s:fi
RESEARCH

Swiss Finance Institute Research Paper Series N°20-65

How Integrated are Credit and Equity Markets? Evidence From Index Options

Pierre Collin-Dufresne
Ecole Polytechnique Fédérale de Lausanne, Swiss Finance Institute, and NBER

Benjamin Junge
Capital Fund Management

Anders B. Trolle
Copenhagen Business School

How integrated are credit and equity markets? Evidence from index options*

Pierre Collin-Dufresne† Benjamin Junge‡ Anders B. Trolle§

Abstract

We study the extent to which credit index (CDX) options are priced consistently with S&P 500 (SPX) equity index options. We derive analytical expressions for CDX and SPX options within a structural credit-risk model with stochastic volatility and jumps using new results for pricing compound options via multivariate affine transform analysis. The model captures many aspects of the joint dynamics of CDX and SPX options; however, it cannot reconcile the relative levels of option prices, suggesting that credit and equity markets are not fully integrated. A strategy of selling CDX volatility yields significantly higher excess returns than selling SPX volatility.

JEL Classification: G12, G13

Keywords: Credit risk, CDX, CDX options, SPX, SPX options, structural models

This version: October 25, 2022

Contains Internet Appendix

*We thank Jack Bao (discussant), Jan Ericsson (discussant), David Lando, Hugues Langlois (discussant), Allan Mortensen, Yoshio Nozawa (discussant), Nicki Rasmussen, Martin Scheicher, and seminar participants at the AFA 2022 annual meeting, the CEPR Advanced Forum for Financial Economics, the EFA 2020 annual meeting, the 10th ITAM Finance conference, the 2nd LFE Workshop in Finance at ICEF, the 2021 SFI Research Days, the Virtual Derivatives Workshop, the UCLA Virtual Finance Workshop, Boston University, Erasmus University, Florida International University, HEC Paris, Sharif University of Technology, Tilburg University, Tinbergen Institute, University College Dublin, and University of Zurich for comments and suggestions. Collin-Dufresne gratefully acknowledges research support from the Swiss Finance Institute. Trolle gratefully acknowledges support from the Danish Finance Institute and the Center for Financial Frictions (FRIC), grant no. DNRF102. The views expressed in this publication are those of the authors and do not purport to reflect the opinions or views of Capital Fund Management.

†EPFL and Swiss Finance Institute. E-mail: pierre.collin-dufresne@epfl.ch

‡Capital Fund Management.

§Copenhagen Business School. E-mail: abtr.fi@cbs.dk

1 Introduction

Classic financial theory views corporate debt and equity as contingent claims on the firm's underlying asset value (Merton (1974)). Accordingly, credit spreads and equity returns should be tightly connected, because they depend on the same set of risk factors in the asset value process. Consistent with much of the literature on structural models, this is how we define "integration" in this paper.[1]

Early tests of *first-generation* structural models find that these models tend to underpredict the level of credit spreads, especially for investment-grade bonds (Jones, Mason, and Rosenfeld (1984), Huang and Huang (2012)).

Instead, more complex *second-generation* structural models, which allow for time-varying risk premia and/or richer asset value dynamics, are more successful at explaining the level of credit spreads (Cremers, Driessen, and Maenhout (2008), Chen, Collin-Dufresne, and Goldstein (2009), Du, Elkamhi, and Ericsson (2019)). In particular, Cremers et al. (2008) demonstrate a close connection between credit spreads and prices of equity index options. More recently, Culp, Nozawa, and Veronesi (2018) propose to use equity options and contingent-claim pricing to construct "pseudo firms" whose derived credit spreads they find to be consistent with actual credit spreads, suggesting "a good deal of integration between corporate bond and options markets."[2]

In this paper we extend the question of integration between credit and equity markets to higher-order moments by investigating whether, in addition to credit spreads, structural models can also match the relative prices of credit and equity index options. Specifically, we use a novel data set of options on a broad credit index to infer implied credit volatilities across a range of moneyness and maturities. We characterize the dynamics of the resulting credit-implied volatility surface and its relation to the volatility surface obtained from equity

[1] Admittedly this is a restrictive definition. A broader definition of integration might only require that all prices are compatible with a common pricing kernel; see, e.g., Chen and Knez (1995) and Sandulescu (2020).
[2] See Culp et al. (2018, p. 458).

index options, and we explore whether the two surfaces and their time variation are consistent when examined through the lens of a rich structural model.

Credit indexes constitute the most liquid component of the corporate credit derivatives market.[3] We focus on the credit index for North American investment-grade firms—the CDX North American Investment Grade Index, henceforth denoted CDX. The years after the financial crisis saw the development of an active credit index options market. Our first contribution is to characterize trading activity in CDX options since trade reporting became mandatory at the end of 2012. Trades are generally large with about two-thirds of the trades having a notional that is at or above the level where the reported notional is capped (typically either USD 100 million or USD 110 million).[4] We estimate that the average daily trading volume during our sample period was USD 4.35 billion, but trading volume exhibits an upward trend and peaks at the height of the COVID-19 crisis in March 2020, where we estimate that it reached an average of USD 11.08 billion per day. In the vast majority of option trades, the underlying is the five-year on-the-run (i.e., most recently issued) CDX contract, and these options are the focus of the paper. Furthermore, we show that trading activity is concentrated in relatively short-term (up to three to four months) options, and that there is relatively more trading in high-strike options.

Next, we use composite dealer quotes to characterize the pricing of CDX options and the relation to S&P 500 (SPX) options.[5] CDX implied volatility smiles are consistently positively skewed, which is economically consistent with the well-known negative skew of SPX implied volatility smiles, once one accounts for the fact that CDX options are quoted in terms of implied credit-spread volatilities. Since high credit spreads typically coincide with

[3]See Collin-Dufresne, Junge, and Trolle (2020) for a detailed description of this market.

[4]Trading between clients and dealers almost exclusively takes place over the counter, while interdealer trading often takes place on dedicated trading platforms. For the subset of trades that are executed on the main interdealer trading platform we have additional data from which we can infer that the capped trades on that platform have an average trade size of USD 353 million.

[5]We follow standard market practice and express CDX option prices in terms of log-normal implied credit-spread volatilities using a reduced-form model.

low equity values, the positive (negative) skews of credit (equity) implied volatility smiles are consistent with a higher premium for options that pay off in bad economic states, where equity values are low and credit spreads are high.

We also investigate the joint dynamics of the underlying index, volatility, and skewness—both within each market and across markets. In particular, we find that much like CDX and SPX returns are highly (negatively) correlated, the smile dynamics are also correlated. Specifically, at-the-money (ATM) CDX and SPX implied volatilities are highly positively correlated, while the skewness of CDX and SPX volatility smiles are negatively correlated.

Since the model-independent analysis shows a strong connection between CDX and SPX options, we next investigate if they can be linked through a rich structural credit-risk model. We consider a general specification for the asset value dynamics of a representative index constituent in which both idiosyncratic and systematic risk have a diffusive and jump component. In addition, the common factor exhibits stochastic volatility and a variance-dependent jump intensity. We allow for both short-term and long-term debt in order to generate a term structure of credit spreads. Indexes and index options are given as compound options, and we develop new results on multivariate transform analysis for affine processes to price these options analytically, thereby facilitating our empirical analysis.[6]

We estimate the model using weekly data on the CDX term structure, the SPX level, and the SPX option surface (as well as short- and long-term index leverage ratios and the index dividend yield), and then price the CDX option surface out-of-sample. Consistent with the data, the fitted CDX implied volatility surfaces are consistently positively skewed; moreover, the magnitude and variation in skewness generated by the model is similar to that observed in the data. The model also largely replicates the joint index-volatility-skewness dynamics

[6]Our model builds on the classic structural approach to pricing corporate debt (Merton (1974), Geske (1977)). Carr and Wu (2010) propose a "hybrid" pricing framework where credit default swaps (CDSs) are priced using a reduced-form approach given an exogenous default intensity and equity options are priced using standard transform analysis applied to the underlying default-adjusted stock price process. This is unlike in traditional structural models, where the stock price, bond price, and default time are determined endogenously by the dynamics of the underlying asset value process.

observed in the data, both within the CDX market and across the two markets.

However, the model cannot match the level of the CDX implied volatility surfaces. Indeed, the CDX implied volatilities generated by the model are, on average, 28 percent lower than those observed in the market. Viewed through the lens of the model, this suggests that market prices of CDX options are too expensive relative to SPX options indicating that credit and equity markets are not fully integrated.[7]

We explore the robustness of our findings along several dimensions. First, our model assumes an infinite number of homogeneous constituents in the two indexes—the "large homogeneous pool" (LHP) approximation of Vasicek (1987)—in order to obtain analytic pricing formulas. We extend the model and perform some numerical analyses to investigate the effects of heterogeneity and a finite number of index constituents, and find that these are unlikely to explain our empirical results.

Second, while our analysis does not require the two indexes to be identical in terms of constituents, it requires a high degree of similarity in terms of index risk characteristics. We compare the two indexes in terms of the distributions of rating, leverage, and total and systematic asset return volatility across constituents—four characteristics that are central to our structural model. We find the distributions to be very similar in terms of mean and median values, even though the SPX distributions display more dispersion. In particular, because index option prices are increasing in systematic asset volatility, one potential resolution of the observed price differential for CDX options could be a higher average systematic asset volatility among CDX constituents, but in fact we find it to be marginally lower.

Third, the relative valuation analysis requires that the two option contracts span similar economic states. By converting the option strikes to a common scale, namely in terms of asset value, we show that this is indeed the case.

[7] We also consider the reverse estimation approach, where we fit to the CDX option surface and price the SPX option surface out-of-sample. Consistent with our main analysis, in this case the model fails to match the level of the SPX implied volatility surface.

Finally, we corroborate our results on the relative valuation of CDX and SPX options by comparing the profitability of selling volatility in the two markets. We show that a strategy of selling CDX volatility yields significantly higher average excess returns and Sharpe ratios than selling SPX volatility.[8] A short-long strategy of selling CDX volatility vs. buying SPX volatility also generates a high Sharpe ratio, although lower than what is attained by selling CDX volatility outright. On the other hand, its higher-order moments are more attractive, with the return distribution being roughly symmetric (instead of highly negatively skewed) and much less leptokurtic.

We discuss, in the conclusion, several possibilities for follow-up research. Clearly, in interpreting our results, we face the joint hypothesis problem (e.g., Fama (1970)) that we can never definitively tell apart whether they reflect lack of integration between the two markets or model misspecification. Although our model incorporates salient features of asset value dynamics, it would be relevant to explore whether our findings hold true in various model extensions. Adding credit-specific factors to the model seems particularly promising, and we suggest one such extension—systematic variation in bankruptcy costs—and show how it can be incorporated in our model.

Another possibility is that there are institutional features that can cause market segmentation and distort the relative prices of index options. For instance, even if CDX and SPX options are close substitutes, they are not treated as such by regulators in the context of credit-risk hedging by financial institutions. We provide suggestive evidence for a significant regulatory-driven demand from banks for CDX options; however, quantifying such a demand and linking it to variation in the relative valuation of index options is left for future research.

The paper is related to several strands of literature. The model is related to Bai, Goldstein, and Yang (2019b) who focus on pricing equity index options in a structural model using the LHP approximation. Relative to their paper, we also treat credit index options,

[8]For instance, a strategy of selling an equally weighted portfolio of option straddles (appropriately sized) yields a Sharpe ratio of 1.744 in the CDX market compared to a Sharpe ratio of 0.659 in the SPX market.

allow option expiries to differ from debt maturity (thereby treating options as true compound options on the firm asset value), and derive full analytical solutions to option prices in a more general stochastic-volatility jump-diffusion setting using new results on multivariate transform analysis for affine processes.[9] Our results on multivariate transform analysis generalize the univariate analysis of Duffie, Pan, and Singleton (2000) and have many applications beyond our specific use in this paper for valuing compound options.[10]

In contrast to the aforementioned papers on the level of credit spreads, a number of papers provide evidence that points towards imperfectly integrated equity and corporate credit markets. Collin-Dufresne, Goldstein, and Martin (2001) find that a large fraction of changes in credit spreads cannot be explained by variables suggested by the Merton (1974) model; further, the unexplained residuals seem to be driven by few common factors which subsequent papers have linked to illiquidity factors (Friewald and Nagler (2019)) or intermediary balance-sheet factors (He, Khorrami, and Song (2020)). A number of recent papers (Chordia, Goyal, Nozawa, Subrahmanyam, and Tong (2017), Choi and Kim (2018), and Bai, Bali, and Wen (2019a)) document differences in the set of factors and characteristics that explain the cross-sections of corporate bond and stock returns. Schaefer and Strebulaev (2008) find that the Merton (1974) model produces reasonable sensitivities of bond returns to stock returns, although a sizable excess bond return volatility remains, which Bao and Pan (2013) link to time-varying bond illiquidity. Kapadia and Pu (2012) find short-lived divergences between CDS and stock prices, especially for firms with high arbitrage costs. A common feature of all these papers is that they study bond returns or credit spread changes of individual firms, for which illiquidity effects are likely to be important. In contrast, we focus on a highly liquid credit index and its options.

[9] Allowing option expiries to differ from debt maturity is important in our setting where option expiries are typically less than four months while the underlying credit index has a maturity of approximately five years. Bai et al. (2019b) derive option prices up to an expectation that is computed via numerical integration.

[10] For instance, our results can be used to value complex "cliquet outperformance options," that depend on the maximum realization of one or several prices at various fixed dates prior to the option maturity, in general affine (equity, commodity, currency, or fixed income) models.

Finally, the paper is related to a recent literature on the relative pricing of CDX tranche swaps and SPX options (Coval, Jurek, and Stafford (2009), Collin-Dufresne, Goldstein, and Yang (2012), and Seo and Wachter (2018)). In principle, this literature also provides insights into the integration of equity and credit derivatives markets. However, in practice the relative pricing of these instruments is complicated by several factors: CDX tranche swaps are long-dated contracts, while the most liquid SPX options have short expiries;[11] the range of (negative) economic states that are spanned by CDX tranche swaps is much wider than that spanned by SPX options (Collin-Dufresne et al. (2012)); and trading in CDX tranche swaps has languished after the financial crisis. In contrast, CDX and SPX options are much more closely aligned in terms of which option maturities are liquid and the range of economic states that are spanned. Moreover, CDX options have flourished after the financial crisis.[12]

The paper is structured as follows: Section 2 describes the CDX options market and the transaction and quote data. Section 3 characterizes the relation between CDX and SPX options. Section 4 presents the structural model, Section 5 shows how to use multivariate transform analysis with affine processes to price indexes and index options, Section 6 describes model estimation and results, and Section 7 discusses robustness checks. Section 8 concludes. Proofs are given in the Appendix, and an Internet Appendix contains supplementary results.

2 CDX and CDX options

2.1 CDX

A CDX is a credit default swap that provides default protection on a set of companies belonging to an index, with the notional of the swap divided evenly among the index constituents.

[11] This literature, therefore, uses less liquid long-term SPX options that are traded over the counter.

[12] Based on all (capped) trade reports since 2013 and aggregating across all North American credit indexes, we find that trading volume in tranche swaps is only 9% of the trading volume in options.

We focus on the investment-grade CDX that provides default protection on 125 investment-grade companies. CDX contracts are issued with initial maturities between one and ten years. A new set of CDX contracts referencing a "refreshed" index is issued every March and September.[13] The most recently launched contracts are called on-the-run; all previously launched contracts are referred to as off-the-run. Most trading activity is in the five-year on-the-run contract. Virtually all such trades are centrally cleared and executed on dedicated trading platforms (so-called swap execution facilities or SEFs) at very low transaction costs; see Collin-Dufresne et al. (2020) for details about the market structure and transaction costs of CDX.

Each swap has a fixed coupon of $C = 100$ bps and, when entering into the swap, the counterparties exchange an upfront amount equal to the present value of the swap.[14] When an index constituent defaults, the loss is settled in the same way as a single-name CDS, and the outstanding notional of the swap is reduced. From then on, the swap references a new version of the index without the defaulted name. For quotation purposes, the upfront amount of the swap is converted to a spread, which is the value of the fixed coupon C that would be required for the upfront amount to be zero. This conversion is explained in Section IA.1 of the Internet Appendix.

2.2 CDX options

A CDX option is an option to enter into a CDX contract at a given strike price. A payer option gives the right to buy credit protection (paying the strike and the subsequent coupons) while a receiver option gives the right to sell credit protection (receiving the strike and the

[13] These *roll dates* are March 20 and September 20 (in the second half of 2014, the roll date was postponed to October 6, due to delays in signing up market participants to the 2014 ISDA Credit Derivatives Definitions). The index constituents are selected among the investment-grade companies that have the most liquid single-name CDSs traded on them. Each index is identified by its series number.

[14] Throughout the paper, we assume that coupons are paid continuously at a rate C, which greatly simplifies notation. In reality, coupons are paid quarterly on standardized coupon dates.

subsequent coupons). Options are European style and are quoted for a wide set of strikes and monthly expirations. Options expire on the third Wednesday of each month. Contractually, the option payoff is given in upfront terms. However, for quotation purposes it is standard practice to write the payoff in spread terms and express the option price as a log-normal spread implied volatility. Details—including how defaults during the life of the option are handled—are provided in Section IA.1 of the Internet Appendix. Note that a payer (receiver) option is a call (put) option on the upfront amount/spread.

2.3 Trading of CDX options

To understand the trading activity in CDX options, we analyze all reported transactions from December 31, 2012 (when reporting to swap data repositories became mandatory) to the end of our sample period on April 30, 2020. Table 1 displays descriptive statistics of the transaction data. For completeness, the table also reports statistics on CDX transactions. In contrast to CDX, trading in CDX options predominantly takes place over the counter, and the SEF trades that we do observe are almost exclusively interdealer trades. Central clearing is also less prevalent in CDX options than in CDX.[15]

CDX option trades are relatively infrequent (18 trades per day, on average) but large in size. The median of the reported trade sizes is USD 100 million. However, about two-thirds of the trades are reported with a capped notional which implies that trade sizes are typically much larger.[16] For the subset of trades that take place on the main interdealer trading platform (GFI SEF), we have additional data from which we can infer that the capped trades in that subset have an average trade size of USD 353 million.[17] The average

[15]For CDX, five-year on-the-run (and immediate off-the-run) trades are, with a few exceptions, required to be executed on SEFs and be centrally cleared. For CDX options, there are no such requirements.

[16]The level of the cap is determined by the Commodity Futures Trading Commission and varies over time and with option strike. In most trade reports, the notional is capped at either USD 100 million or USD 110 million.

[17]Daily market activity reports from the GFI SEF show that the aggregate uncapped notional amount traded is USD 108,410 million for CDX options during the period from October 2, 2013 to April 30, 2020. Identifying

daily trading volume based on the capped trade reports is USD 1.44 billion. Assuming that capped trades in general have the same average trade size as those on the GFI SEF, we obtain an estimate of the true average daily trading volume of USD 4.35 billion.[18] Note that this is a downward-biased estimate because the trade reporting requirement only concerns trades for which at least one counterparty is a US institution.

Figure 1 shows the evolution in trading activity on a monthly basis. Panels A and B show the average daily trading volume for CDX and CDX options, respectively, while Panels C and D show the average number of trades per day. Underscoring the growing popularity of CDX options, the trading volume exhibits an upward trend during the sample period. The average daily trading volume based on the capped trade reports (estimated true volume) has increased from USD 0.88 billion (USD 2.72 billion) in January 2013 to USD 2.08 billion (USD 6.23 billion) in April 2020. Trading volume peaks at the height of the COVID-19 crisis in March 2020 at USD 3.59 billion (USD 11.08 billion) per day. The highest trade count for CDX options is in February 2020 at 88 trades per day, on average.

Table 1 also shows that in the vast majority of option trades, the underlying CDX is the five-year on-the-run contract. Therefore, we focus on those options in the remainder of the paper.

Table 2 shows the distribution of trading volume across moneyness and option maturity. We define moneyness as

$$m = \frac{\log\left(\frac{K}{F(\tau)}\right)}{\sigma^{ATM}\sqrt{\tau}}, \tag{1}$$

where K is the strike, $F(\tau)$ is the forward spread, σ^{ATM} is the ATM log-normal spread

GFI SEF trades in the transaction data shows that the aggregate capped notional amount is USD 34,829 million, with 300 capped trades that have an average capped trade size of USD 108 million. This implies that the true average trade size of the capped trades is USD 353.27 (=108 + (108,410 - 34,829)/300) million.

[18] Compared with CDX option trades, CDX trades are more frequent (202 trades per day, on average) but smaller in size with a median trade size of USD 50 million and less than a quarter of the trade sizes being above the cap. The average daily trading volume based on the capped trade reports is USD 11.13 billion but we estimate that the true volume is USD 17.80 billion using the same method as for CDX options.

implied volatility, and τ is the maturity. Intuitively, m measures the number of standard deviations that an option is in or out of the money given log-normally distributed spreads. The table shows that there is more trading in high-strike than low-strike options. It also shows that trading is concentrated in relatively short-term options with maturities out to three to four months.

2.4 CDX option quotes

To have synchronized data across the option surface, we use quotes rather than trades. Quotes are obtained from Markit and are composites of "dealer runs" sent from dealers to clients. We use end-of-day quotes. The sample period is from February 24, 2012 until April 30, 2020.

Details on the quote data is given in Sections IA.2 and IA.3 of the Internet Appendix. There, we find that when option maturities become very short (typically less than one week), dealers stop quoting prices. Beyond that, there are almost always quotes for at least three monthly expirations. At longer maturities, quotes are more sporadic. In light of these findings as well as the evidence on option transactions (Table 2), on each observation date we select the first three monthly expirations among the options that have more than two weeks to expiration. These options are denoted M1, M2, and M3. The average option maturities are 29.9, 60.2, and 90.6 calendar days, respectively.

For each maturity, we consider 13 moneyness "buckets": $-3.25 < m \leq -2.75$, $-2.75 < m \leq -2.25$, ... , $2.75 < m \leq 3.25$, where m is defined in (1). Within each bucket, we search for the option that is closest to the mid-point of the interval. We only search among out-of-the-money (OTM) options due to their higher liquidity. In the ATM category, we give priority to payer options.

The result of this data-sorting is a uniform maturity-moneyness grid that preserves the information in the data without overweighing those dates on which more maturities and/or

strikes are quoted. In the Internet Appendix, we show that quotations are tilted towards higher-strike options. This probably reflects both the higher interest in trading those options (see Table 2) and the fact that the risk-neutral spread distribution is heavily skewed towards higher spreads (see below) so that deep OTM payer options (by our moneyness measure) have meaningful prices even when deep OTM receiver options have little value.

2.5 SPX option quotes

SPX options trade on the Chicago Board Options Exchange (CBOE) and from there we get end-of-day quotes. Regular SPX options expire on the third Friday of each month (there are also weekly and end-of-month expirations that we do not consider). On each observation date, we search for the three SPX option maturities that are closest to the three CDX option maturities. These SPX options either expire two days after or five days before; hence, there is a close match in maturity between SPX and CDX options. The average SPX option maturities are 30.6, 61.2, and 91.5 calendar days, respectively.

For each maturity, we then find the OTM options that are closest to the mid-points of the following 13 moneyness intervals: $-8.5 < m \leq -7.5$, $-7.5 < m \leq -6.5$, ... , $3.5 < m \leq 4.5$, where m is again defined in (1), but with $F(\tau)$ denoting the forward SPX value. Note that the m-range is not directly comparable across CDX and SPX options (one is in spread terms, the other is in price terms). Rather, given the m-range for CDX options, we choose the m-range for SPX options so that the moneyness range is roughly similar when expressed on a common scale, namely in asset-value terms, see Section 7.3.

3 Stylized facts

To provide an initial sense of the data, Figure 2 shows weekly CDX and SPX implied volatility smiles for the two-month maturity. Weekly data is sampled each Wednesday.[19] It is immediately apparent that implied volatility smiles for CDX options are positively skewed, in stark contrast to the negatively skewed SPX implied volatility smiles. This is economically intuitive in that bad economic states are characterized by low equity prices and high credit spreads; therefore, if such states carry a high risk and/or price of risk, prices of OTM SPX put options and OTM CDX call options will be elevated.

To summarize the information in implied volatilities across moneyness, option maturity, and time, we follow the approach in Foresi and Wu (2005). On each date and for each option maturity, we run the following cross-sectional regression

$$\sigma^{IV}(m) = \beta_0 + \beta_1 m + \beta_2 m^2 + \epsilon, \tag{2}$$

where m is the measure of moneyness given in (1), and ϵ is an error term. In this regression, β_0 captures the ATM implied volatility, β_1 captures the skewness of the implied volatility smile, and β_2 captures the curvature of the implied volatility smile. The β-coefficients are very highly correlated across option maturity; therefore, for ease of exposition, we average the β-coefficients across option maturity to produce single time series of β_0, β_1, and β_2. Note that β_2 is sensitive to the moneyness range which varies over time, especially for CDX options (see Figure IA3 in the Internet Appendix). This variation introduces noise in the estimate of curvature. For this reason, we mainly focus on the dynamics of volatility and skewness.

Figure 3 provides an overview of the data with the left (right) panels showing data for the CDX (SPX) market. The top-left panel shows time series of the 1Y and 5Y CDX spreads.

[19] If Wednesday is not a trading day, we consider the preceding Tuesday instead. The sample comprises 427 weekly observation dates from February 29, 2012 to April 29, 2020.

Normally, the CDX term structure is strongly upward sloping; however, during the COVID-19 crisis the slope flattens as the 1Y spread increases more than the 5Y. At the peak of the crisis, the 5Y spread reaches 151 bps.

The middle-left panel (blue line) shows the time series of CDX volatility. Clearly, CDX volatility exhibits significant variation; in particular, it spikes during the COVID-19 crisis in March 2020 when it reaches a maximum of 1.35 relative to the sample average of 0.47. Moreover, variation in CDX and SPX volatility (middle-right panel) appears to be highly correlated.

The lower-left panel (blue line) shows the time series of CDX skewness. This confirms the observation in Figure 2 that the CDX implied volatility smiles are always positively skewed. CDX skewness varies over time and reaches a maximum of 0.149 during the COVID-19 crisis relative to a sample average of 0.073. It appears that variation in CDX and SPX skewness (lower-right panel) is moderately negatively correlated so that, when the SPX volatility smile becomes more skewed towards OTM put options, the CDX volatility smile tends to become more skewed towards OTM call options.[20]

Next, we investigate more formally the joint dynamics of the underlying index, volatility, and skewness—both within each market and across markets. To this end, the left part of Table 3 reports correlations (in weekly changes) between the log CDX spread, CDX volatility, CDX skewness, log SPX index, SPX volatility, and SPX skewness. To make sure that our findings are not driven by the COVID-19 crisis, we report results both for the full sample (Panel A) and for an ex-COVID-19 sample that ends on December 31, 2019 (Panel B). The shading of each cell is proportional to the absolute value of the correlation. For CDX, there is a highly positive correlation between changes in spread and volatility (0.62), which is consistent with the positively skewed implied volatility smiles. We also observe a somewhat

[20] One exception is during the COVID-19 crisis; initially, both CDX and SPX skewness becomes more pronounced, but CDX skewness reverses already on March 9 while SPX skewness reverses on March 18. Figure IA11 in the Internet Appendix shows the smile dynamics during the COVID-19 crisis.

weaker positive correlation between changes in spread and skewness (0.20), and a moderately positive correlation between changes in volatility and skewness (0.39). For SPX, the table confirms the well-known negative return-volatility correlation (-0.86), positive return-skewness correlation (0.74), and negative volatility-skewness correlation (-0.80). Regarding the cross-market interactions, we highlight the strongly negative correlation between CDX spread changes and SPX returns (-0.80), the highly positive correlation between volatility changes (0.69), and a somewhat more moderate negative correlation between skewness changes (-0.33). This correlation structure is robust to excluding the COVID-19 period.

4 A structural model for pricing index options

We now propose a structural model to price credit and equity index options consistently with the debt and equity claims on each firm in the index. Asset value dynamics have a factor structure where both idiosyncratic and systematic risk have a diffusive and jump component, and the common factor in addition features stochastic volatility and a variance-dependent jump intensity. We model each individual firm's CDS and equity following Merton's (1974) seminal paper as, respectively, a put and call option on the firm's asset value. To address the term structure of credit spreads, we allow the outstanding debt to have different maturities as in Geske (1977), and we use the LHP approximation of Vasicek (1987) to model the index portfolios. Indexes and index options are given as compound options, and in Section 5 we develop new results on multivariate transform analysis for affine processes to price these options analytically.

4.1 The firms' assets

We assume that each individual firm in the index has an asset value A_t^i that is driven by a common component A_t, which has stochastic volatility (ω_t) and is exposed to systematic

Brownian (dW_t) and pure-jump (dN_t) shocks, and a firm-specific residual component, which is exposed to idiosyncratic Brownian (dW_t^i) and pure-jump (dN_t^i) shocks. Specifically, we assume that the risk-neutral asset value dynamics of (ex-ante identical) individual firms are given by

$$\begin{aligned}
\frac{dA_t^i}{A_t^i} &= \frac{dA_t}{A_t} + \sigma_i dW_t^i + (e^{\gamma_i} - 1)dN_t^i - \lambda_i \nu_i dt \\
\frac{dA_t}{A_t} &= (r - \delta)dt + \sqrt{\omega_t} dW_t + (e^{\gamma} - 1)dN_t - \lambda_t \nu dt \\
d\omega_t &= \kappa(\bar{\omega} - \omega_t)dt + \sigma_\omega \sqrt{\omega_t}\{\rho_\omega dW_t + \sqrt{1 - {\rho_\omega}^2} dZ_t\},
\end{aligned}$$

where W_t^i, W_t, and Z_t are independent Brownian motions, N_t and N_t^i are independent Poisson counting processes with intensities $\lambda_t = \lambda_0 + \lambda_\omega \omega_t$ and λ_i, respectively, $\gamma \sim \mathcal{N}(m, v)$ and $\gamma_i \sim \mathcal{N}(m_i, v_i)$ are independent normal random variables, and we define $\nu = \mathbb{E}[e^{\gamma} - 1] = e^{m + \frac{v}{2}} - 1$ and $\nu_i = \mathbb{E}[e^{\gamma_i} - 1] = e^{m_i + \frac{v_i}{2}} - 1$. We assume that all payouts, δA_t^i, generated by the firm's assets go to equity holders.

It is helpful to define $a_t^i = \log A_t^i$, $a_t = \log A_t$, and $m_t^i = a_t^i - a_t$, with m_t^i capturing firm-specific risk. The state vector

$$x_t = [a_t, \omega_t]$$

captures the systematic risk components, whereas the relevant state vector when considering a specific firm can be defined as:

$$x_t^i = [a_t, \omega_t, m_t^i].$$

The dynamics of all the variables are given in Appendix A.1, but here we note three properties that will be instrumental to deriving index option values: (i) both x_t and x_t^i are affine jump-diffusion Markov processes (as defined in Duffie et al. (2000)), (ii) $\forall i$ m_t^i are independent of x_t, and (iii) $\forall i$ a_T^i have i.i.d. distributions conditional on x_T.

4.2 The firms' debt

We consider a simplified debt structure with two outstanding zero-coupon bonds: a short-term bond with principal D_1 and maturity date T_1, and a long-term bond with principal D_2 and maturity date $T_2 > T_1$.[21] We assume that repayments of principals are made by equity holders, via "out-of-pocket" side payments, so that the asset value process is not affected.[22] Thus, equity holders will choose to default at T_1 if the continuation value from holding on to the equity is worth less than the principal payment D_1 they owe to debt holders at that time. This determines an endogenous default threshold, Φ_{T_1}, at T_1, where Φ_{T_1} is the asset value such that, right after D_1 has been paid by equity holders, the equity value equals D_1. At T_2, the default threshold is D_2, as in the standard Merton (1974) model. In case of default, we assume that a fraction α of assets is paid out to debt holders, while a fraction $1-\alpha$ is lost because of bankruptcy costs. Finally, if the firm defaults at T_1, we assume that payments to debt holders are proportional to principal, so that holders of the short-term bond are paid a fraction $R_1 = \alpha\frac{D_1}{D_1+D_2}$ of assets, while holders of the long-term bond are paid a fraction $R_2 = \alpha\frac{D_2}{D_1+D_2}$.

4.3 Bond, equity, and CDS valuation

Consider any firm i and let $t \leq T_1$. The value of the short-term bond is given by

$$B_t^{T_1,i} = e^{-r(T_1-t)}\Big(D_1\mathbb{E}_t[\mathbf{1}_{\left\{A^i_{T_1}\geq\Phi_{T_1}\right\}}] + \mathbb{E}_t[R_1A^i_{T_1}\mathbf{1}_{\left\{A^i_{T_1}<\Phi_{T_1}\right\}}]\Big),$$

where the first term is the present value of the bond's principle when it is repaid and the second term is the present value of the bond's recovery amount when the firm defaults at

[21] This is the simplest debt structure that allows us to get a term structure of credit spreads and generate variation in the risky annuity for long-term CDX contracts. The model can handle any number of bonds.

[22] This is a standard assumption in dynamic capital structure models (Black and Cox (1976), Leland (1994)).

T_1. The value of the long-term bond is given by

$$B_t^{T_2,i} = e^{-r(T_1-t)}\mathbb{E}_t[R_2 A_{T_1}^i \mathbf{1}_{\left\{A_{T_1}^i < \Phi_{T_1}\right\}}] + e^{-r(T_2-t)}\Big(D_2\mathbb{E}_t[\mathbf{1}_{\left\{A_{T_1}^i \geq \Phi_{T_1}, A_{T_2}^i \geq D_2\right\}}] + \mathbb{E}_t[\alpha A_{T_2}^i \mathbf{1}_{\left\{A_{T_1}^i \geq \Phi_{T_1}, A_{T_2}^i < D_2\right\}}]\Big),$$

where the first term is the present value of the bond's recovery amount when the firm defaults at T_1, and the second and third terms are, respectively, the present values of the bond's principle when it is repaid and the bond's recovery amount when the firm defaults at T_2, provided that the firm did not default at T_1.

The equity value is given by the asset value less the value of the two bonds and the present value of the expected bankruptcy costs; that is,

$$\begin{aligned} S_t^i = A_t^i &- e^{-r(T_1-t)}\Big(D_1\mathbb{E}_t[\mathbf{1}_{\left\{A_{T_1}^i \geq \Phi_{T_1}\right\}}] + \mathbb{E}_t[A_{T_1}^i \mathbf{1}_{\left\{A_{T_1}^i < \Phi_{T_1}\right\}}]\Big) \\ &- e^{-r(T_2-t)}\Big(D_2\mathbb{E}_t[\mathbf{1}_{\left\{A_{T_1}^i \geq \Phi_{T_1}, A_{T_2}^i \geq D_2\right\}}] + \mathbb{E}_t[A_{T_2}^i \mathbf{1}_{\left\{A_{T_1}^i \geq \Phi, A_{T_2}^i < D_2\right\}}]\Big). \end{aligned} \tag{3}$$

Consider a unit-notional CDS contract from t to T_2. The value of the protection leg is

$$V_t^{\text{Protection leg},i} = e^{-r(T_1-t)}\mathbb{E}_t[(1-\frac{\alpha A_{T_1}^i}{D_1+D_2})\mathbf{1}_{\left\{A_{T_1}^i < \Phi\right\}}] + e^{-r(T_2-t)}\mathbb{E}_t[(1-\frac{\alpha A_{T_2}^i}{D_2})\mathbf{1}_{\left\{A_{T_1}^i \geq \Phi, A_{T_2}^i < D_2\right\}}],$$

where the first term is the present value of loss given default (LGD) at T_1 and the second term is the present value of LGD at T_2, provided that the firm did not default at T_1. The value of the premium leg with a coupon rate of C paid continuously is

$$V_t^{\text{Premium leg},i} = \left(\int_t^{T_1} e^{-r(u-t)}du + \int_{T_1}^{T_2} e^{-r(u-t)}du\mathbb{E}_t[\mathbf{1}_{\left\{A_{T_1}^i \geq \Phi\right\}}]\right) \times C,$$

where the coupon up until date T_1 always has to paid because the firm cannot default before T_1 (the first term), whereas the coupon from T_1 to T_2 only has to be paid if the firm did not

default at T_1 (the second term). Therefore, the upfront amount of the CDS contract is

$$\begin{aligned} U_t^i =& V_t^{\text{Protection leg},i} - V_t^{\text{Premium leg},i} \\ =& e^{-r(T_1-t)}\Big((1+C_1)\mathbb{E}_t[\mathbf{1}_{\left\{A^i_{T_1}<\Phi_{T_1}\right\}}] - \frac{\alpha}{D_1+D_2}\mathbb{E}_t[A^i_{T_1}\mathbf{1}_{\left\{A^i_{T_1}<\Phi_{T_1}\right\}}] - C_1\Big) \\ &+ e^{-r(T_2-t)}\Big(\mathbb{E}_t[\mathbf{1}_{\left\{A^i_{T_1}\geq\Phi_{T_1},A^i_{T_2}<D_2\right\}}] - \frac{\alpha}{D_2}\mathbb{E}_t[A^i_{T_2}\mathbf{1}_{\left\{A^i_{T_1}\geq\Phi_{T_1},A^i_{T_2}<D_2\right\}}]\Big) - C_0, \end{aligned} \tag{4}$$

where we have defined $C_0 = C\int_t^{T_1} e^{-r(u-t)}du$ and $C_1 = C\int_{T_1}^{T_2} e^{-r(u-T_1)}du$.

4.4 The default boundary at T_1

Valuation in the previous section depends on the default boundary at T_1. Note that after the payment of D_1 is made, the equity value becomes

$$S^i_{T_1}(a^i_{T_1},\omega_{T_1}) = A^i_{T_1} - e^{-r(T_2-T_1)}\Big(D_2\mathbb{E}_{T_1}[\mathbf{1}_{\left\{A^i_{T_2}\geq D_2\right\}}] + \mathbb{E}_{T_1}[A^i_{T_2}\mathbf{1}_{\left\{A^i_{T_2}<D_2\right\}}]\Big).$$

Therefore, the default boundary $\Phi(\omega)$, such that it is optimal to default at T_1 if $A_{T_1} \leq \Phi(\omega_{T_1})$, is given by the solution to the equation $S^i_{T_1}(\log\Phi(\omega),\omega) = D_1$. To obtain analytical valuations, we approximate the log-default boundary with an affine function:

$$\log\Phi(\omega) \approx \phi_0 + \phi_1\omega. \tag{5}$$

We verify in Section IA.5 of the Internet Appendix that (5) is an accurate approximation.

4.5 CDX and SPX

The upfront amount of the CDX is a simple average of the upfront amounts of the $N = 125$ single-name CDSs for the index constituents. Because N is large, we approximate the index upfront amount by letting $N \to \infty$. In this case, we obtain a simple analytical expression

for the index upfront amount via the law of large numbers, which in turn allows us to price CDX options analytically. From (4), the index upfront amount, conditional on the common factors $x_t = \{a_t, \omega_t\}$, is given by

$$\begin{aligned}
U_t(x_t) &= \lim_{N\to\infty} \frac{1}{N}\sum_{i=1}^{N} U_t^i \\
&= \mathbb{E}[U_t^i | x_t] \\
&= e^{-r(T_1-t)}\Big((1+C_1)\mathbb{E}[\mathbf{1}_{\left\{A^i_{T_1}<\Phi(\omega_{T_1})\right\}} \,|\, x_t] - \frac{\alpha}{D_1+D_2}\mathbb{E}[A^i_{T_1}\mathbf{1}_{\left\{A^i_{T_1}<\Phi(\omega_{T_1})\right\}} \,|\, x_t] - C_1\Big) \\
&\quad + e^{-r(T_2-t)}\Big(\mathbb{E}[\mathbf{1}_{\left\{A^i_{T_1}\geq\Phi(\omega_{T_1}), A^i_{T_2}<D_2\right\}} \,|\, x_t] - \frac{\alpha}{D_2}\mathbb{E}[A^i_{T_2}\mathbf{1}_{\left\{A^i_{T_1}\geq\Phi(\omega_{T_1}), A^i_{T_2}<D_2\right\}} \,|\, x_t]\Big) - C_0.
\end{aligned}$$

Similarly, from (3), the value of the SPX is given by

$$\begin{aligned}
S_t(x_t) &= \lim_{N\to\infty} \frac{1}{N}\sum_{i=1}^{N} S_t^i \\
&= \mathbb{E}[S_t^i | x_t] \\
&= A_t - e^{-r(T_1-t)}\Big(D_1\mathbb{E}[\mathbf{1}_{\left\{A^i_{T_1}\geq\Phi(\omega_{T_1})\right\}} \,|\, x_t] + \mathbb{E}[A^i_{T_1}\mathbf{1}_{\left\{A^i_{T_1}<\Phi(\omega_{T_1})\right\}} \,|\, x_t]\Big) \\
&\quad - e^{-r(T_2-t)}\Big(D_2\mathbb{E}[\mathbf{1}_{\left\{A^i_{T_1}\geq\Phi(\omega_{T_1}), A^i_{T_2}\geq D_2\right\}} \,|\, x_t] + \mathbb{E}[A^i_{T_2}\mathbf{1}_{\left\{A^i_{T_1}\geq\Phi(\omega_{T_1}), A^i_{T_2}<D_2\right\}}\} \,|\, x_t]\Big).
\end{aligned}$$

4.6 CDX and SPX options

The time-0 value of a CDX call option with strike K and expiration at T_0 is (where we use the notation: $\mathbb{E}_0[\cdot] := \mathbb{E}[\cdot \,|\, x_0]$)

$$\begin{aligned}
C_0^{CDX} &= e^{-rT_0}\mathbb{E}_0[\max(U_{T_0}(x_{T_0}) - K, 0)] \\
&= e^{-rT_0}\mathbb{E}_0[(U_{T_0}(x_{T_0}) - K)\mathbf{1}_{\left\{A_{T_0}<\underline{A}(\omega_{T_0})\right\}}] \\
&= e^{-rT_1}\Big((1+C_1)\mathbb{E}_0[\mathbf{1}_{\left\{A_{T_0}<\underline{A}(\omega_{T_0}), A^i_{T_1}<\Phi(\omega_{T_1})\right\}}] - \frac{\alpha}{D_1+D_2}\mathbb{E}_0[A^i_{T_1}\mathbf{1}_{\left\{A_{T_0}<\underline{A}(\omega_{T_0}), A^i_{T_1}<\Phi(\omega_{T_1})\right\}}]\Big)
\end{aligned}$$

$$+ e^{-rT_2}\Big(\mathbb{E}_0[\mathbf{1}_{\left\{A_{T_0}<\underline{A}(\omega_{T_0}),A^i_{T_1}\geq\Phi(\omega_{T_1}),A^i_{T_2}<D_2\right\}}] - \frac{\alpha}{D_2}\mathbb{E}_0[A^i_{T_2}\mathbf{1}_{\left\{A_{T_0}<\underline{A}(\omega_{T_0}),A^i_{T_1}\geq\Phi(\omega_{T_1}),A^i_{T_2}<D_2\right\}}]\Big)$$
$$- e^{-rT_0}\tilde{K}\mathbb{E}_0[\mathbf{1}_{\left\{A_{T_0}<\underline{A}(\omega_{T_0})\right\}}],$$

where $\tilde{K} = K + C_0 + C_1 e^{-r(T_1-T_0)}$ and $\underline{a}(\omega) = \log \underline{A}(\omega)$ is the exercise boundary such that it is optimal to exercise the CDX call at T_0 when $a_{T_0} \leq \underline{a}(\omega_{T_0})$. It is implicitly defined by the equation $U_{T_0}(\underline{a}(\omega), \omega) = K$ (using the fact that, for a given ω, $U_{T_0}(a, \omega)$ is decreasing in a). To value CDX options analytically, we approximate the exercise boundary with an affine function:

$$\underline{a}(\omega) = \underline{a}_0 + \underline{a}_1\omega. \tag{6}$$

Similarly, the time-0 value of an SPX call option with strike K and expiration at T_0 is

$$\begin{aligned}
C_0^{SPX} &= e^{-rT_0}\mathbb{E}_0[\max(S_{T_0}(x_{T_0}) - K, 0)] \\
&= e^{-rT_0}\mathbb{E}_0[(S_{T_0}(x_{T_0}) - K)\mathbf{1}_{\left\{A_{T_0}\geq\overline{A}(\omega_{T_0})\right\}}] \\
&= e^{-rT_0}\mathbb{E}_0[A_{T_0}\mathbf{1}_{\left\{A_{T_0}\geq\overline{A}(\omega_{T_0})\right\}}] - e^{-rT_1}\Big(D_1\mathbb{E}_0[\mathbf{1}_{\left\{A_{T_0}\geq\overline{A}(\omega_{T_0}),A^i_{T_1}\geq\Phi(\omega_{T_1})\right\}}] + \mathbb{E}_0[A^i_{T_1}\mathbf{1}_{\left\{A_{T_0}\geq\overline{A}(\omega_{T_0}),A^i_{T_1}<\Phi(\omega_{T_1})\right\}}]\Big) \\
&\quad - e^{-rT_2}\Big(D_2\mathbb{E}_0[\mathbf{1}_{\left\{A_{T_0}\geq\overline{A}(\omega_{T_0}),A^i_{T_1}\geq\Phi(\omega_{T_1}),A^i_{T_2}\geq D_2\right\}}] + \mathbb{E}_0[A^i_{T_2}\mathbf{1}_{\left\{A_{T_0}\geq\overline{A}(\omega_{T_0}),A^i_{T_1}\geq\Phi(\omega_{T_1}),A^i_{T_2}<D_2\right\}}]\Big) \\
&\quad - e^{-rT_0}K\mathbb{E}_0[\mathbf{1}_{\left\{A_{T_0}\geq\overline{A}(\omega_{T_0})\right\}}],
\end{aligned}$$

where $\overline{a}(\omega) = \log \overline{A}(\omega)$ is the exercise boundary such that it is optimal to exercise the SPX call at T_0 if $a_{T_0} \geq \overline{a}(\omega_{T_0})$, and which is implicitly defined by the equation $S_{T_0}(\underline{a}(\omega), \omega) = K$ (using the fact that, for a given ω, $S_{T_0}(a, \omega)$ is increasing in a). To value SPX options analytically, we approximate the exercise boundary with an affine function:

$$\overline{a}(\omega) = \overline{a}_0 + \overline{a}_1\omega. \tag{7}$$

We verify in Section IA.5 of the Internet Appendix that (6) and (7) are accurate approximations to the respective exercise boundaries.

5 Multivariate transform analysis for affine processes

The valuation of indexes and index options described above can be reduced to computing the following *generalized affine transform*:

$$\mathcal{G}^{\alpha}_{\boldsymbol{\beta}}(y_1,\ldots,y_n;\overline{X}_{T_0},\boldsymbol{T}) = \mathbb{E}[e^{\alpha\cdot X_{T_n}}\mathbf{1}_{\left\{\beta_1\cdot X_{T_1}\leq y_1,\ldots,\beta_n\cdot X_{T_n}\leq y_n\right\}}\,|\,\overline{X}_{T_0}] \tag{8}$$

defined for an N-dimensional affine state vector X_t with a subvector $\overline{X}_t$ (that is, $X_t = \left[\begin{smallmatrix}\overline{X}_t\\ \underline{X}_t\end{smallmatrix}\right]$), a vector $\boldsymbol{T} = \{T_0,\ldots,T_n\}$ of increasing dates, an (N,n)-matrix $\boldsymbol{\beta}$ with column vectors β_i (that is, $\boldsymbol{\beta} = \{\beta_1,\ldots,\beta_n\}$), and an N-vector α.

This is a multivariate extension of the generalized affine transform presented in the classic paper by Duffie et al. (2000), who consider the case with $n = 1$ and $\overline{X}_t = X_t$, and use it to solve the valuation of standard derivative contracts, such as European call and put options, written on an underlying with N-dimensional affine dynamics.

The multidimensional case we present here is useful to handle derivatives with more complex payoffs involving multiple dates, such as compound options and cliquet options, or with payoffs that depend on several underlyings, such as index outperformance options or basket options.

Duffie et al. (2000) obtained the univariate solution using the Fourier inversion theorem of Gil-Pelaez (1951). Here we follow a similar approach by relying on the multidimensional version of that theorem derived in Shephard (1991).

To solve the generalized affine transform, we first rewrite (where to simplify notation, we

drop the dependence on $\boldsymbol{T}$):

$$\begin{aligned}\mathcal{G}^{\alpha}_{\boldsymbol{\beta}}(y_1,\ldots,y_n;\,\overline{X}_{T_0}) &= \mathbb{E}[e^{\alpha\cdot X_{T_n}}\,|\,\overline{X}_{T_0}]\,\mathbb{E}^{\alpha}[\mathbf{1}_{\left\{\beta_1\cdot X_{T_1}\le y_1,\ldots,\beta_n\cdot X_{T_n}\le y_n\right\}}\,|\,\overline{X}_{T_0}]\\ &:= \Psi(\alpha;\overline{X}_{T_0},T_0,T_n)\,G^{\alpha}_{\boldsymbol{\beta}}(y_1,\ldots,y_n;\,\overline{X}_{T_0}),\end{aligned} \tag{9}$$

where, for some n-dimensional parameter vector α,

$$\Psi(\alpha;\overline{X}_{T_0},T_0,T) := \mathbb{E}[e^{\alpha\cdot X_T}\,|\,\overline{X}_{T_0}] \tag{10}$$

is the moment generating function of X_T conditional on the subvector $\overline{X}_{T_0}$, which in general need not have an exponential affine solution. Instead, the classic exponential affine moment generating function that defines the affine process X_t is:[23]

$$\Psi(\alpha;X_{T_0},T_0,T) := \mathbb{E}[e^{\alpha\cdot X_T}\,|\,X_{T_0}] \tag{11}$$

$$= e^{b_\alpha(T_0,T)+c_\alpha(T_0,T)X_{T_0}}, \tag{12}$$

where $b_\alpha(T_0,T)$ and $c_\alpha(T_0,T)$ are deterministic functions.[24]

Observe that $G^{\alpha}_{\boldsymbol{\beta}}(y_1,\ldots,y_n;\,\overline{X}_{T_0}) \equiv \mathbb{P}^{\alpha}(\beta_i\cdot X_{T_i}\le y_i\ \forall i=1,\ldots,n)$ is the multivariate cumulative distribution function (conditional on T_0, $\overline{X}_{T_0}$) of the n random variables $x_i = \beta_i\cdot X_{T_i},\ \ i=1,\ldots,n$ under the probability measure $\mathbb{P}^{\alpha}$ defined by

$$\frac{d\mathbb{P}^{\alpha}}{d\mathbb{P}} = \frac{e^{\alpha\cdot X_{T_n}}}{\Psi(\alpha;\overline{X}_{T_0},T_0,T_n)}.$$

We then obtain the following theorem from multivariate Fourier inversion:

[23] We note the slight abuse of notation: $\Psi(\beta;X,t,T)$ and $\Psi(\beta;\overline{X},t,T)$ are different functions! We hope this leads to no confusion as the two vectors X and $\overline{X}$ have different sizes.

[24] These functions are related to the generator of the affine process via a system of ODEs, see Duffie, Filipović, and Schachermayer (2003).

Theorem 1. *Define*

$$\begin{aligned}\mathcal{U}(y_1,\ldots,y_n) =& 2^n G^{\alpha}_{\{\beta_1,\ldots,\beta_n\}}(y_1,\ldots,y_n)\\ &- 2^{n-1}\left[G^{\alpha}_{\{\beta_2,\ldots,\beta_n\}}(y_2,\ldots,y_n)+\ldots+G^{\alpha}_{\{\beta_1,\ldots,\beta_{n-1}\}}(y_1,\ldots,y_{n-1})\right]\\ &+ 2^{n-2}\left[G^{\alpha}_{\{\beta_3,\ldots,\beta_n\}}(y_3,\ldots,y_n)+\ldots+G^{\alpha}_{\{\beta_1,\ldots,\beta_{n-2}\}}(y_1,\ldots,y_{n-2})\right]\\ &+\ldots+(-1)^n.\end{aligned}$$

Then, if n is odd we have:

$$\mathcal{U}(y_1,\ldots,y_n) = \frac{(-2)^n}{(2\pi)^n}\int_0^{\infty}\ldots\int_0^{\infty} 2\mathrm{i}^{n-1}\underset{u_2}{\Delta}\cdots\underset{u_n}{\Delta} Im\left[\frac{e^{-\mathrm{i}\,u\cdot y}\Psi^{\alpha}(\mathrm{i}u_1\beta_1,\ldots,\mathrm{i}u_n\beta_n;\overline{X}_{T_0},T_0,T_1,\ldots,T_n)}{u_1\ldots u_n}\right]du_1\ldots du_n,$$

and if n is even we have:

$$\mathcal{U}(y_1,\ldots,y_n) = \frac{(-2)^n}{(2\pi)^n}\int_0^{\infty}\ldots\int_0^{\infty} 2\mathrm{i}^{n}\underset{u_2}{\Delta}\cdots\underset{u_n}{\Delta} Re\left[\frac{e^{-\mathrm{i}\,u\cdot y}\Psi^{\alpha}(\mathrm{i}u_1\beta_1,\ldots,\mathrm{i}u_n\beta_n;\overline{X}_{T_0},T_0,T_1,\ldots,T_n)}{u_1\ldots u_n}\right]du_1\ldots du_n,$$

where for $1\leq j\leq n$ and $f:\mathbb{R}^n\to\mathbb{R}$ the operator $\underset{u_j}{\Delta}$ is defined by

$$\underset{u_j}{\Delta} f(u) = f(u_1,\ldots,u_{j-1},u_j,u_{j+1},\ldots,u_n)+f(u_1,\ldots,u_{j-1},-u_j,u_{j+1},\ldots,u_n),$$

and for all $j\geq 1$:

$$\Psi^{\alpha}(\beta_1,\ldots,\beta_j;\overline{X}_{T_0},T_0,T_1,\ldots,T_j) = \frac{\Psi(\beta_1,\ldots,\beta_{j-1},\beta_j+\alpha;\overline{X}_{T_0},T_0,T_1,\ldots,T_j)}{\Psi(\alpha;\overline{X}_{T_0},T_0,T_j)}.$$

For $j=1$ the conditional moment generating function is defined in (10), and for all $j>1$

we define recursively:

$$\Psi(\beta_1,\ldots,\beta_j;\overline{X}_{T_0},T_0,T_1,\ldots,T_j)=\Psi(\beta_1,\ldots,\beta_{j-2},\beta_{j-1}+c_{\beta_j}(T_{j-1},T_j);\overline{X}_{T_0},T_0,T_1,\ldots,T_{j-1})e^{b_{\beta_j}(T_{j-1},T_j)}.$$

Proof. See Appendix A.2. □

Note that for $n=1$ our theorem recovers the transform inversion formula of Duffie et al. (2000), Proposition 2:

Corollary 1. *Using Theorem 1 in the definition (9) for the case $n=1$ and with $\overline{X}_t=X_t$ we obtain:*

$$\mathcal{G}^{\alpha}_{\beta_1}(y_1;X_{T_0},T_0,T_1)=\frac{\Psi(\alpha;X_{T_0},T_0,T_1)}{2}-\frac{1}{\pi}\int_0^{\infty}Im\left[\frac{e^{-\mathrm{i}\,u_1y_1}\Psi(\alpha+\mathrm{i}u_1\beta_1;X_{T_0},T_0,T_1)}{u_1}\right]du_1.$$

All indexes and index options are valued with Theorem 1 applied to the three-dimensional affine process $X_t=x^i_t$, using as subvector either $\overline{X}_t=x_t$ or $\overline{X}_t=x^i_t$ (Section IA.4 of the Internet Appendix shows how all expectations in the pricing formulas in Section 4 can be expressed in terms of the generalized transform (8)). For this purpose, we present in the next theorem closed-form solutions to the two moment generating functions (10) and (11). While the exponential affine solution in (12) is standard, an exponential affine solution to (10) does not automatically follow and, indeed, obtains here only because when considering the affine process $x^i_t=[x_t,m^i_t]$, the subvector process x_t is independent of m^i_t.

Theorem 2. *For the affine process $X_t:=x^i_t=[x_t,m^i_t]$ we obtain (for conditionning subvectors respectively given by (i) $\overline{X}_t=x^i_t$ and (ii) $\overline{X}_t=x_t$):*

$$(i)\;\;\Psi(\beta;x^i_t,t,T):=\mathbb{E}[e^{\beta\cdot x^i_T}\,|\,x^i_t]=e^{b_\beta(t,T)+c_\beta(t,T)x^i_t}$$

$$(ii)\;\;\Psi(\beta;x_t,t,T):=\mathbb{E}[e^{\beta\cdot x^i_T}\,|\,x_t]=e^{\zeta(\beta_3)T+B(T-t;\beta_1,\beta_2)+\beta_1a_t+C(T-t;\beta_1,\beta_2)\omega_t},$$

where $\beta = [\beta_1, \beta_2, \beta_3]$ *is a vector of parameters and*

$$b_\beta(t,T) = \zeta(\beta_3)(T-t) + B(T-t;\beta_1,\beta_2)$$
$$c_\beta(t,T) = \begin{bmatrix} \beta_1 \\ C(T-t;\beta_1,\beta_2) \\ \beta_3 \end{bmatrix},$$

where the functions $\zeta(\beta_3)$*,* $B(T-t;\beta_1,\beta_2)$*, and* $C(T-t;\beta_1,\beta_2)$ *have closed-form solutions given in Equations (17), (18), and (19) below.*

Proof. See Appendix A.3 □

6 The relative pricing of index options

6.1 Calibration procedure

The main empirical analysis consists of fitting the model to the CDX term structure, the SPX level, and the SPX option surface, and then price the CDX option surface out-of-sample. As a robustness check, we also conduct the reverse exercise, fitting to the CDX option surface and pricing the SPX option surface out-of-sample. In particular, we force a perfect fit to the 1Y and 5Y CDX and the SPX level (as well as the SPX dividend yield and the short- and long-term index leverage ratios), and minimizes the sum of squared pricing errors for index options.[25] It is especially important to price the 5Y CDX and the SPX level accurately; otherwise, it is difficult to interpret option pricing errors.

As in Collin-Dufresne et al. (2012), the parameters governing the dynamics of the common factors are held fixed for each 6-month period over which a CDX series is on-the-run. The common factors and the remaining parameters change from each observation date to the next. As in Section 3, we use weekly data. Additional details on the estimation is given in

[25] See Section IA.8 of the Internet Appendix for details on the computation of the index leverage ratios using Compustat data. The SPX dividend yield is obtained from the put-call parity relation for SPX options.

Section IA.7 of the Internet Appendix.

A number of parameters are fixed ex ante (we have verified that our results are robust to reasonable variations in these parameters). First, the idiosyncratic jump risk is largely pinned down by the 1Y CDX, which is essentially a deep out-of-the-money put option on firm assets. This makes it difficult to identify all idiosyncratic jump parameters. We set $m_i = -5$ and $v_i = 0$, implying that an idiosyncratic jump leads to almost certain default for a company, and calibrate only the idiosyncratic jump intensity. Second, bankruptcy costs are set to 20%, corresponding to $\alpha = 0.80$, which is roughly in line with empirical estimates (see, e.g., Andrade and Kaplan (1998) and Davydenko, Strebulaev, and Zhao (2012)). Third, the risk-free interest rate is set to the two-month rate from the bootstrapped LIBOR/swap curve. Fourth, in the common factor dynamics, the parameters σ_ω and ρ_ω are invariant under a change of measure. In the context of calibrating stochastic-volatility jump-diffusion models to equity index options, Broadie, Chernov, and Johannes (2007) stress the importance of *time-series consistency*; i.e., restricting those parameters that are invariant under a change of measure to their values under the physical measure. In Section IA.7 of the Internet Appendix, we show that setting $\sigma_\omega = 0.20$ and $\rho_\omega = -0.70$ makes the corresponding vol-of-vol and correlation parameters for SPX returns largely consistent with recent time series studies. We verify ex post that similar values for σ_ω and ρ_ω are obtained from the time series of the calibrated factors.

6.2 Results

Table 4 reports the sample mean and sample standard deviation of the calibrated parameters, with Panels A and B showing results when calibrating to SPX and CDX options, respectively (the table reports values of $\ell_1 = \frac{D_1}{A_t}$ and $\ell_2 = \frac{D_2}{A_t}$ instead of D_1 and D_2).[26] In

[26] Tables IA.1 and IA.2 in the Internet Appendix report parameter estimates for each time period over which a CDX series is on-the-run.

both cases, there is very strong evidence for stochastic volatility and variance-dependent jump intensities with λ_0 estimated to be close to zero.[27] It is instructive to compare the two sets of estimates in terms of the implications for the unconditional systematic and total asset volatility ($\sqrt{\bar{\omega} + \lambda(m^2 + v)}$ and $\sqrt{\bar{\omega} + \sigma_i^2 + \lambda(m^2 + v) + \lambda_i(m_i^2 + v_i)}$, respectively, where $\lambda = \lambda_0 + \lambda_\omega \bar{\omega}$), and the resulting unconditional correlation between firm asset values. The underlying indexes depend on total asset risk and given that we always calibrate to the index levels, it is unsurprising that total asset volatility is very similar across the two calibrations (0.39 vs. 0.38). Index options, on the other hand, largely depend on systematic asset risk which can therefore differ across the two calibrations; indeed, the systematic asset volatility is lower when calibrating to SPX options (0.21 vs. 0.27). Consequently, the asset correlation implied from SPX options is lower than implied from CDX options (0.30 vs. 0.51).[28] This provides the first indication that the model will not match both sets of index options simultaneously; we can expect that calibrating to SPX options will tend to underprice CDX options and calibrating to CDX options will tend to overprice SPX options.

To assess the fit to options, on each observation date we compute the mean pricing error (ME) and root mean squared pricing error (RMSE) across each option surface, where pricing errors are given as the relative difference between fitted and actual implied volatilities, $\frac{\hat{\sigma}^{IV} - \sigma^{IV}}{\sigma^{IV}}$. Table 5 reports the sample means of the resulting ME and RMSE time series. Consider first the results when calibrating to SPX options. The in-sample fit is very good

[27] We verify that values of $\sigma_{_\omega}$ and $\rho_{_\omega}$ obtained from the time series of the calibrated factors are consistent with their ex-ante pre-determined values. We estimate $\sigma_{_\omega}$ as the standard deviation of $\frac{\omega_{t+1} - \omega_t}{\sqrt{\omega_t}}$ times $\sqrt{52}$ and $\rho_{_\omega}$ as the correlation between $\frac{\log A_{t+1} - \log A_t}{\sqrt{\omega_t}}$ and $\frac{\omega_{t+1} - \omega_t}{\sqrt{\omega_t}}$. For the ex-COVID-19 sample, we get $\sigma_{_\omega} = 0.21$ and $\rho_{_\omega} = -0.77$ when calibrating to SPX options, and $\sigma_{_\omega} = 0.25$ and $\rho_{_\omega} = -0.55$ when calibrating to CDX options, which are roughly in line with the pre-determined values. Including the COVID-19 period leads to slightly higher estimates of $\sigma_{_\omega}$.

[28] To put these correlations in perspective we directly compute pairwise correlations of daily asset returns among index constituents per calendar quarter, and then average across quarters (see Section IA.12 of the Internet Appendix for details on the computation of asset returns). We require each return time series to comprise at least 50 daily returns in the respective quarter. The average pairwise asset correlations are remarkably similar for the two indexes, equal to 0.29 for SPX and 0.28 for CDX. The extent to which risk-neutral correlations inferred from index options exceed the physical correlation depends, in particular in the presence of jumps, on risk premia and is beyond the scope of this paper.

with an average ME of essentially zero and not statistically significant. On the other hand, the out-of-sample fit to CDX options produces an average ME of -0.283, which is highly statistically significant (that the out-of-sample CDX RMSE is larger than the in-sample SPX RMSE is to be expected). That is, as alluded to above, fitted CDX option prices are, on average, lower than market prices.

Consider next the results when calibrating to CDX options. These are the mirror-image of the previous results. The in-sample fit to CDX options is very good with an insignificant average ME, while the out-of-sample fit to SPX options has an average ME of 0.49, which again is highly statistically significant.

Figure 4 shows the time series of the out-of-sample ME for CDX options when calibrating to SPX options (blue line) and the out-of-sample ME for SPX options, when calibrating to CDX options (red line). The two lines almost always have opposite sign and they are highly negatively correlated (correlation coefficient of -0.81) so that if the mispricing worsens according to one calibration, it usually also does so according to the other, confirming the robustness of the results. We note that there is a tendency for the mispricing to decrease over time.

To further investigate model performance, we focus on the version calibrated to SPX options. First, we investigate which dimensions of the CDX option surface the model has difficulty matching; to do so, we run the regression (2) on the fitted implied volatilities and measure the model fit in terms of how close the β-estimates obtained from the fitted data are to the original β-estimates. In Figure 3, the red lines show the β-estimates from the fitted data. The figure confirms the model's accurate (in-sample) fit to SPX options in terms of both volatility (middle-right panel) and skewness (lower-right panel). The figure also shows that the model has a relatively accurate (out-of-sample) fit to CDX skewness (lower-left panel). However, the figure shows that the model has a poor (out-of-sample) fit to CDX volatility. While the model appears to capture the variation in volatility relatively well, the

level of model-implied volatility is consistently lower than the market; indeed, the sample means of β_0^{CDX} in the data and the fitted data are 0.47 and 0.33, respectively.

Next, we investigate the extent to which the model captures the index-volatility-skewness correlation structure discussed in Section 3. The correlations computed from the fitted data are reported in the right part of Table 3. Within the SPX market, there is a close (in-sample) match to the data. More importantly, within the CDX market, there is a relatively good (out-of-sample) match to the correlation between spread and volatility (0.49 vs. 0.62 in the data) but somewhat too low correlations between volatility and skewness (0.11 vs. 0.20 in the data) and between spread and skewness (0.22 vs. 0.39 in the data). Regarding the cross-market interactions, the model largely captures the correlation between SPX and CDX volatility (0.83 vs. 0.69 in the data) and between SPX and CDX skewness (-0.25 vs. -0.33 in the data) as well as the remaining "off-diagonal" correlations.[29] These findings hold true in the ex-COVID-19 sample.

To summarize, the model captures many aspects of the joint dynamics of the credit and equity index options data. However, it is not able to capture the relative levels of CDX and SPX option prices. In particular, calibrating the model to the SPX implied volatility surface produces a CDX implied volatility surface that, while largely having the correct shape, is consistently below the market.

6.3 Understanding the sources of volatilities and smiles

In the model, index volatility is driven by several sources, namely the financial leverage effect as well as stochastic volatility and jumps in the systematic asset factor. Let I_t denote the index (either the SPX level or the CDX spread) in which case the instantaneous variance of

[29] Note that, by design of the estimation procedure, the correlation between SPX returns and CDX spread changes is matched exactly.

index returns is given as

$$\underbrace{\left(\frac{\partial I_t}{\partial A_t}\frac{A_t}{I_t}\right)^2\omega_t}_{\text{Financial leverage}}+\underbrace{\left(\frac{\partial I_t}{\partial \omega_t}\frac{1}{I_t}\sigma_{\omega}\right)^2\omega_t}_{\text{Stochastic asset vol}}+\underbrace{2\frac{\partial I_t}{\partial A_t}\frac{\partial I_t}{\partial \omega_t}\frac{A_t}{I_t^2}\sigma_{\omega}\rho_{\omega}\omega_t}_{\text{Covariance}}+\underbrace{\lambda_t\mathbb{E}\left[\left(\frac{I(A_{t-}e^{\gamma},\omega_t)}{I(A_{t-},\omega_t)}-1\right)^2\right]}_{\text{Jumps}}. \quad (13)$$

To provide intuition about the model, in this section we show how these different elements affect both the relative levels of index volatility as well as the shapes of the index implied volatility smiles. For illustration, we focus on two-month options.

We start with the parameter estimates from Panel A in Table 4. The instantaneous volatility of simple asset returns, $\sqrt{\omega_t+\lambda_t\mathbb{E}[(e^{\gamma}-1)^2]}$, is 0.116. We consider four versions of the model which all have this systematic asset volatility, but differ in terms of its sources. For each model version, we re-calibrate A_t, σ_i, λ_i, ℓ_1, ℓ_2, and δ to the sample means of the 1Y and 5Y CDX upfronts, the SPX level, the SPX dividend yield, and the index leverage ratios, so that these quantities are held constant across versions.

First, as a natural benchmark, we consider a version with deterministic diffusive volatility ($\omega_t = 0.0135, \sigma_{\omega} = \rho_{\omega} = \lambda_0 = \lambda_{\omega} = 0$), in which case only the financial leverage effect is present. The instantaneous volatility of CDX and SPX returns are 0.151 and 0.245, respectively, giving an *index volatility ratio* of 1.62. Figure 5 (blue lines) shows the implied volatility smiles. Both curves are quite flat, and in striking contrast to the data, the CDX implied volatility smile exhibits a negative slope.[30]

Second, we turn on stochastic asset volatility, but with zero correlation between asset returns and volatility ($\omega_t = 0.0135, \sigma_{\omega} = 0.2, \rho_{\omega} = \lambda_0 = \lambda_{\omega} = 0$). This adds the second term in (13), which originates from the fact that the index value depends directly on ω_t. However, this term is greater for CDX than SPX (we can think of the CDX and SPX as, respectively, a deep OTM and ITM option on the asset value so that in relative terms CDX

[30] In Section IA.9 of the Internet Appendix, we prove analytically that in the classic Merton (1974) model the leverage effect generates a negative implied volatility skew for both credit and equity options.

is more sensitive to ω_t) causing CDX volatility to increase relative to SPX volatility, with the index volatility ratio increasing to 1.67. For the implied volatility smile, a stochastic ω_t has two effects. The first is to make the return distribution more leptokurtic which increases the curvature of the smile. The second effect is to generate positive correlation between the index value and variance (both of which depend positively on ω_t) which, other things equal, skews the smile towards higher strikes. Figure 5 (red lines) shows that both implied volatility smiles exhibit more curvature; in addition, for CDX the second effect is sufficiently strong to overturn the leverage effect resulting in a positively skewed smile.

Third, we add negative correlation between asset returns and volatility ($\omega_t = 0.0135, \sigma_{_\omega} = 0.2, \rho_{_\omega} = -0.70, \lambda_0 = \lambda_\omega = 0$), which adds the third term in (13). This terms is positive for CDX (because $\frac{\partial I_t}{\partial A_t} < 0$ and $\frac{\partial I_t}{\partial \omega_t} > 0$) but negative for SPX (because $\frac{\partial I_t}{\partial A_t} > 0$ and $\frac{\partial I_t}{\partial \omega_t} > 0$), so it further increases CDX volatility relative to SPX volatility, with the index volatility ratio increasing to 1.94. For the implied volatility smile, a negative $\rho_{_\omega}$ makes the asset return distribution negatively skewed, decreasing SPX return skewness and increasing CDX return skewness (because of opposite signs of $\frac{\partial I_t}{\partial A_t}$) and amplifying the skewed smiles as shown in Figure 5 (yellow lines).

Fourth, we consider the full model with jumps (where the systematic parameters are as in Panel A in Table 4). This shifts systematic risk from diffusive risk towards jump risk. The fourth term in (13) is greater for CDX than SPX causing the index volatility ratio to increase further to 2.17. For the implied volatility smile, asset-value jumps with a negative mean jump size make the asset return distribution both more leptokurtic and negatively skewed, and Figure 5 (purple lines) shows that jumps attenuate the already skewed smiles.

The upshot is that both stochastic volatility and jumps have a significant effect on the relative valuation of CDX and SPX options in terms of both the level and shape of the index implied volatility smiles.

7 Robustness and additional empirical results

We conduct several robustness checks regarding the LHP approximation, the similarities in the compositions of the CDX and SPX indexes, and the overlap in the asset value states spanned by CDX and SPX options. We also corroborate our model-dependent results on the relative valuation of CDX and SPX options by investigating the investment performance of trading strategies that sell volatility in the two options markets.

7.1 The large homogeneous portfolio approximation

The LHP approximation of Vasicek (1987) requires that all firms within the index are ex-ante identical, so that conditioning on the common systematic state-variables, one can apply the law of large number. In reality, firms in the CDX and SPX exhibit significant heterogeneity (see below). In Section IA.10 of the Internet Appendix, we solve an extension of the model that allows for heterogeneity in leverage across firms. Specifically, we allow for two different groups of firms that are each homogeneous, and derive analytical solutions to index option prices by using the LHP approximation within each group. We show that, relative to the benchmark model, matching the mean, dispersion, and skewness of the leverage distribution of index constituents leads to lower CDX option prices relative to SPX option prices, hence exacerbating the valuation differential.

Second, the LHP approximation assumes that there are an infinite number of index constituents. In Section IA.11 of the Internet Appendix, we use simulations to price index options for a finite number of index constituents and quantify the bias in the analytical option pricing formulas. We show that the (downward) bias is small, but greater for CDX options than for SPX options because the CDX index has fewer constituents. Therefore, accounting for the actual number of index constituents would raise CDX option prices relative to SPX option prices; however, the effect is small relative to the magnitude of the valuation

differential.

7.2 Comparison of index compositions

Our analysis does not require the two indexes to be identical in terms of names, but rather in terms of risk characteristics. To compare the indexes, we focus on four risk characteristics of the underlying constituents that are central to the structural model: rating (as a proxy for the physical-measure default probability), leverage, and total and systematic asset return volatility.[31]

Figure 6 compares the indexes in terms of leverage and ratings. Panels A and B show the distribution of firm-quarter leverage observations for the CDX and SPX constituents, respectively.[32] Clearly, the distribution for SPX constituents has a higher dispersion with relatively more low-leverage (even unlevered) and high-leverage firms. However, on average, leverage is similar across the two indexes with a mean (median) of 0.277 (0.244) for CDX vs. 0.238 (0.200) for SPX.

Panels C and D show the distribution of firm-quarter rating observations for the two sets of index constituents.[33] Again, the distribution for SPX constituents has a higher dispersion, but for both indexes the mean and median rating is BBB+.[34]

Figure 7 compares the indexes in terms of asset return volatility. Panels A and B show the distribution of firm-quarter observations of total asset return volatility for the CDX and SPX

[31] Section IA.12 of the Internet Appendix details the computation of asset return volatility. In a nutshell, asset returns are leverage-weighted averages of stock and synthetic bond returns, where stock returns are from CRSP and synthetic bond returns are computed using single-name CDS data from Markit. The systematic component of asset return volatility is obtained from a one-factor model.

[32] In the figure, we focus on total leverage. In the Internet Appendix, we split total leverage into short- and long-term leverage and find similar results, see Figure IA12. The fraction of CDX (SPX) constituents for which we are able to compute leverage varies between 0.832 and 0.888 (0.892 and 0.984).

[33] Note that ratings data in Compustat is only available up until third quarter of 2017. During this time period, the fraction of CDX (SPX) constituents with ratings information varies between 0.888 and 0.912 (0.864 and 0.892).

[34] When the CDX index is refreshed every six months, it consists only of investment-grade firms (i.e., those rated BBB- and above). The few BB-rated firm-quarter observations in the figure come from firms that were downgraded after index launch.

index constituents, respectively. While the distribution for SPX constituents displays slightly higher dispersion (standard deviation of 0.068 for CDX vs. 0.080 for SPX), the average asset volatility is very similar with a mean (median) of 0.167 (0.154) for CDX vs. 0.173 (0.158) for SPX.

Since the non-diversifiable component of volatility is the crucial driver of index option value, we plot the distribution of firm-quarter observations of systematic asset return volatility in Panels C and D. These distributions are strikingly similar with a mean (median) [standard deviation] of 0.092 (0.085) [0.045] for CDX vs. 0.098 (0.089) [0.052] for SPX.

Given these results, it seems unlikely that differences in the risk characteristics that drive valuation in our structural model (such as leverage, total and systematic volatility) can explain our findings. In particular, a potential explanation for the observed price discrepancy between CDX and SPX options could be a relatively higher systematic asset return volatility among CDX constituents, but this is clearly not what we observe in the data.

7.3 Comparison of asset values spanned by index options

The relative pricing argument we rely on is more palatable if the two option markets span similar economic states.[35] Since, CDX and SPX options are quoted using different models, their strike ranges are not readily comparable. Instead, we translate them to strike ranges in terms of the common asset factor, A_{T_0}. In doing so, we use the model calibrated to SPX options and condition on $\omega = \mathbb{E}_0[\omega_{T_0}]$.

For CDX options, A^{min} is the value of the common factor below which the highest-strike call option expires in the money, and A^{max} is the value above which the lowest-strike put option expires in the money.[36] Similarly, for SPX options, A^{min} is the value of the common

[35] Intuitively, if the two markets span different states, then the comparison would rely on "extrapolation" into the tails of the distribution, which might be less robust. For example, Collin-Dufresne et al. (2012), show that the effective strike of super-senior CDX tranches is much deeper out-of-the-money than the deepest OTM quoted strike for SPX options, so that relative price comparisons are very model dependent.

[36] Recall that $U_{T_0}(\log A, \omega)$ is decreasing in A; therefore, A^{min} solves $U_{T_0}(\log A^{min}, \omega) = K^{max}$ and A^{max}

factor below which the lowest-strike put option expires in the money, and A^{max} is the value above which the highest-strike call option expires in the money.[37]

Figure 8 plots the time series of the strike range of CDX and SPX options in terms of the common asset factor. Specifically, on each observation date and for each option maturity, we express A^{min} and A^{max} relative to the forward asset value, A^{fwd}; that is, as $\frac{A^{min}-A^{fwd}}{A^{fwd}}$ and $\frac{A^{max}-A^{fwd}}{A^{fwd}}$. Clearly, CDX and SPX options span roughly the same asset values; if anything, the range is greater for SPX options. For instance, for the two-month option maturity, the average strike range is -21.0% to 12.0% for CDX options and -27.4% to 11.4% for SPX options.

7.4 Trading CDX vs. SPX options

Our model suggests that market prices of CDX options are too expensive relative to SPX options. To corroborate this result, we compare the profitability of selling volatility in the two markets. We consider a strategy of selling ATM straddles within each maturity category on a daily basis and with a holding period of one day (a short holding period ensures that the delta remains close to zero). In addition to holding the option premium in a margin account, we assume that an initial amount of capital is required when selling options. We further assume that the required capital is proportional to the option premium and adjust the proportionality factor to achieve a 10% unconditional annualized volatility of realized excess returns within each option maturity category.[38]

Table 6 shows summary statistics of returns for each option maturity as well as for an

solves $U_{T_0}(\log A^{max}, \omega) = K^{min}$.

[37] Recall that $S_{T_0}(\log A, \omega)$ is increasing in A; therefore, A^{min} solves $S_{T_0}(\log A^{min}, \omega) = K^{min}$ and A^{max} solves $S_{T_0}(\log A^{max}, \omega) = K^{max}$.

[38] A similar approach is taken in Duarte, Longstaff, and Yu (2007) in their analysis of fixed income arbitrage strategies. The choice of 10% is inconsequential for our conclusions. Section IA.13 of the Internet Appendix provides more details on the trading strategy. It also shows that the results are robust to assuming that the required capital is constant over time (rather than varying with the option premium).

equally weighted (EW) portfolio of the three option maturities.[39] Across all maturities and both including and excluding the COVID-19 crisis, selling CDX volatility generates higher and more statistically significant average excess returns and higher Sharpe ratios than selling SPX volatility. For instance, for the full sample (Panel A), the EW portfolio generates an annualized Sharpe ratio of 1.744 in the CDX market vs. 0.659 in the SPX market. Because of the large increase in volatility during the COVID-19 crisis, the strategy in both markets performs better during the ex-COVID-19 sample (Panel B).[40]

We also consider a short-long strategy of selling CDX straddles vs. buying SPX straddles.[41] This strategy generates high Sharpe ratios, that are typically higher than that of selling SPX volatility outright, but lower than selling CDX volatility outright. For instance, for the full sample, trading the EW portfolios against each other generates an annualized Sharpe ratio of 0.877. Further, the higher-order moments of the long-short strategy are more attractive, with the return distributions being roughly symmetric (instead of highly negatively skewed) and much less leptokurtic. Figure 9 shows the evolution of one dollar invested in each of the EW strategies at the beginning of the sample. Clearly, the short-long strategy avoids the occasional large drawdowns from selling volatility outright.

8 Conclusion

In recent years, a liquid market for credit index (CDX) options has developed. We study the extent to which these options are priced consistently with S&P 500 (SPX) equity index options. We consider a rich structural credit-risk model where both idiosyncratic and

[39] When computing performance, we only consider returns on those days where returns are available for all option maturities and for both markets.

[40] A contemporaneous paper by Ammann and Moerke (2019) constructs synthetic variance swap contracts from CDX options and finds that selling CDX variance swaps generates higher Sharpe ratios than selling SPX variance swaps in a pre-COVID-19 sample. See also Chen, Doshi, and Seo (2020).

[41] We assume that the same amount of capital is required when buying SPX straddles as when selling them so that we maintain a 10% unconditional annualized volatility of realized excess returns. The short-long strategy then allocates 50% of funds to selling CDX straddles and 50% to buying SPX straddles.

systematic asset risk have a diffusive and jump component, and where the common factor exhibits stochastic volatility and a variance-dependent jump intensity. Using the large homogeneous portfolio approximation and new results on multivariate transform analysis for affine processes we obtain analytical solutions to indexes and index options, which are compound options in our structural modelling framework. Estimating the model, we find that it captures many aspects of the joint dynamics of CDX and SPX options. However, according to the model, market prices of CDX options are too expensive relative to SPX options, suggesting that credit and equity markets are not fully integrated—at least not in the strong sense suggested by classic Merton (1974)-style structural models, where both credit and equity options are priced by the same set of risk factors that drive the asset value process. This result is further corroborated by a model-independent analysis of option trading strategies, which shows that selling CDX volatility yields significantly higher average excess returns and Sharpe ratios than selling SPX volatility.

Our findings suggest at least two lines for future research. First, although our model incorporates salient features of asset value dynamics, it can surely be extended further, for instance, by adding multifactor systematic and idiosyncratic stochastic volatility, or allowing for a more complex default boundary.[42] Of particular interest would be to incorporate credit-specific risk factors. A natural candidate for such a factor would be systematic variation in bankruptcy costs, and we show in Section IA.14 of the Internet Appendix how to add this feature, while keeping analytical expressions for all derivatives prices.[43] It is an open question as to whether these and other model extensions can account for the observed discrepancy between CDX and SPX option prices.

Another line of research would be searching for institutional features that can cause

[42] For example, in a paper subsequent to ours, Doshi, Ericsson, Fournier, and Seo (2021) explore whether a first-passage-time structural model with priced asset variance risk can reconcile pricing across CDX and SPX option markets.

[43] Another plausible candidate would be a credit-specific liquidity factor, as suggested by Bao and Pan (2013) and Friewald and Nagler (2019).

market segmentation and a persistent price discrepancy. For instance, Basel III regulation has created a significant demand for CDX call options from banks who seek to hedge their credit valuation adjustment (CVA) exposures in order to reduce their regulatory capital.[44] Using regulatory filings on risk-weighted assets for CVA from eight global systemically important US banks, we show in the Section IA.15 of the Internet Appendix that the size of this hedging demand could potentially account of a large fraction of the trading activity in CDX options. Thus, demand pressure, along the lines of Gârleanu, Pedersen, and Poteshman (2009), could distort the relative prices of CDX and SPX options.

[44] In the aftermath of the financial crisis, the Basel III regulation introduced a new capital charge—the CVA risk charge—to cover the risk of deterioration in the credit worthiness of counterparties. Both CDX and CDX options are eligible hedge instruments, but due to a discrepancy between the regulatory and accounting treatment of counterparty risk, many banks prefer to use CDX options; see, e.g., Becker (2014).

Appendix A Proofs

A.1 Dynamics of the state variables

We can rewrite the individual firm asset value as[45]

$$A_T^i = A_T e^{-\frac{1}{2}{\sigma_i}^2 T + \sigma_i W_T^i} e^{-\lambda_i \nu_i T + \gamma_i N_T^i}, \tag{14}$$

where the common factor $a_t = \log A_t$ has dynamics:

$$da_t = (r - \delta - \lambda_t \nu - \frac{1}{2}\omega_t)dt + \sqrt{\omega_t} dW_t + \gamma dN_t. \tag{15}$$

Note that the state vector

$$x_t = [a_t, \omega_t]$$

follows an affine jump-diffusion process; see, e.g., Duffie et al. (2000).

It is helpful to define $a_T^i = \log A_T^i = \log A_T + \log M_T^i$ for some strictly positive martingale $M_t^i = e^{m_t^i}$ so that $A_t^i = e^{a_t + m_t^i}$ with:

$$dm_t^i = -(\frac{1}{2}{\sigma_i}^2 + \lambda_i \nu_i)dt + \sigma_i dW_t^i + \gamma_i dN_t^i. \tag{16}$$

Then, the state when considering a specific firm can be defined as:

$$x_t^i = [a_t, \omega_t, m_t^i]$$

We note that the m_t^i are independent of the state x_t and that the A_T^i have i.i.d. distributions conditional on x_t, which will be helpful when deriving CDX and SPX values.

[45] Note the abuse of notation here (and throughout the Appendix): γN denotes the sum of N i.i.d. random variables with the same distribution as γ.

A.2 Proof of Theorem 1

Proof. The theorem follows directly from applying Theorems 5 and 6 of Shephard (1991) to recover the cumulative joint distribution of the n random variables $x_j := \beta_j \cdot X_{T_j}\ \forall j = 1, \dots n$ under the $\mathbb{P}^\alpha$ measure, that is $G^\alpha_{\boldsymbol{\beta}}(y_1, \dots, y_n) = \mathbb{P}^\alpha(x_1 \leq y_1, \dots, x_n \leq y_n)$, from its characteristic function defined as:

$$\begin{aligned}\varphi(u_1, \dots, u_n) &= \mathbb{E}^\alpha\left[e^{\mathrm{i}\,(u_1 x_1 + \dots + u_n x_n)}\right] \\ &= \Psi^\alpha(\mathrm{i}u_1\beta_1, \dots, \mathrm{i}u_n\beta_n; \overline{X}_{T_0}, T_0, T_1, \dots, T_n),\end{aligned}$$

where the moment generating function can be computed as follows $\forall j \geq 1$:

$$\begin{aligned}\Psi^\alpha(\beta_1, \dots, \beta_j; \overline{X}_{T_0}, T_0, T_1, \dots, T_j) &:= \mathbb{E}^\alpha[e^{\beta_1 \cdot X_{T_1} + \dots + \beta_j \cdot X_{T_j}} \,|\, \overline{X}_{T_0}] \\ &= \frac{1}{\Psi(\alpha; \overline{X}_{T_0}, T_0, T_j)} \mathbb{E}[e^{\beta_1 \cdot X_{T_1} + \dots + (\beta_j + \alpha) \cdot X_{T_j}} \,|\, \overline{X}_{T_0}] \\ &= \frac{\Psi(\beta_1, \dots, \beta_{j-1}, \beta_j + \alpha; \overline{X}_{T_0}, T_0, T_1, \dots, T_j)}{\Psi(\alpha; \overline{X}_{T_0}, T_0, T_j)}.\end{aligned}$$

For any set of N-dimensional vectors $\beta_j\ j = 1, \dots, n$, we have

$$\begin{aligned}\Psi(\beta_1, \dots, \beta_j; \overline{X}_{T_0}, T_0, T_1, \dots, T_j) &:= \mathbb{E}[e^{\beta_1 \cdot X_{T_1} + \dots + \beta_j \cdot X_{T_j}} \,|\, \overline{X}_{T_0}] \\ &= \mathbb{E}\left[e^{\beta_1 \cdot X_{T_1} + \dots + \beta_{j-1} \cdot X_{T_{j-1}}} \mathbb{E}[e^{\beta_j \cdot X_{T_j}} \,|\, X_{T_{j-1}}] \,|\, \overline{X}_{T_0}\right] \\ &= \mathbb{E}\left[e^{\beta_1 \cdot X_{T_1} + \dots + \beta_{j-1} \cdot X_{T_{j-1}}} \Psi(\beta_j; X_{T_{j-1}}, T_{j-1}, T_j) \,|\, \overline{X}_{T_0}\right] \\ &= \mathbb{E}\left[e^{\beta_1 \cdot X_{T_1} + \dots + \beta_{j-1} \cdot X_{T_{j-1}}} e^{b_{\beta_j}(T_{j-1}, T_j) + c_{\beta_j}(T_{j-1}, T_j) \cdot X_{T_{j-1}}} \,|\, \overline{X}_{T_0}\right] \\ &= \Psi(\beta_1, \dots, \beta_{j-2}, \beta_{j-1} + c_{\beta_j}(T_{j-1}, T_j); \overline{X}_{T_0}, T_0, T_1, \dots, T_{j-1}) e^{b_{\beta_j}(T_{j-1}, T_j)}.\end{aligned}$$

We thus obtain an explicit recursive solution for the relevant multivariate characteristic function in terms of the two deterministic functions $b_\beta(t, T)$ and $c_\beta(t, T)$ in (12). □

A.3 Proof of Theorem 2

Proof. To prove the first result:

$$\begin{aligned}\Psi(\beta; x_t^i, t, T) &:= \mathbb{E}[e^{\beta \cdot x_T^i} \mid x_t^i] \\ &= \mathbb{E}[e^{\beta_1 a_T + \beta_2 \omega_T + \beta_3 m_T^i} \mid x_t^i] \\ &= \mathbb{E}[e^{\beta_3 m_T^i} \mid m_t^i]\, \mathbb{E}[e^{\beta_1 a_T + \beta_2 \omega_T} \mid x_t] \\ &= e^{\beta_3 m_t^i + \zeta(\beta_3)(T-t) + \beta_1 a_t + B(T-t;\beta_1,\beta_2) + C(T-t;\beta_1,\beta_2)\omega_t},\end{aligned}$$

where we use the fact that m_t^i is independent of a_t, ω_t and Lemmas 1 and 2 below.

To prove the second result, we proceed similarly:

$$\begin{aligned}\Psi(\beta; x_t, t, T) &:= \mathbb{E}[e^{\beta \cdot x_T^i} \mid x_t] \\ &= \mathbb{E}[e^{\beta_1 a_T + \beta_2 \omega_T + \beta_3 m_T^i} \mid x_t] \\ &= \mathbb{E}[e^{\beta_3 m_T^i}]\mathbb{E}[e^{\beta_1 a_T + \beta_2 \omega_T} \mid x_t] \\ &= e^{\zeta(\beta_3)T + \beta_1 a_t + B(T-t;\beta_1,\beta_2) + C(T-t;\beta_1,\beta_2)\omega_t}.\end{aligned}$$

□

Lemma 1.

$$\mathbb{E}[e^{\beta_3 m_T^i} \mid m_t^i] = e^{\beta_3 m_t^i + \zeta(\beta_3)(T-t)},$$

where

$$\zeta(\beta_3) = -\frac{1}{2}{\sigma_i}^2 \beta_3(1-\beta_3) - \lambda_i(\beta_3 \nu_i - \nu^i(\beta_3)) \tag{17}$$

and (for some scalar β):

$$\nu^i(\beta) = \mathbb{E}[e^{\gamma_i \beta} - 1] = e^{m_i \beta + \frac{1}{2} v_i \beta^2} - 1.$$

Proof. Follows from the definition of m_t^i in Equation (16). □

Lemma 2.

$$\mathbb{E}[e^{\beta_1 a_T + \beta_2 \omega_T} \mid x_t] = e^{\beta_1 a_t + B(T-t;\beta_1,\beta_2) + C(T-t;\beta_1,\beta_2)\omega_t},$$

where $B(T-t;\beta_1,\beta_2)$ and $C(T-t;\beta_1,\beta_2)$ are deterministic functions given below.

Proof. Using the law of iterated expectation, we seek a candidate solution $M_t = e^{\beta_1 a_t + B(T-t) + C(T-t)\omega_t}$ that is a martingale; i.e., such that $E_t[\frac{dM_t}{M_{t^-}}] = 0$. This implies

$$\begin{aligned} 0 = &- \dot{B} - \dot{C}\,\omega_t + \beta_1(r - \delta - \frac{1}{2}\omega_t) - \beta_1(\lambda_0 + \lambda_\omega \omega_t)\nu + C\kappa(\bar{\omega} - \omega_t) \\ &+ \frac{1}{2}\beta_1^2 \omega_t + \frac{1}{2} C^2 \sigma_\omega^2 \omega_t + \beta_1 C \rho_\omega \sigma_\omega \omega_t + (\lambda_0 + \lambda_\omega \omega_t)\nu(\beta_1), \end{aligned}$$

where (for some scalar β):

$$\nu(\beta) = \mathbb{E}[e^{\gamma \beta} - 1] = e^{m\beta + \frac{1}{2} v \beta^2} - 1.$$

This implies the following system of ordinary differential equations:

$$\begin{aligned} \dot{B} &= \beta_1(r - \delta) + \lambda_0(\nu(\beta_1) - \beta_1 \nu) + \kappa \bar{\omega} C \\ \dot{C} &= P - QC + \frac{1}{2}\sigma_\omega^2 C^2, \end{aligned}$$

where

$$P = \frac{1}{2}\beta_1(\beta_1 - 1) + \lambda_\omega(\nu(\beta_1) - \beta_1\nu)$$
$$Q = \kappa - \beta_1\rho_\omega\sigma_\omega,$$

which must be solved subject to the boundary conditions $B(0) = 0$ and $C(0) = \beta_2$. The solution is given by

$$B(\tau) = \beta_1(r-\delta)\tau + \lambda_0(\nu(\beta_1) - \beta_1\nu)\tau + \frac{\kappa\bar{\omega}}{\sigma_\omega^2}\left((Q-d)\tau - 2\log\left(\frac{1-ce^{-d\tau}}{1-c}\right)\right) \tag{18}$$

$$C(\tau) = \frac{(Q-d) - (Q+d)ce^{-d\tau}}{\sigma_\omega^2(1-ce^{-d\tau})}, \tag{19}$$

where

$$d = \sqrt{Q^2 - 2P\sigma_\omega^2}$$
$$c = \frac{Q - d - \beta_2\sigma_\omega^2}{Q + d - \beta_2\sigma_\omega^2}.$$

□

References

Ammann, Manuel, and Mathis Moerke, 2019, Credit variance risk premiums, Working paper, University of St.Gallen.

Andrade, Gregor, and Steven N. Kaplan, 1998, How costly is financial (not economic) distress? Evidence from highly leveraged transactions that became distressed, *Journal of Finance* 53, 1443–1494.

Bai, Jennie, Turan G. Bali, and Quan Wen, 2019a, Common risk factors in the cross-section of corporate bond returns, *Journal of Financial Economics* 131, 619–642.

Bai, Jennie, Robert S. Goldstein, and Fan Yang, 2019b, The leverage effect and the basket-index put spread, *Journal of Financial Economics* 131, 186–205.

Bao, Jack, and Jun Pan, 2013, Bond illiquidity and excess volatility, *Review of Financial Studies* 26, 3068–3103.

Becker, Lucas, 2014, CVA hedge losses prompt focus on swaptions and guarantees, *Risk Magazine* .

Black, Fischer, and John C. Cox, 1976, Valuing corporate securities: Some effects of bond indentures provisions, *Journal of Finance* 31, 351–367.

Broadie, Mark, Mikhail Chernov, and Michael Johannes, 2007, Model specification and risk premia: Evidence from futures options, *Journal of Finance* 62, 1453–1490.

Carr, Peter, and Liuren Wu, 2010, Stock options and credit default swaps: A joint framework for valuation and estimation, *Journal of Financial Econometrics* 8, 409–449.

Chen, Long, Pierre Collin-Dufresne, and Robert S. Goldstein, 2009, On the relation between the credit spread puzzle and the equity premium puzzle, *Review of Financial Studies* 22, 3367–3409.

Chen, Steven Shu-Hsi, Hitesh Doshi, and Sang Byung Seo, 2020, Ex ante risk in the corporate bond market: Evidence from synthetic options, Working paper, University of Houston.

Chen, Zhiwu, and Peter J. Knez, 1995, Measurement of market integration and arbitrage, *The Review of Financial Studies* 8, 287–325.

Choi, Jaewon, and Yongjun Kim, 2018, Anomalies and market (dis)integration, *Journal of Monetary Economics* 100, 16–34.

Chordia, Tarun, Amit Goyal, Yoshio Nozawa, Avanidhar Subrahmanyam, and Qing Tong, 2017, Are capital market anomalies common to equity and corporate bond markets? an empirical investigation, *Journal of Financial and Quantitative Analysis* 52, 1301–1342.

Collin-Dufresne, Pierre, Robert S. Goldstein, and J. Spencer Martin, 2001, The determinants of credit spread changes, *Journal of Finance* 56, 2177–2207.

Collin-Dufresne, Pierre, Robert S. Goldstein, and Fan Yang, 2012, On the relative pricing of long-maturity index options and collateralized debt obligations, *Journal of Finance* 67, 1983–2014.

Collin-Dufresne, Pierre, Benjamin Junge, and Anders B. Trolle, 2020, Market structure and transaction costs of index CDSs, *Journal of Finance* 75, 2719–2763.

Coval, Joshua, Jakub Jurek, and Erik Stafford, 2009, Economic catastrophe bonds, *American Economic Review* 99, 628–666.

Cremers, Martijn, Joost Driessen, and Pascal Maenhout, 2008, Explaining the level of credit spreads: Option-implied jump risk premia in a firm value model, *Review of Financial Studies* 21, 2209–2242.

Culp, Christopher L., Yoshio Nozawa, and Pietro Veronesi, 2018, Option-based credit spreads, *American Economic Review* 108, 454–488.

Davydenko, Sergei A., Ilya A. Strebulaev, and Xiaofei Zhao, 2012, A market-based study of the cost of default, *Review of Financial Studies* 25, 2959–2999.

Doshi, Hitesh, Jan Ericsson, Mathieu Fournier, and Sang Byung Seo, 2021, Asset variance risk and compound option prices, Working paper, McGill University.

Du, Du, Redouane Elkamhi, and Jan Ericsson, 2019, Time-varying asset volatility and the credit spread puzzle, *Journal of Finance* 74, 1841–1885.

Duarte, Jefferson, Francis A. Longstaff, and Fan Yu, 2007, Risk and return in fixed-income arbitrage: Nickels in front of a steamroller?, *Review of Financial Studies* 20, 769–811.

Duffie, Darrell, Damir Filipović, and Walter Schachermayer, 2003, Affine processes and applications in finance, *Annals of Applied Probability* 13, 984–1053.

Duffie, Darrell, Jun Pan, and Kenneth J. Singleton, 2000, Transform analysis and asset pricing for affine jump-diffusions, *Econometrica* 68, 1343–1376.

Fama, Eugene F., 1970, Efficient capital markets: A review of theory and empirical work, *Journal of Finance* 25, 383–417.

Foresi, Silverio, and Liuren Wu, 2005, Crash-o-phobia: A domestic fear or a worldwide concern, *Journal of Derivatives* 13, 8–21.

Friewald, Nils, and Florian Nagler, 2019, Over-the-counter market frictions and yield spread changes, *Journal of Finance* 74, 3217–3257.

Gârleanu, Nicolae, Lasse H. Pedersen, and Allen M. Poteshman, 2009, Demand-based option pricing, *Review of Financial Studies* 22, 4259–4299.

Geske, Robert, 1977, The valuation of corporate liabilities as compound options, *Journal of Financial and Quantitative Analysis* 12, 541–552.

Gil-Pelaez, J., 1951, Note on the inversion theorem, *Biometrika* 38, 481–482.

He, Zhiguo, Paymon Khorrami, and Zhaogang Song, 2020, Commonality in credit spread changes: Dealer inventory and intermediary distress, Working paper, University of Chicago.

Huang, Jing-Zhi, and Ming Huang, 2012, How much of the corporate-treasury yield spread is due to credit risk?, *Review of Asset Pricing Studies* 2, 153–202.

Jones, Philip E., Scott P. Mason, and Eric Rosenfeld, 1984, Contingent claims analysis of corporate capital structures: An empirical investigation, *Journal of Finance* 39, 611–25.

Kapadia, Nikunj, and Xiaoling Pu, 2012, Limited arbitrage between equity and credit markets, *Journal of Financial Economics* 105, 542–564.

Leland, Hayne E., 1994, Optimal capital structure, endogenous bankruptcy, and the term structure of credit spreads, *Journal of Finance* 49, 1213–1252.

Merton, Robert C., 1974, On the pricing of corporate debt: The risk structure of interest rates, *Journal of Finance* 29, 449–470.

Newey, Whitney K., and Kenneth D. West, 1987, A simple, positive semi-definite, heteroskedasticity and autocorrelation consistent covariance matrix, *Econometrica* 55, 703–708.

Sandulescu, Mirela, 2020, How integrated are corporate bond and stock markets? Working paper, University of Michigan.

Schaefer, Stephen M., and Ilya A. Strebulaev, 2008, Structural models of credit risk are useful: Evidence from hedge ratios on corporate bonds, *Journal of Financial Economics* 90, 1–19.

Seo, Sang Byung, and Jessica Wachter, 2018, Do rare events explain CDX tranche spreads?, *Journal of Finance* 73, 2343–2383.

Shephard, Neil, 1991, From characteristic function to distribution function: a simple framework for the theory, *Econometric Theory* 7, 519–529.

Vasicek, Oldrich, 1987, Probability of loss on a loan portfolio, KMV Corporation.

	CDX	CDX options
Trades per day	202	18
Median trade size (in million USD)	50	100
Capped trade size (% of trades)	22.3	66.5
Average daily volume (in million USD)	11,133	1,442
Five-year tenor (% of trades)	96.1	98.1
On-the-run series (% of trades)	88.9	94.0
On-SEF execution (% of trades)	83.9	3.8
Cleared (% of trades)	90.4	17.6
Payer (% of trades)	—	63.1

Table 1: Descriptive statistics for CDX and CDX option trades

The table shows descriptive statistics for CDX and CDX option trades. Tenor is the initial time to expiration of the CDX contract (the underlying CDX contract in case of CDX options). The on-the-run series is the most recently launched CDX contract. Typically, reported trade sizes are capped when the notional amount traded exceeds USD 100 million or USD 110 million. The sample period is December 31, 2012 to April 30, 2020. The sample comprises 371,693 CDX trades and 32,669 CDX option trades.

	Days to expiration						
Moneyness	< 15	15–44	45–74	75–104	105–134	≥ 135	Total
$m < -1.5$	0.20	0.24	0.06	0.01	0.00	0.00	0.52
$-1.5 \leq m < -0.5$	0.94	3.99	2.94	1.62	0.54	0.39	10.42
$\lvert m \rvert \leq 0.5$	2.12	15.28	9.61	6.48	2.27	1.28	37.03
$0.5 < m \leq 1.5$	1.53	9.01	10.34	8.75	4.17	2.30	36.10
$m > 1.5$	1.42	5.96	4.45	2.65	0.97	0.47	15.92
Total	6.21	34.47	27.40	19.51	7.95	4.45	

Table 2: Distribution of trading volume across the volatility surface

The table shows the percentage of CDX option volume across the volatility surface. Moneyness is defined as $m = \log(K/F(\tau))/(\sigma\sqrt{\tau})$, where K is the strike, $F(\tau)$ is the front-end-protected τ-forward spread, σ is at-the-money implied volatility, $\tau = d/365$ is time to expiration, and d is days to expiration. The underlying of all options is the five-year on-the-run index. The sample period is December 31, 2012 to April 30, 2020. The sample comprises 28,409 CDX option trades.

Panel A: Full sample

	Data					Model				
	ΔI^{CDX}	$\Delta\beta_0^{CDX}$	$\Delta\beta_1^{CDX}$	ΔI^{SPX}	$\Delta\beta_0^{SPX}$	ΔI^{CDX}	$\Delta\beta_0^{CDX}$	$\Delta\beta_1^{CDX}$	ΔI^{SPX}	$\Delta\beta_0^{SPX}$
$\Delta\beta_0^{CDX}$	0.62					0.49				
$\Delta\beta_1^{CDX}$	0.20	0.39				0.11	0.22			
ΔI^{SPX}	-0.80	-0.65	-0.23			-0.80	-0.60	-0.11		
$\Delta\beta_0^{SPX}$	0.67	0.69	0.22	-0.86		0.68	0.83	0.12	-0.85	
$\Delta\beta_1^{SPX}$	-0.65	-0.58	-0.33	0.74	-0.80	-0.68	-0.68	-0.25	0.70	-0.74

Panel B: Ex-COVID-19 sample

	Data					Model				
	ΔI^{CDX}	$\Delta\beta_0^{CDX}$	$\Delta\beta_1^{CDX}$	ΔI^{SPX}	$\Delta\beta_0^{SPX}$	ΔI^{CDX}	$\Delta\beta_0^{CDX}$	$\Delta\beta_1^{CDX}$	ΔI^{SPX}	$\Delta\beta_0^{SPX}$
$\Delta\beta_0^{CDX}$	0.56					0.40				
$\Delta\beta_1^{CDX}$	0.22	0.53				0.15	0.33			
ΔI^{SPX}	-0.79	-0.56	-0.28			-0.79	-0.62	-0.17		
$\Delta\beta_0^{SPX}$	0.67	0.62	0.31	-0.83		0.63	0.86	0.20	-0.81	
$\Delta\beta_1^{SPX}$	-0.55	-0.49	-0.33	0.62	-0.69	-0.56	-0.55	-0.30	0.68	-0.69

Table 3: Correlations within and across markets

The table reports correlations between weekly changes in the log CDX spread (ΔI^{CDX}), CDX volatility ($\Delta\beta_0^{CDX}$), CDX skewness ($\Delta\beta_1^{CDX}$), log SPX index (ΔI^{SPX}; i.e., the log SPX return), SPX volatility ($\Delta\beta_0^{SPX}$), and SPX skewness ($\Delta\beta_1^{SPX}$). The correlation matrices to the left ("Data") are computed from the data, and those to the right ("Model") are computed from the fitted data using the model calibrated to SPX options. The shading of each cell is proportional to the absolute value of the correlation. The full sample period is February 29, 2012 to April 29, 2020 (427 weekly observations). The ex-COVID-19 sample period is February 29, 2012 to December 31, 2019 (410 weekly observations).

	ω_t	κ	$\bar{\omega}$	λ_0	λ_ω	m	$\sqrt{v}$	A_t	σ_i	λ_i	ℓ_1	ℓ_2	δ
Panel A: Calibration to SPX options													
Mean	0.0101	1.074	0.0310	0.000	8.33	-0.171	0.160	2905.8	0.284	0.001	0.034	0.227	0.015
St. dev.	0.0065	0.831	0.0126	0.000	5.32	0.052	0.030	689.5	0.039	0.001	0.003	0.014	0.003
Panel B: Calibration to CDX options													
Mean	0.0185	1.751	0.0247	0.021	63.96	-0.045	0.167	2905.8	0.212	0.001	0.034	0.227	0.015
St. dev.	0.0179	0.914	0.0089	0.129	39.33	0.038	0.027	689.6	0.073	0.001	0.003	0.014	0.003

Table 4: Parameter estimates

The table reports the sample mean and sample standard deviation of the calibrated parameters. Note that it reports values of $\ell_1 = \frac{D_1}{A_t}$ and $\ell_2 = \frac{D_2}{A_t}$ instead of D_1 and D_2. A number of model parameters are fixed in advance: $m_i = -5$, $v_i = 0$, $\alpha = 0.8$, $\sigma_\omega = 0.20$ and $\rho_\omega = -0.70$. The sample period is February 29, 2012 to April 29, 2020 (427 weekly observations).

	SPX options		CDX options	
Calibrated to	ME	RMSE	ME	RMSE
Panel A: Full sample				
SPX options	-0.003	0.085	-0.283	0.296
	(-0.66)		(-12.47)	
CDX options	0.493	0.590	-0.003	0.033
	(16.74)		(-1.56)	
Panel B: Ex-COVID-19 sample				
SPX options	-0.002	0.085	-0.289	0.301
	(-0.48)		(-13.01)	
CDX options	0.500	0.596	-0.003	0.031
	(17.04)		(-1.69)	

Table 5: Pricing errors

On each observation date, we compute the mean pricing error (ME) and root mean squared pricing error (RMSE) for SPX options and CDX options, where pricing errors are given as the relative difference between fitted and actual implied volatilities. The table reports sample means of the resulting ME and RMSE time series. In parenthesis are t-statistics corrected for heteroscedasticity and serial correlation up to 52 lags using the approach of Newey and West (1987). The full sample period is February 29, 2012 to April 29, 2020 (427 weekly observations). The ex-COVID-19 sample period is February 29, 2012 to December 31, 2019 (410 weekly observations).

	CDX options				SPX options				CDX vs. SPX options			
	M1	M2	M3	EW	M1	M2	M3	EW	M1	M2	M3	EW
Panel A: Full sample												
Mean	0.122	0.154	0.189	0.155	0.052	0.073	0.069	0.064	0.035	0.041	0.060	0.045
t-stat	3.125	3.842	4.742	4.208	1.514	2.052	1.919	1.880	1.865	2.153	3.167	2.623
Std.dev.	0.100	0.100	0.100	0.089	0.100	0.100	0.100	0.098	0.057	0.057	0.057	0.052
SR	1.217	1.539	1.888	1.744	0.515	0.726	0.692	0.659	0.613	0.710	1.051	0.877
Skewness	-2.051	-2.378	-1.493	-2.219	-2.497	-2.277	-2.101	-2.285	-0.236	0.069	0.205	0.142
Kurtosis	14.167	19.322	19.149	17.586	17.593	16.775	15.177	16.125	9.008	10.395	12.045	9.772
Panel B: Ex-COVID-19 sample												
Mean	0.157	0.206	0.238	0.200	0.081	0.119	0.125	0.108	0.038	0.043	0.057	0.046
t-stat	4.105	5.344	6.276	5.757	2.418	3.481	3.635	3.269	1.932	2.163	2.815	2.539
Std.dev.	0.100	0.100	0.100	0.087	0.100	0.100	0.100	0.098	0.059	0.059	0.059	0.053
SR	1.568	2.055	2.383	2.291	0.811	1.187	1.248	1.106	0.647	0.731	0.963	0.868
Skewness	-1.802	-1.781	-1.122	-1.717	-2.598	-2.285	-1.980	-2.314	-0.327	0.020	0.175	0.072
Kurtosis	12.718	14.466	19.333	14.476	19.176	18.696	15.770	17.950	9.399	10.810	12.372	10.226

Table 6: Summary statistics of trading strategies

In each market and for each option maturity category, the strategy sells closest-to-ATM straddles each trading day with a holding period of one day. We assume that the strategy requires an initial amount of capital proportional to the option premium, and we adjust the proportionality factor to achieve a 10% unconditional annualized volatility of realized excess returns for each option maturity. "EW" denotes an equally weighted portfolio of the three option maturities. "CDX vs. SPX options" denotes a short-long strategy that allocates 50% of funds to selling CDX straddles and 50% to buying SPX straddles. Means, standard deviations, and Sharpe ratios ("SR") are annualized. t-statistics are corrected for heteroscedasticity and serial correlation up to four lags using the approach of Newey and West (1987). The full sample consists of 1881 daily returns between February 28, 2012 and April 30, 2020. The ex-COVID-19 sample consists of 1801 daily returns between February 28, 2012 and December 31, 2019.

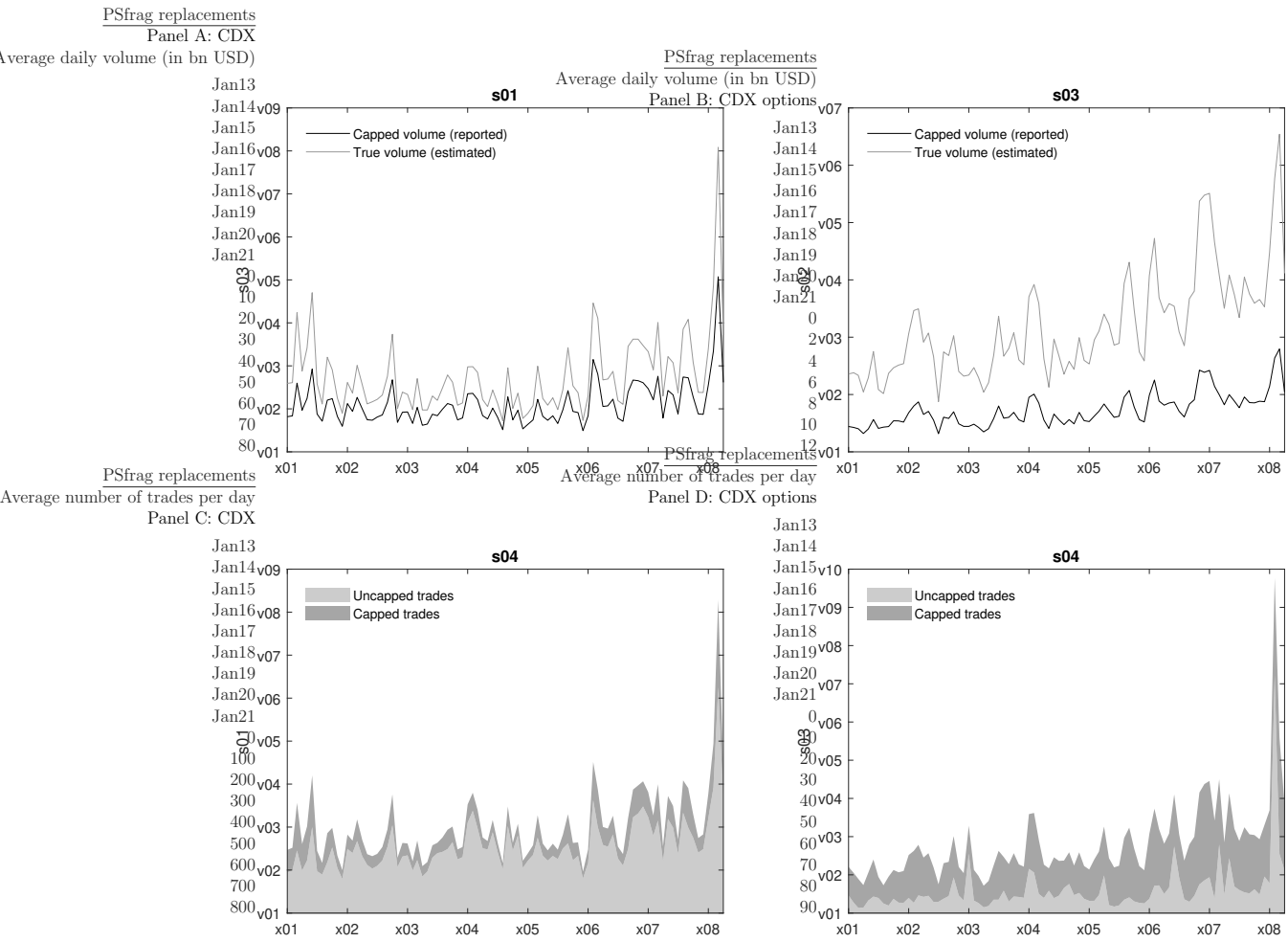

Figure 1: Trading activity for CDX and CDX options

Panels A and B show the average daily trading volume for CDX and CDX options. Panels C and D show the average number of trades per day for CDX and CDX options. Daily market activity reports from the GFI SEF are used to compute the average amount by which the actual notionals of capped trades on the GFI SEF exceed the reported notionals. This is done separately for CDX and CDX options (see Footnote 17 for details). The estimated true volume in Panels A and B is obtained by adding the average amount to the reported notionals for all capped trades. The frequency of observations is monthly. The sample period is December 31, 2012 to April 30, 2020 (88 observations).

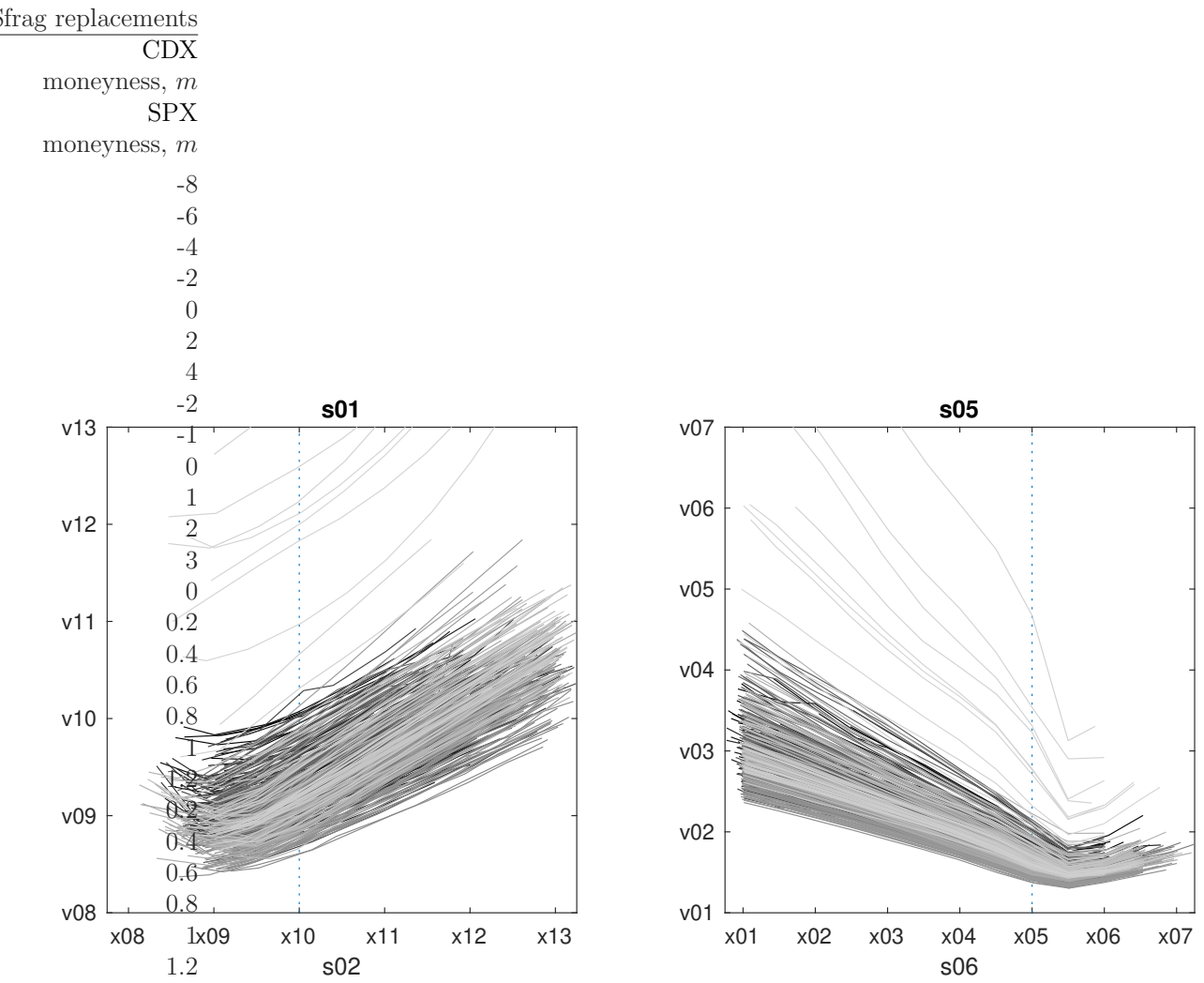

Figure 2: CDX and SPX implied volatility smiles

The figure shows weekly (Wednesday) two-month implied volatility smiles for CDX and SPX. CDX data is displayed in the left panel and SPX data is displayed in the right panel. Moneyness is defined as $m = \log(K/F(\tau))/(\sigma\sqrt{\tau})$, where K is the strike, $F(\tau)$ is the forward (front-end-protected) spread in case of CDX options and the forward price in case of SPX options, σ is the at-the-money implied volatility, and τ is the maturity of the option. The sample period is February 29, 2012 to April 29, 2020 (426 observations).

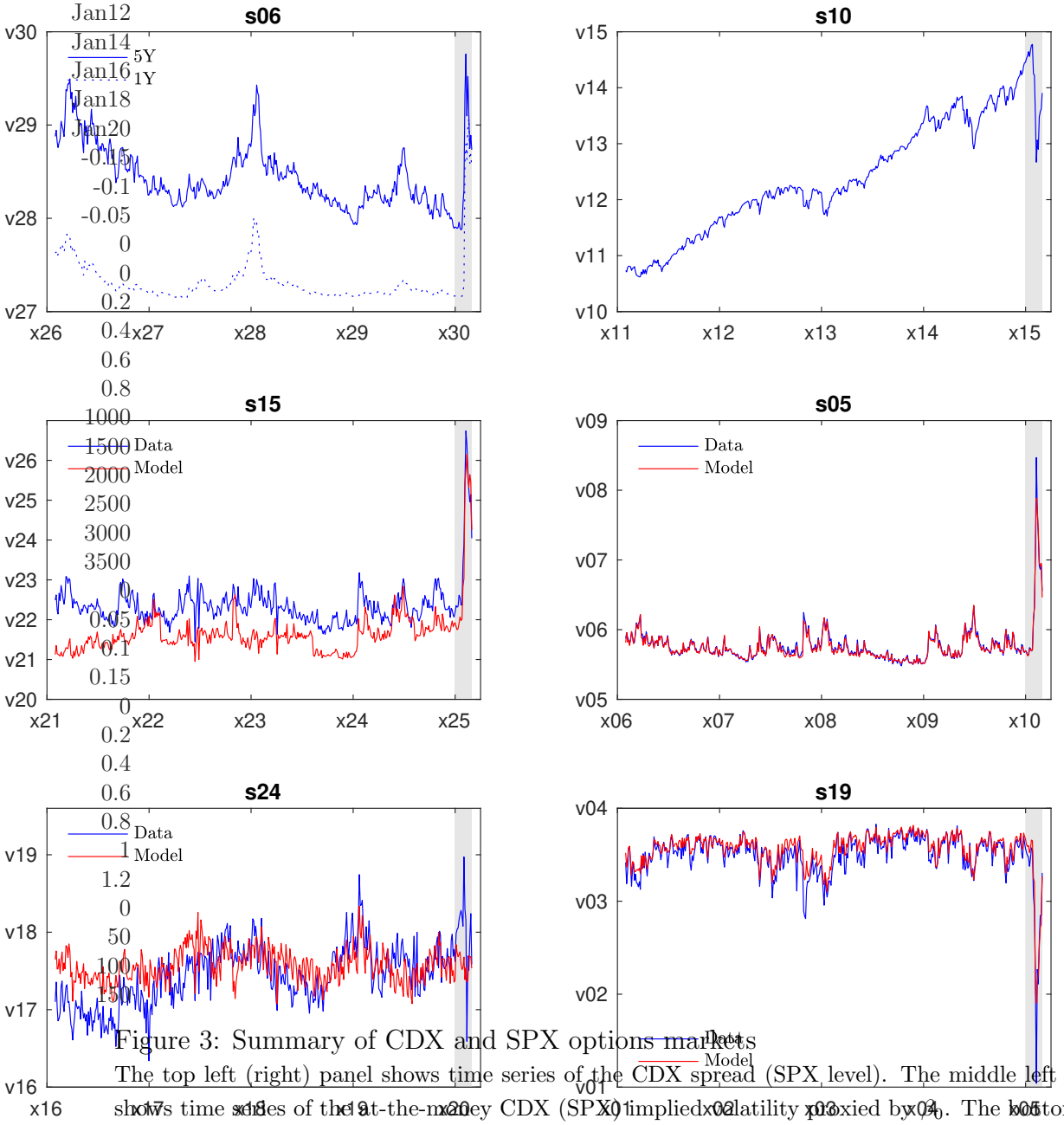

Figure 3: Summary of CDX and SPX options markets

The top left (right) panel shows time series of the CDX spread (SPX level). The middle left (right) panel shows time series of the at-the-money CDX (SPX) implied volatility proxied by β_0. The bottom left (right) panel shows time series of the skewness of the CDX (SPX) implied volatility smile proxied by β_1. Blue lines show the data. Red lines show the fitted data for the model calibrated to SPX options. The sample period is February 29, 2012 to April 29, 2020 (427 weekly observations). The shaded area marks the COVID-19 period starting on January 1, 2020.

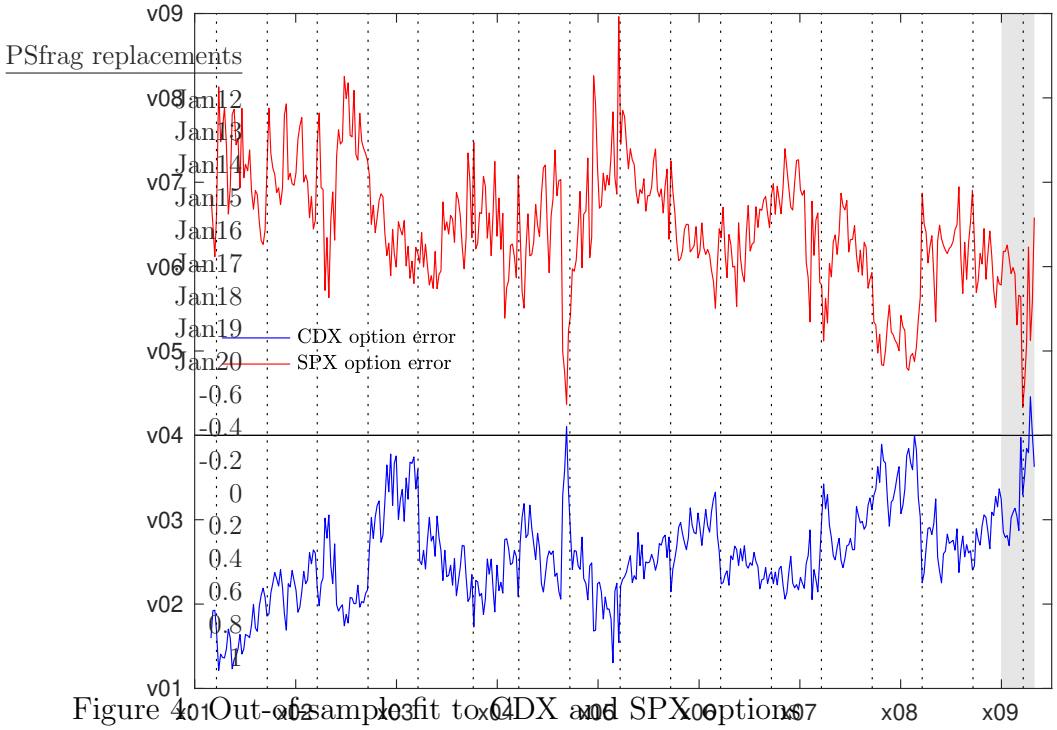

Figure 4: Out-of-sample fit to CDX and SPX options

On each observation date, we compute the mean out-of-sample pricing error (ME); that is, for the model calibrated to SPX options, we compute the pricing error for CDX options (blue line) and for the model calibrated to CDX options, we compute the pricing error for SPX options (red line). Pricing errors are given as the relative difference between fitted and actual implied volatilities. Vertical dotted lines mark CDX roll dates. The sample period is February 29, 2012 to April 29, 2020 (427 weekly observations). The shaded area marks the COVID-19 period starting on January 1, 2020.

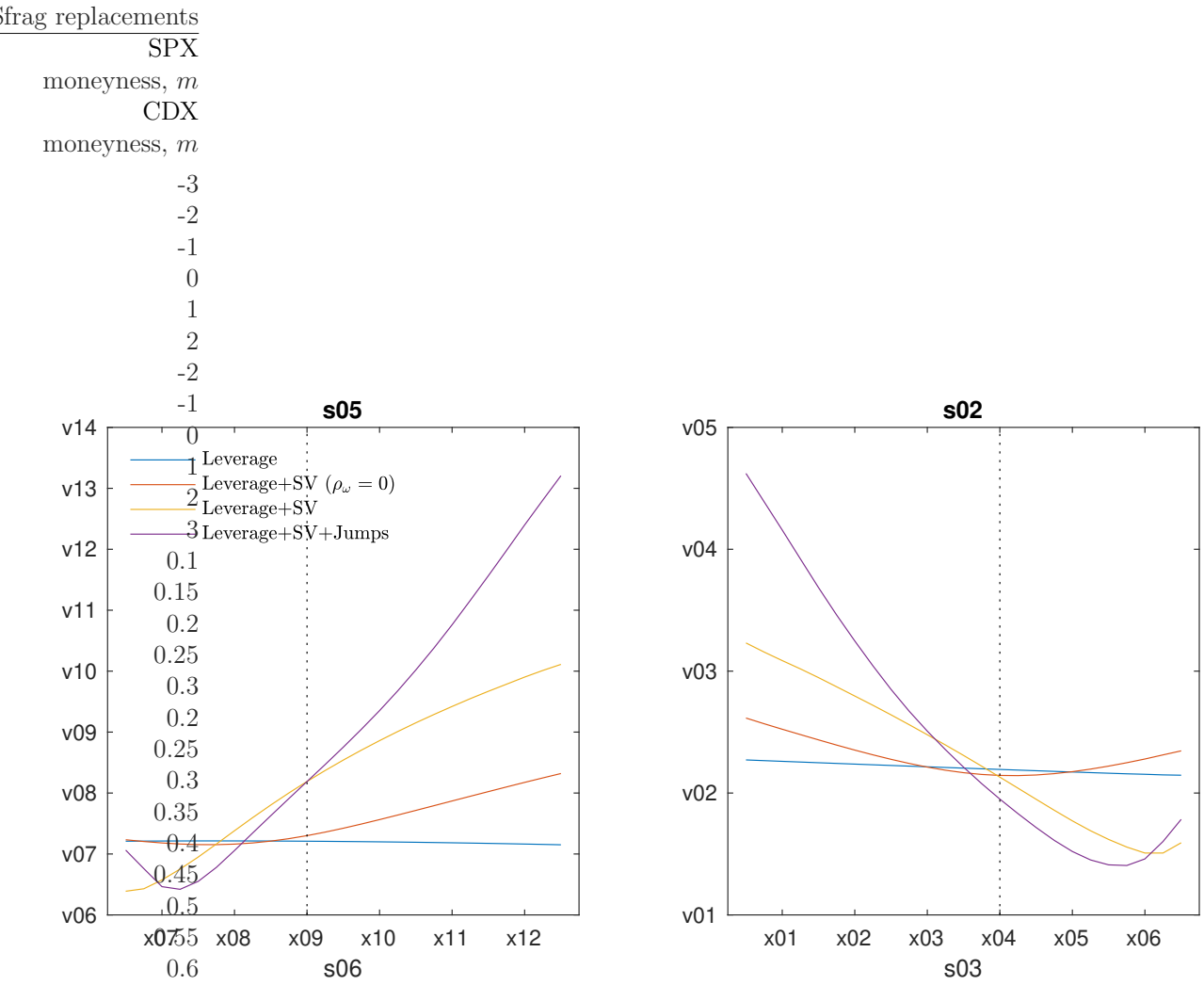

Figure 5: Sources of implied volatility smiles

The figure shows how the financial leverage effect and stochastic volatility (SV) and jumps in the systematic asset factor affect the implied volatility smiles for CDX and SPX options with a two-month maturity. The first model (blue lines) has deterministic systematic asset volatility ($\omega_t = 0.0135, \sigma_\omega = \rho_\omega = \lambda_0 = \lambda_\omega = 0$) and the smiles are only due to the financial leverage effect. The second model (red lines) adds SV, but with zero correlation between asset returns and volatility ($\omega_t = 0.0135, \sigma_\omega = 0.2, \rho_\omega = \lambda_0 = \lambda_\omega = 0$). The third model (yellow lines) adds negative correlation between asset returns and volatility ($\omega_t = 0.0135, \sigma_\omega = 0.2, \rho_\omega = -0.70, \lambda_0 = \lambda_\omega = 0$). The fourth model (purple lines) adds jumps ($\omega_t = 0.0101, \sigma_\omega = 0.2, \rho_\omega = -0.70, \lambda_0 = 0.000, \lambda_\omega = 8.33, m = -0.171, \sqrt{v} = 0.160$). All model specifications have the same instantaneous volatility of the systematic asset factor. For each model, A_t, σ_i, λ_i, ℓ_1, ℓ_2, and δ are calibrated to match the sample means of 1Y and 5Y CDX upfronts, the SPX level, the SPX dividend yield, and the index leverage ratios. The remaining parameters are given in Panel A of Table 4.

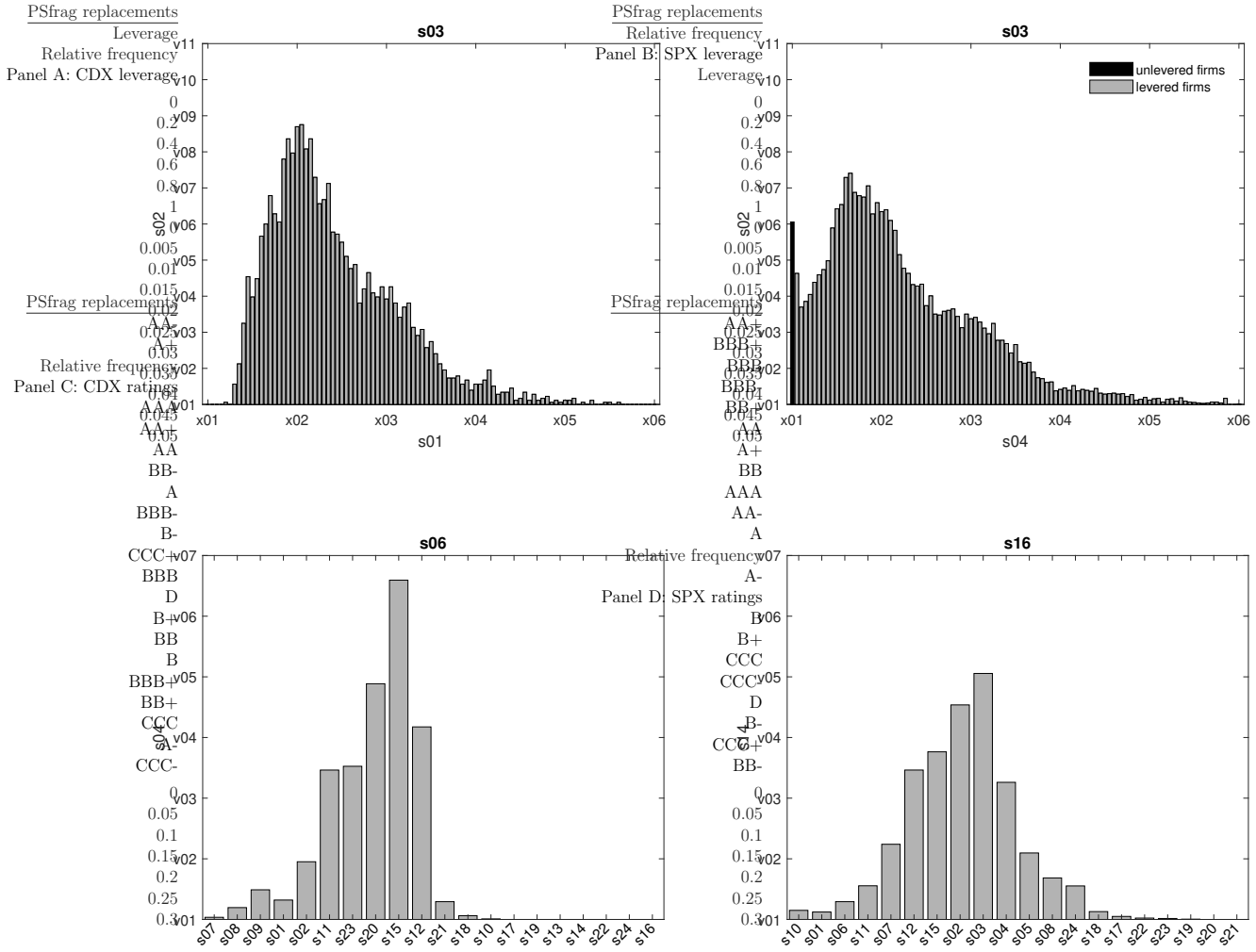

Figure 6: Distributions of leverage and ratings across index constituents

Panels A and B show the distribution of firm-quarter leverage observations for CDX and SPX constituents, respectively, between the first quarter of 2012 and the first quarter of 2020. Leverage is defined as book value of debt over the sum of book value of debt and market value of equity. Panels C and D show the distribution of firm-quarter rating observations for CDX and SPX constituents, respectively, between the first quarter of 2012 and the third quarter of 2017.

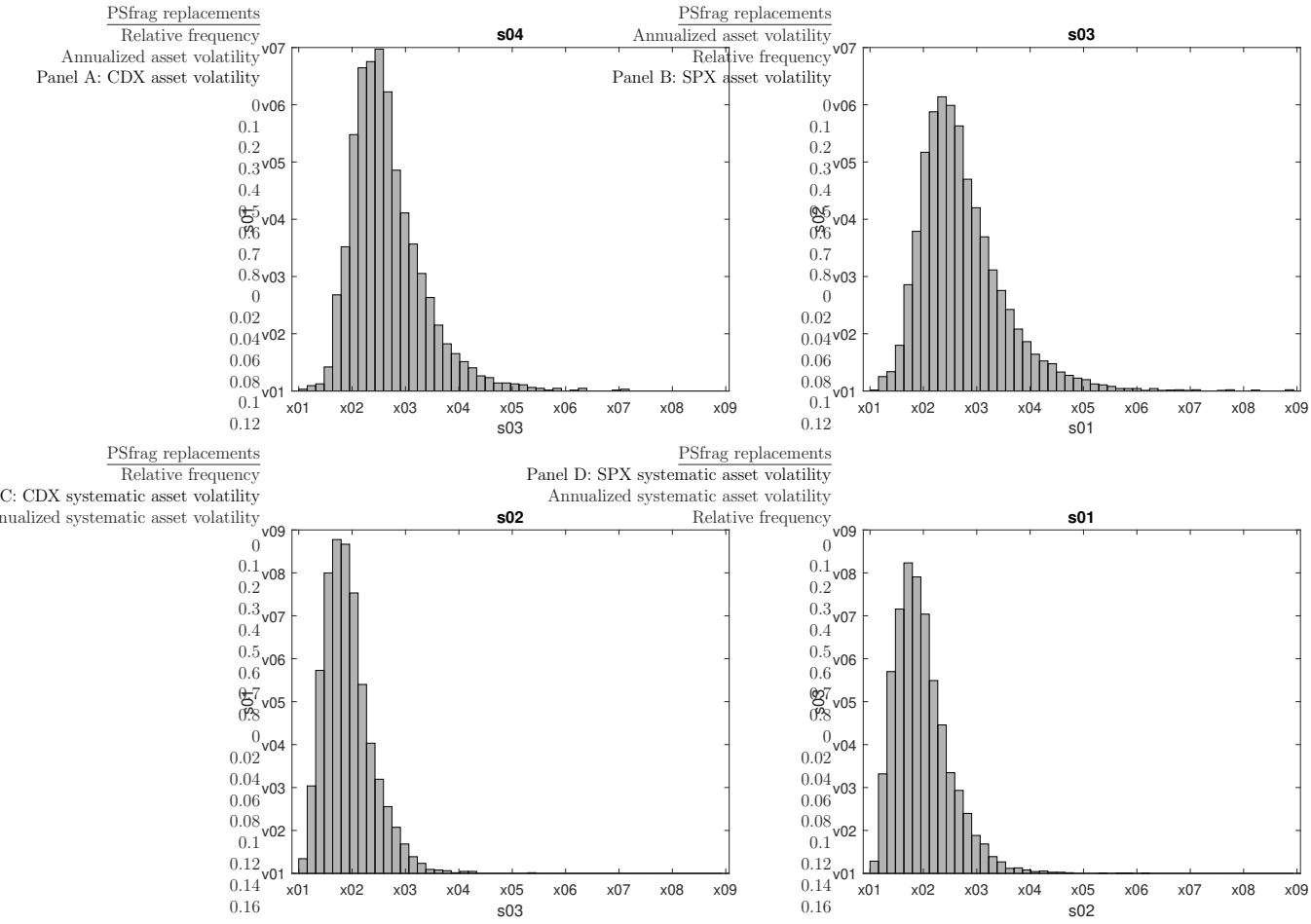

Figure 7: Distributions of asset volatility across index constituents

Panels A and B (C and D) show the distribution of firm-quarter total (systematic) asset return volatility for CDX and SPX constituents, respectively. Asset returns are computed using daily data from January 3, 2012 to December 31, 2019.

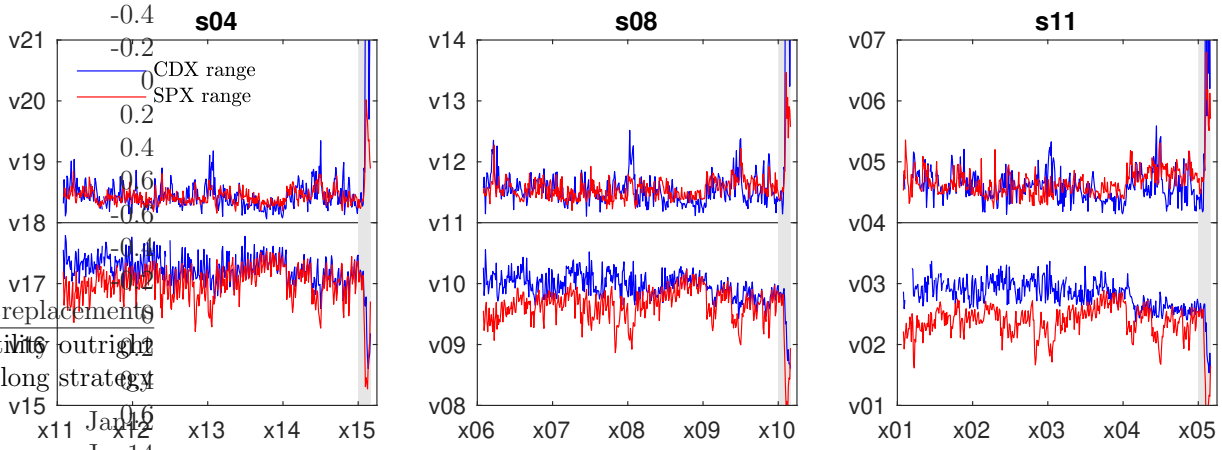

Figure 8: Range of asset values spanned by options

The figure shows $\frac{A^{min}-A^{fwd}}{A^{fwd}}$ and $\frac{A^{max}-A^{fwd}}{A^{fwd}}$ for CDX and SPX options. A^{fwd} is the forward value of the common factor. For CDX options, A^{min} solves $U_{T_0}(\log A^{min}, \omega) = K^{max}$ and A^{max} solves $U_{T_0}(\log A^{max}, \omega) = K^{min}$. For SPX options, A^{min} solves $S_{T_0}(\log A^{min}, \omega) = K^{min}$ and A^{max} solves $S_{T_0}(\log A^{max}, \omega) = K^{max}$. We use the model calibrated to SPX options and always condition on $\omega = \mathbb{E}_0[\omega_{T_0}]$. The sample period is February 29, 2012 to April 29, 2020 (427 weekly observations). The shaded area marks the COVID-19 period starting on January 1, 2020.

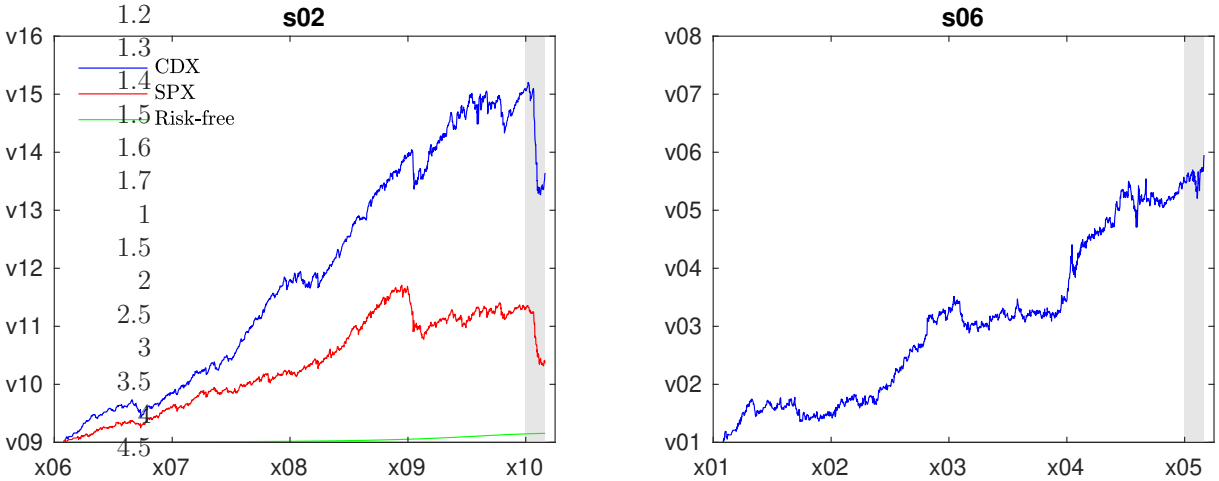

Figure 9: Cumulative performance of trading strategies

The figure shows the evolution of one dollar invested in each of the EW strategies at the beginning of the sample (see Table 6 for details on the trading strategies). The left panel shows the performance of selling CDX and SPX straddles outright. The right panel shows the performance of the short-long strategy that allocates 50% of funds to selling CDX straddles and 50% to buying SPX straddles. On those trading days where options returns are not available, we invest at the risk-free rate. The sample period is from February 24, 2012 to April 30, 2020 (2042 daily observations). The shaded area marks the COVID-19 period starting on January 1, 2020.

Internet Appendix to: How integrated are credit and equity markets? Evidence from index options

IA.1 CDX spreads and implied volatilities

This section explains how to convert upfront amounts to spreads and option prices to spread implied volatilities.

IA.1.1 CDX spread

Consider a CDX contract with $N = 125$ equally-weighted constituents, maturity T, and premium paid continuously at a rate of C. To lighten notation, we assume that the initial notional is one. The fraction of index constituents that have not defaulted at time t (which corresponds to the outstanding notional) is then given by

$$f(t) = \frac{1}{N} \sum_{i=1}^{N} \mathbf{1}_{\{\tau_i > t\}},$$

where τ_i is the default time of firm i. Similarly, the cumulative default losses between index inception and time t is given by

$$L(t) = \frac{1}{N} \sum_{i=1}^{N} \ell_i \mathbf{1}_{\{\tau_i \leq t\}},$$

where ℓ_i is the default loss of firm i.

The time-t value of the contract from the perspective of the buyer of protection is

$$V(t,T) = V^{Prot}(t,T) - C \times \mathcal{A}(t,T),$$

where $V^{Prot}(t,T)$ is the value of the protection leg given by

$$V^{Prot}(t,T) = \mathbb{E}_t \left[\int_t^T e^{-\int_t^u r(s)ds} dL(u) \right],$$

and $\mathcal{A}(t,T)$ is the risky annuity value given by

$$\mathcal{A}(t,T) = \mathbb{E}_t \left[\int_t^T e^{-\int_t^u r(s)ds} f(u)du \right].$$

Although CDX contracts are *traded* in terms of an upfront amount and a fixed coupon, they are typically *quoted* in terms of a spread, which is the size of the coupon such that the upfront amount is zero. When converting between upfront amount and spread, the market standard is to assume i) that index constituents are homogenous (i.e., identical in terms of default intensity and default loss), ii) a constant default intensity λ, iii) a loss-given-default of $(1-R)$ with a recovery rate of $R = 40\%$, and iv) that interest rates and defaults are independent.[1] With these assumptions, we have

$$\overline{V}^{Prot}(t,T) = \lambda(1-R)f(t)\int_t^T P(t,u)e^{-\lambda(u-t)}du$$

and

$$\overline{\mathcal{A}}(t,T) = f(t)\int_t^T P(t,u)e^{-\lambda(u-t)}du.$$

For a given $V(t,T)$, λ is first calibrated so that

$$V(t,T) = \overline{V}^{Prot}(t,T) - C \times \overline{\mathcal{A}}(t,T) = (\lambda(1-R) - C)\,\overline{\mathcal{A}}(t,T),$$

and the spread is then given by

$$\overline{Spr}(t,T) = \lambda(1-R).$$

Alternatively, CDX contracts can be quoted in terms of *points upfront* (PUF) which is the

[1] These are the assumptions behind the so-called the ISDA Standard Model. In the following, overlined quantities are calculated under these assumptions.

upfront amount per unit of outstanding notional. In our case, this is given by

$$U(t,T) = \frac{1}{f(t)} V(t,T).$$

IA.1.2 Forward CDX spread

Consider a CDX call option bought at time 0, with option expiry at time T_0, CDX maturity at time T, and strike in PUF terms of K^U. The option payoff is

$$\left(V(T_0,T) + (L(T_0) - L(0)) - f(0)K^U\right)^+.$$

Exercise will cost $f(0)K^U$. In return, the option-holder enters into the version of the CDX contract that prevails at time T_0 (which has a value of $V(T_0,T)$) and receives the realized default losses during the life of the option (which has a value of $L(T_0) - L(0)$). The latter feature is called *front-end protection* (FEP).

Equivalently, we can write the option payoff as

$$\left(V^{FEP}(T_0,T) - f(0)K^U\right)^+, \tag{IA1}$$

where $V^{FEP}(T_0,T)$ is the value of a front-end protected CDX contract for which the protection leg incorporates the default losses between times 0 and T_0.

At time $0 \leq t < T_0$, the value of this *forward-starting* CDX contract is

$$V^{FEP}(t;T_0,T) = V^{Prot,FEP}(t;T_0,T) - C \times \mathcal{A}(t;T_0,T),$$

where

$$V^{Prot,FEP}(t;T_0,T) = \mathbb{E}_t\left[\int_{T_0}^{T} e^{-\int_t^u r(s)ds} dL(u)\right] + \mathbb{E}_t\left[e^{-\int_t^{T_0} r(s)ds}(L(T_0) - L(0))\right]$$

and

$$\mathcal{A}(t;T_0,T)=\mathbb{E}_t\left[\int_{T_0}^{T}e^{-\int_t^u r(s)ds}f(u)du\right].$$

To express this value as a spread, we use the same assumptions as above so that

$$\overline{V}^{Prot,FEP}(t;T_0,T)=\lambda(1-R)f(t)\int_{T_0}^{T}P(t,u)e^{-\lambda(u-t)}du+(1-R)P(t,T_0)\left(f(0)-f(t)e^{-\lambda(T_0-t)}\right)$$

and

$$\overline{\mathcal{A}}(t;T_0,T)=f(t)\int_{T_0}^{T}P(t,u)e^{-\lambda(u-t)}du.$$

For a given $V^{FEP}(t;T_0,T)$ (obtained via put-call parity, see Section IA.2), λ is first calibrated so that

$$V^{FEP}(t;T_0,T)=\overline{V}^{Prot,FEP}(t;T_0,T)-C\times\overline{\mathcal{A}}(t;T_0,T),$$

and the front-end protected forward spread is then given by

$$\overline{Spr}^{FEP}(t;T_0,T)=\frac{\overline{V}^{Prot,FEP}(t;T_0,T)}{\overline{\mathcal{A}}(t;T_0,T)}. \tag{IA2}$$

IA.1.3 Spread implied volatilities

For the purpose of expressing option prices as implied volatilities, we write the option payoff (IA1) in spread terms as

$$\left(\left(\overline{Spr}^{FEP}(T_0,T)-C\right)\overline{\mathcal{A}}(T_0,T)-f(0)K^U\right)^+=\left(\overline{Spr}^{FEP}(T_0,T)-K^{Spr}\right)^+\overline{\mathcal{A}}(T_0,T),$$

where

$$K^{Spr}=\frac{f(0)K^U}{\overline{\mathcal{A}}(T_0,T)}+C.$$

is the strike in spread terms. K^{Spr} is itself stochastic and to get a strike known at $0 \leq t < T_0$ we replace $\overline{\mathcal{A}}(T_0, T)$ with its time-t forward value, $\frac{1}{P(t,T_0)}\overline{\mathcal{A}}(t; T_0, T)$, to get

$$K^{Spr} \approx \frac{f(0)K^U P(t, T_0)}{\overline{\mathcal{A}}(t; T_0, T)} + C. \tag{IA3}$$

This is the equation we will use to convert between strikes in upfront terms and spread terms.[2]

The CDX call option price is given by

$$\begin{aligned} C(t; T_0, T, K) &= \mathbb{E}_t \left[e^{-\int_t^{T_0} r(s)ds} \left(\overline{Spr}^{FEP}(T_0, T) - K^{Spr} \right)^+ \overline{\mathcal{A}}(T_0, T) \right] \\ &= \overline{\mathcal{A}}(t; T_0, T) \tilde{\mathbb{E}}_t \left[\left(\overline{Spr}^{FEP}(T_0, T) - K^{Spr} \right)^+ \right], \end{aligned}$$

where $\tilde{\mathbb{E}}_t[\cdot]$ denotes expectation taken with respect to the annuity measure that has $\overline{\mathcal{A}}(t; T_0, T)$ as numeraire.[3] The forward spread (IA2) is a martingale under the annuity measure and—assuming that it follows a driftless geometric Brownian motion—we get a Black (1976)-type option price formula. This allows us to express option prices as log-normal spread implied volatilities.[4]

IA.2 Markit credit option data

This section describes Markit's credit option data and the cleaning and data processing procedures we employ.

[2] Clearly, the conversion is exact for $K^U = 0$.

[3] A technical issue arises if all the index constituents were to default prior to option expiry; see, e.g., Morini and Brigo (2011). However, the risk of this is negligible given realistic spreads and short option maturities.

[4] Pedersen (2003) presents an alternative model that can be used to back out log-normal spread implied volatilities. That model must be solved numerically, but avoids the strike approximation (IA3). As shown by White (2014), the two models generate very similar implied volatilities.

IA.2.1 Data description

As part of its credit option data, Markit records pricing information for European options on the CDX North American Investment Grade (hereafter, CDX) index. Each record uniquely identifies the CDX option contracts it refers to by specifying the underlying CDX contract as well as the strike price and maturity of the options.[5] The underlying CDX contract is identified by the index's series and version numbers and the contract tenor, i.e., the time to maturity with which the contract was initially launched. The option maturity is identified by the month and the year in which the option expires. The option strike is not given directly in terms of the points upfront (PUF) used for settlement, see (IA1). Instead, the strike is given in terms of a spread. At option maturity, this spread is converted to PUF using the ISDA Standard Model along with the prevailing discount curve.[6] Because of interest rate uncertainty, the strike in terms of PUF is, strictly speaking, not known before option expiry. However, interest rate uncertainty is second-order in our context; therefore, at any point in time prior to option expiry, we convert the strike from spread to PUF by assuming that the discount curve at expiry coincides with the prevailing forward curve.

The pricing information consists of bid and offer composite quotes and the corresponding quote mid-points. Quotes are relative to a so-called reference level because CDX options are conventionally traded with "with delta", i.e., together with a delta hedge in the underlying CDX contract. The quoted spread at which the delta hedge will be executed is called the reference level. The amount that will be executed is a percentage of the option's notional amount and specified via a quoted delta.[7] Both the reference level and the delta are con-

[5] Records contain pricing information for payer and receiver options with the same strike price and maturity.

[6] The zero curve used by the ISDA Standard Model is constructed from LIBOR money market rates (for maturities up to one year) and swap rates (for longer maturities). Specifically, it uses 1M, 2M, 3M, 6M, and 1Y USD LIBOR rates (before June 3, 2013 the 9M rate was used as well) and annual USD LIBOR swap rates from the 2Y maturity onwards (with quarterly floating leg payments and semi-annual fixed leg payments). For details, see the interest rate curve specifications on the homepage of the ISDA CDS Standard Model.

[7] The quoted delta actually is the percentage of the option's notional that will be executed for hedging purposes and therefore it is not necessarily equal to the option's delta. In particular, it is positive for both payer and receiver options.

ventionally quoted along with the option's bid and offer prices. The composite quotes are averages over the most recent quotes that market-making credit derivatives dealers contribute for a given reference level prior to 5:30 p.m. New York time. Both the reference level and averages of the quoted payer and receiver deltas are recorded in addition to the composite quotes.

The pricing information also contains the number of dealers who contribute quotes to the calculation of the composite and the number of unique quotes that dealers contributed throughout the trading day. In this context unique means that the quote count does not increase if a dealer repeatedly contributes the same quote for a given reference level.

Markit made some changes to the reporting format of the credit option data since they initially offered the data. Specifically, data coverage expanded to options for which Markit does not observe dealer quotes on a given date and instead uses a proprietary pricing model to determine option prices. These records are flagged as "estimated" in the data and we disregard them entirely. We only use "observed" records that are based on actual dealer quotes and collected in the same way as described above.[8]

IA.2.2 Data cleaning

The raw data comprise 301,673 records for CDX options. We remove 150 duplicate records. Where necessary, we determine the option expiry date as the third Wednesday of the month that corresponds to the expiry-month-expiry-year tuple specified in the raw data, and we remove one record with quote date after the determined expiry date. We also remove three records with negative bid-ask spreads and 73 records with quote dates that do not fall on a

[8]There are minor changes to the reporting format such as expiry dates being recorded instead of the month and year in which the option expires. The records also provide additional information that was not available in the original reporting format such as front-end protected forward prices and spreads. We prefer to determine front-end protected forward spreads ourselves (see next section) to have a consistent set of data throughout. Our data comprises of records in the original reporting format for the period up to and including September 11, 2017. Thereafter, all records are in the new reporting format.

weekday. Finally, we remove 176 records that do not specify the strike price of the options.

IA.2.3 Data processing

The remaining 301,270 records are grouped into 22,296 option strips. Each strip of options is characterized by the underlying CDX contract, the options' expiry date, and the reference level at which the options are quoted on a given day.[9] Formally, on a given day and for a given underlying CDX contract, expiry date, and reference level, a strip comprises of a set of strikes, $\Sigma_C = \{K_{C,1}, K_{C,2}, \ldots, K_{C,m}\}$, at which payer options are quoted and a set of strikes, $\Sigma_P = \{K_{P,1}, K_{P,2}, \ldots, K_{P,n}\}$, at which receiver options are quoted.

To compute the spread implied volatilities of the options in a strip, we need the value of the underlying forward-starting front-end protected CDX contract. This value is not directly observable. However, it can be inferred via put-call parity. Specifically, it is backed out from that part of the strip's strike grid on which both payer and receiver options are quoted, which is denoted by $\Sigma = \Sigma_C \cap \Sigma_P$. If $\Sigma = \emptyset$, there is no strike at which both payer and receiver options are quoted and we discard the option strip, which is the case for three strips. On the other hand, if $\Sigma \neq \emptyset$, there is at least one strike at which payer and receiver options are quoted and we proceed as follows.

Let $C(t; T_0, T, K^U)$ and $P(t; T_0, T, K^U)$ denote the time-t mid-quotes of payer and receiver options, respectively, with expiry at T_0 and PUF strike K^U on the current CDX version. Then, put-call parity asserts that

$$C(t; T_0, T, K^U) - P(t; T_0, T, K^U) = V^{FEP}(t; T_0, T) - D(t, T_0) f(t) K^U,$$

[9] Often, there are several reference levels for the same option expiry. In this case, we take that reference level whose strip length is longest (i.e., the one with the largest number of strikes). Should that not result in a unique match then we consider the number of quotes (we select the reference level with the largest number of quotes), the number of quoting dealers (again selecting the reference level that is quoted by the largest number of dealers), and the average spread across the options (selecting the reference level that is quoted with the tightest spread).

where $D(t, T_0)$ is the discount factor for date T_0, and $V^{FEP}(t; T_0, T)$ is the time-t value of the T_0-starting front-end protected CDX contract. Therefore, V^{FEP} can be inferred as the constant term in the following linear regression across all strikes in Σ:

$$C(t; T_0, T, K_n^U) - P(t; T_0, T, K_n^U) = \alpha + \beta D(t, T_0) f(t) K_n^U + \epsilon_n, \qquad K_n^U \in \Sigma. \tag{IA4}$$

If $N = |\Sigma| > 1$, we estimate the regression in Equation (IA4) by least-squares and remove 13 strips for which $R^2 < 98.5\%$. For the remaining strips, we re-estimate the regression in Equation (IA4) imposing the restriction $\beta = -1$, in which case the least-square estimate of V^{FEP} is given by

$$\widehat{V}^{FEP} = \frac{1}{N} \sum_{n=1}^{N} \left\{ C(t; T_0, T, K_n^U) - P(t; T_0, T, K_n^U) + D(t, T_0) f(t) K_n^U \right\}.$$

Then, we proceed to compute the corresponding front-end protected forward spread (as described in Section IA.1.2) and the spread implied volatilities for all the options in the strip (as described in Section IA.1.3).

Finally, we drop all records for options on off-the-run index series, leaving us with 282,861 records for 20,794 option strips.

IA.3 Details on option quotes

This section provides more detailed information on the option quotes. Figure IA1 shows time series of the CDX option maturities (in calendar days) that are quoted. The time series are color-coded according to the option expiry grid (recall that options expire on the third Wednesday of each month), so that the blue line at the bottom of the figure shows the first maturity on the expiry grid (i.e., the options that expire on the first third Wednesday following the observation date), the red line above the blue line shows the second maturity

on the expiry grid, etc. The time series are broken whenever there are no option quotes for a given maturity.

Clearly, the range of quoted maturities increases over the sample period. This is consistent with the growing trading volume in CDX options (Figure 1).

The left panels in Figure IA2 show time series of the M1, M2, and M3 CDX option maturities (in calendar days). The right panels in Figure IA2 show time series of the maturity difference (in calendar days) between the M1, M2, and M3 CDX options and the maturity-matched SPX options.

The left (right) panels in Figure IA3 show time series of the range of moneyness spanned by CDX (SPX) options.

The left (right) panels in Figure IA4 show time series of the relative bid-ask spreads of at-the-money (ATM) CDX (SPX) options. Unfortunately, there is a period in 2017 and 2018, when bid and ask prices are missing from the Markit data.

IA.4 Computing expectations in pricing formulas

This section shows how all expectations in the pricing formulas in Section 4 are mapped into the generalized transform (8) so that they can be evaluated via Theorem 1.

Default boundary: The expectations in the expression for $S^i_{T_1}$ in Section 4.4 are given as

$$\mathbb{E}_{T_1}[\mathbf{1}_{\left\{A^i_{T_2}\geq D_2\right\}}] = \mathcal{G}^{\{0,0,0\}}_{\{-1,0,-1\}}(-\log D_2; x^i_{T_1}, T_1, T_2)$$
$$\mathbb{E}_{T_1}[A^i_{T_2}\mathbf{1}_{\left\{A^i_{T_2}<D_2\right\}}] = \mathcal{G}^{\{1,0,1\}}_{\{1,0,1\}}(\log D_2; x^i_{T_1}, T_1, T_2).$$

CDX: The expectations in the expression for U_t in Section 4.5 are given as

$$\mathbb{E}[\mathbf{1}_{\left\{A^i_{T_1}<\Phi(\omega_{T_1})\right\}} \mid x_t] = \mathcal{G}^{\{0,0,0\}}_{\{1,-\phi_1,1\}}(\phi_0; x_t, t, T_1)$$

$$\mathbb{E}[A^i_{T_1}\mathbf{1}_{\left\{A^i_{T_1}<\Phi(\omega_{T_1})\right\}} \mid x_t] = \mathcal{G}^{\{1,0,1\}}_{\{1,-\phi_1,1\}}(\phi_0; x_t, t, T_1)$$

$$\mathbb{E}[\mathbf{1}_{\left\{A^i_{T_1}\geq\Phi(\omega_{T_1}),A^i_{T_2}<D_2\right\}} \mid x_t] = \mathcal{G}^{\{0,0,0\}}_{\{-1,\phi_1,-1\},\{1,0,1\}}(-\phi_0, \log D_2; x_t, t, T_1, T_2)$$

$$\mathbb{E}[A^i_{T_2}\mathbf{1}_{\left\{A^i_{T_1}\geq\Phi(\omega_{T_1}),A^i_{T_2}<D_2\right\}} \mid x_t] = \mathcal{G}^{\{1,0,1\}}_{\{-1,\phi_1,-1\},\{1,0,1\}}(-\phi_0, \log D_2; x_t, t, T_1, T_2)$$

SPX: The expectations in the expression for S_t in Section 4.5 are given as

$$\mathbb{E}[\mathbf{1}_{\left\{A^i_{T_1}\geq\Phi(\omega_{T_1})\right\}} \mid x_t] = \mathcal{G}^{\{0,0,0\}}_{\{-1,\phi_1,-1\}}(-\phi_0; x_t, t, T_1)$$

$$\mathbb{E}[A^i_{T_1}\mathbf{1}_{\left\{A^i_{T_1}<\Phi(\omega_{T_1})\right\}} \mid x_t] = \mathcal{G}^{\{1,0,1\}}_{\{1,-\phi_1,1\}}(\phi_0; x_t, t, T_1)$$

$$\mathbb{E}[\mathbf{1}_{\left\{A^i_{T_1}\geq\Phi(\omega_{T_1}),A^i_{T_2}\geq D_2\right\}} \mid x_t] = \mathcal{G}^{\{0,0,0\}}_{\{-1,\phi_1,-1\},\{-1,0,-1\}}(-\phi_0, -\log D_2; x_t, t, T_1, T_2)$$

$$\mathbb{E}[A^i_{T_2}\mathbf{1}_{\left\{A^i_{T_1}\geq\Phi(\omega_{T_1}),A^i_{T_2}<D_2\right\}} \mid x_t] = \mathcal{G}^{\{1,0,1\}}_{\{-1,\phi_1,-1\},\{1,0,1\}}(-\phi_0, \log D_2; x_t, t, T_1, T_2)$$

CDX option: The expectations in the expression for C_0^{CDX} in Section 4.6 are given as

$$\mathbb{E}_0[\mathbf{1}_{\left\{A_{T_0}<\underline{A}(\omega_{T_0})\right\}}] = \mathcal{G}^{\{0,0,0\}}_{\{1,-\underline{a}_1,0\}}(\underline{a}_0; x_0, 0, T_0)$$

$$\mathbb{E}_0[\mathbf{1}_{\left\{A_{T_0}<\underline{A}(\omega_{T_0}),A^i_{T_1}<\Phi(\omega_{T_1})\right\}}] = \mathcal{G}^{\{0,0,0\}}_{\{1,-\underline{a}_1,0\},\{1,-\phi_1,1\}}(\underline{a}_0, \phi_0; x_0, 0, T_0, T_1)$$

$$\mathbb{E}_0[A^i_{T_1}\mathbf{1}_{\left\{A_{T_0}<\underline{A}(\omega_{T_0}),A^i_{T_1}<\Phi(\omega_{T_1})\right\}}] = \mathcal{G}^{\{1,0,1\}}_{\{1,-\underline{a}_1,0\},\{1,-\phi_1,1\}}(\underline{a}_0, \phi_0; x_0, 0, T_0, T_1)$$

$$\mathbb{E}_0[\mathbf{1}_{\left\{A_{T_0}<\underline{A}(\omega_{T_0}),A^i_{T_1}\geq\Phi(\omega_{T_1}),A^i_{T_2}<D_2\right\}}] = \mathcal{G}^{\{0,0,0\}}_{\{1,-\underline{a}_1,0\},\{-1,\phi_1-1,\},\{1,0,1\}}(\underline{a}_0, -\phi_0, \log D_2; x_0, 0, T_0, T_1, T_2)$$

$$\mathbb{E}_0[A^i_{T_2}\mathbf{1}_{\left\{A_{T_0}<\underline{A}(\omega_{T_0}),A^i_{T_1}\geq\Phi(\omega_{T_1}),A^i_{T_2}<D_2\right\}}] = \mathcal{G}^{\{1,0,1\}}_{\{1,-\underline{a}_1,0\},\{-1,\phi_1,-1\},\{1,0,1\}}(\underline{a}_0, -\phi_0, \log D_2; x_0, 0, T_0, T_1, T_2)$$

SPX option: The expectations in the expression for C_0^{SPX} in Section 4.6 are given as

$$\mathbb{E}_0[\mathbf{1}_{\left\{A_{T_0}\geq\overline{A}(\omega_{T_0})\right\}}] = \mathcal{G}^{\{0,0,0\}}_{\{-1,\overline{a}_1,0\}}(-\overline{a}_0; x_0, 0, T_0)$$

$$\mathbb{E}_0[A_{T_0}\mathbf{1}_{\left\{A_{T_0}\geq\overline{A}(\omega_{T_0})\right\}}] = \mathcal{G}^{\{1,0,0\}}_{\{-1,\overline{a}_1,0\}}(-\overline{a}_0; x_0, 0, T_0)$$

$$\mathbb{E}_0[\mathbf{1}_{\left\{A_{T_0}\geq\overline{A}(\omega_{T_0}),A^i_{T_1}\geq\Phi(\omega_{T_1})\right\}}] = \mathcal{G}^{\{0,0,0\}}_{\{-1,\overline{a}_1,0\},\{-1,\phi_1,-1\}}(-\overline{a}_0, -\phi_0; x_0, 0, T_0, T_1)$$

$$\mathbb{E}_0[A^i_{T_1}\mathbf{1}_{\left\{A_{T_0}\geq\overline{A}(\omega_{T_0}),A^i_{T_1}<\Phi(\omega_{T_1})\right\}}] = \mathcal{G}^{\{1,0,1\}}_{\{-1,\overline{a}_1,0\},\{1,-\phi_1,1\}}(-\overline{a}_0, \phi_0; x_0, 0, T_0, T_1)$$

$$\mathbb{E}_0[\mathbf{1}_{\left\{A_{T_0}\geq\overline{A}(\omega_{T_0}),A^i_{T_1}\geq\Phi(\omega_{T_1}),A^i_{T_2}\geq D_2\right\}}] = \mathcal{G}^{\{0,0,0\}}_{\{-1,\overline{a}_1,0\},\{-1,\phi_1-1,\},\{-1,0,-1\}}(-\overline{a}_0, -\phi_0, -\log D_2; x_0, 0, T_0, T_1, T_2)$$

$$\mathbb{E}_0[A^i_{T_2}\mathbf{1}_{\left\{A_{T_0}\geq\overline{A}(\omega_{T_0}),A^i_{T_1}\geq\Phi(\omega_{T_1}),A^i_{T_2}<D_2\right\}}] = \mathcal{G}^{\{1,0,1\}}_{\{-1,\overline{a}_1,0\},\{-1,\phi_1,-1\},\{1,0,1\}}(-\overline{a}_0, -\phi_0, \log D_2; x_0, 0, T_0, T_1, T_2)$$

CDS: We do not need to evaluate single-name credit default swaps (CDSs) in the empirical analysis; for completeness, we include their valuation here. The expectations in the expression for U^i_t in Section 4.3 are given as

$$\mathbb{E}_t[\mathbf{1}_{\left\{A^i_{T_1}<\Phi(\omega_{T_1})\right\}}] = \mathcal{G}^{\{0,0,0\}}_{\{1,-\phi_1,1\}}(\phi_0; x^i_t, t, T_1)$$

$$\mathbb{E}_t[A^i_{T_1}\mathbf{1}_{\left\{A^i_{T_1}<\Phi(\omega_{T_1})\right\}}] = \mathcal{G}^{\{1,0,1\}}_{\{1,-\phi_1,1\}}(\phi_0; x^i_t, t, T_1)$$

$$\mathbb{E}_t[\mathbf{1}_{\left\{A^i_{T_1}\geq\Phi(\omega_{T_1}),A^i_{T_2}<D_2\right\}}] = \mathcal{G}^{\{0,0,0\}}_{\{-1,\phi_1,-1\},\{1,0,1\}}(-\phi_0, \log D_2; x^i_t, t, T_1, T_2)$$

$$\mathbb{E}_t[A^i_{T_2}\mathbf{1}_{\left\{A^i_{T_1}\geq\Phi(\omega_{T_1}),A^i_{T_2}<D_2\right\}}] = \mathcal{G}^{\{1,0,1\}}_{\{-1,\phi_1,-1\},\{1,0,1\}}(-\phi_0, \log D_2; x^i_t, t, T_1, T_2)$$

IA.5 Default and option exercise boundaries

We have performed extensive analyses that show that the default and option exercise boundaries are accurately approximated by affine functions. This section provides a visual illustration.

We parameterize the model as follows: We set the interest rate to its sample mean of

$r = 0.0111$, and assume $T_0 = \frac{2}{12}$, $T_1 = 1$, and $T_2 = 5$ because the average option maturity is two months and the average maturities of the two points on the CDX term structure that we consider are 1 and 5 years, respectively. We set parameter values for the systematic factors to those reported in Panel A of Table 4, and we re-calibrate A_t, σ_i, λ_i, ℓ_1, ℓ_2, and δ to the sample means of 1Y and 5Y CDX upfronts, the SPX level, the SPX dividend yield, and the index leverage ratios. The resulting parameter values are $A_t = 2904.5$, $\sigma_i = 0.280$, $\lambda_i = 0.002$, $\ell_1 = 0.034$, $\ell_2 = 0.226$, and $\delta = 0.015$.

Using this parameterized model we show that the affine functions in Equations (5), (6), and (7) are very close approximations to the actual boundaries for reasonable ω-values. When implementing the pricing formulas, we always linearize the boundaries around the expected future ω-value.

Default boundary: Figure IA5 shows the equity value at T_1, $S^i_{T_1}$, as a function of $a^i_{T_1}$ and ω_{T_1}. Being a call option on the firm asset value, $S^i_{T_1}$ is increasing in both state variables. The black line shows the default boundary; i.e., the set of $\{a^i_{T_1}, \omega_{T_1}\}$-pairs for which $S^i_{T_1}(a^i, \omega) = D_1$.

Figure IA6 shows the default boundary as a function of variance, $\log \Phi(\omega_{T_1})$. The blue line shows the actual boundary, while the red line shows the affine approximation in Equation (5) obtained by linearizing the $\log \Phi(\omega)$-function around $\omega = \mathbb{E}_0[\omega_{T_1}] = 0.0239$.

CDX option exercise boundary: We consider a two-month ATM call option with a strike equal to the forward CDX upfront, $K = -114.9$ bps (results for out-of-the money (OTM) options and different option maturities are similar and available upon request).

Figure IA7 shows the CDX upfront amount at T_0, U_{T_0}, as a function of a_{T_0} and ω_{T_0}. Being essentially a put option on the firm asset value, U_{T_0} is decreasing in a_{T_0} and increasing in ω_{T_0}. The black line shows the option exercise boundary; i.e., the set of $\{a_{T_0}, \omega_{T_0}\}$-pairs for which $U_{T_0}(a, \omega) = K$.

Figure IA8 shows the exercise boundary as a function of variance, $\underline{a}(\omega_{T_0})$. The blue line shows the actual boundary, while the red line shows the affine approximation in Equation (6) obtained by linearizing the $\underline{a}(\omega)$-function around $\omega = \mathbb{E}_0[\omega_{T_0}] = 0.0135$.

SPX option exercise boundary: We consider a two-month ATM call option with a strike equal to the forward SPX value, $K = 2199.5$ (again, results for OTM options and different option maturities are similar and available upon request).

Figure IA9 shows the SPX value at T_0, S_{T_0}, as a function of a_{T_0} and ω_{T_0}. Being essentially a call option on the firm asset value, S_{T_0} is increasing in both state variables. The black line shows the option exercise boundary; i.e., the set of $\{a_{T_0}, \omega_{T_0}\}$-pairs for which $S_{T_0}(a, \omega) = K$.

Figure IA10 shows the exercise boundary as a function of variance, $\overline{a}(\omega_{T_0})$. The blue line shows the actual boundary, while the red line shows the affine approximation in Equation (7) obtained by linearizing the $\overline{a}(\omega)$-function around $\omega = \mathbb{E}_0[\omega_{T_0}] = 0.0135$.

IA.6 Pricing formulas for the jump-diffusion version of the model

Without stochastic volatility, the asset value process becomes a jump-diffusion. In this case, indexes and index options can be valued using an alternative approach that results in closed-form expressions. This section contains the details of the derivation.

IA.6.1 Valuation of CDX and SPX

From (14) and (15) we have[10]

$$A_{T_0} = A_0 e^{(r-\delta-\lambda\nu)T_0+\gamma N_{T_0}+y}$$

[10]Here and throughout the Internet Appendix γN denotes the sum of N i.i.d. random variables with the same distribution as γ.

$$A^i_{T_1} = A_0 e^{(r-\delta-\lambda_i\nu_i-\lambda\nu)T_1+\gamma N_{T_1}+\gamma_i N^i_{T_1}+y+z} = A_{T_0} e^{(r-\delta-\lambda\nu)(T_1-T_0)-\lambda_i\nu_i T_1+\gamma(N_{T_1}-N_{T_0})+\gamma_i N^i_{T_1}+z} \tag{IA5}$$

$$A^i_{T_2} = A_0 e^{(r-\delta-\lambda_i\nu_i-\lambda\nu)T_2+\gamma N_{T_2}+\gamma_i N^i_{T_2}+y+z+x} = A_{T_0} e^{(r-\delta-\lambda\nu)(T_2-T_0)-\lambda_i\nu_i T_2+\gamma(N_{T_2}-N_{T_0})+\gamma_i N^i_{T_2}+z+x},$$

where y, z, and x are independent normal random variables with mean and variance

$$\begin{aligned}
m_y &= -\frac{1}{2}v_y & v_y &= \rho\sigma^2 T_0 \\
m_z &= -\frac{1}{2}v_z & v_z &= (1-\rho)\sigma^2 T_0 + \sigma^2(T_1-T_0) = \sigma^2(T_1-\rho T_0) \\
m_x &= -\frac{1}{2}v_x & v_x &= \sigma^2(T_2-T_1).
\end{aligned}$$

Because, conditional on the number of jumps, future asset values are log-normally distributed, we obtain the following closed-form solutions to all the expectations (basically variants of the standard Merton (1976) jump-diffusion model formula):

$$\mathbb{E}[\mathbf{1}_{\left\{A^i_{T_1}<\Phi\right\}} \mid A_{T_0}] = \sum_{n_1,j_1=0}^{\infty} \mathcal{P}^{T_1-T_0}_{\lambda}(n_1)\mathcal{P}^{T_1}_{\lambda_i}(j_1)\mathcal{N}\left(-d_1^-\right)$$

$$\mathbb{E}[A^i_{T_1}\mathbf{1}_{\left\{A^i_{T_1}<\Phi\right\}} \mid A_{T_0}] = \sum_{n_1,j_1=0}^{\infty} \mathcal{P}^{T_1-T_0}_{\lambda}(n_1)\mathcal{P}^{T_1}_{\lambda_i}(j_1) A_{T_0} e^{(r-\delta-\lambda\nu)(T_1-T_0)-\lambda_i\nu_i T_1+n_1 m+j_1 m_i+\frac{1}{2}(n_1 v+j_1 v_i)}\mathcal{N}\left(-d_1^+\right)$$

$$\mathbb{E}[\mathbf{1}_{\left\{A^i_{T_1}\geq\Phi, A^i_{T_2}<D_2\right\}} \mid A_{T_0}] = \sum_{n_1,n_2,j_1,j_2=0}^{\infty} \mathcal{P}^{T_1-T_0}_{\lambda}(n_1)\mathcal{P}^{T_2-T_1}_{\lambda}(n_2)\mathcal{P}^{T_1}_{\lambda_i}(j_1)\mathcal{P}^{T_2-T_1}_{\lambda_i}(j_2)\mathcal{N}_2(d_1^-,-d_2^-;-\rho)$$

$$\begin{aligned}
\mathbb{E}[A^i_{T_2}\mathbf{1}_{\left\{A^i_{T_1}\geq\Phi, A^i_{T_2}<D_2\right\}} \mid A_{T_0}] = &\sum_{n_1,n_2,j_1,j_2=0}^{\infty} \mathcal{P}^{T_1-T_0}_{\lambda}(n_1)\mathcal{P}^{T_2-T_1}_{\lambda}(n_2)\mathcal{P}^{T_1}_{\lambda_i}(j_1)\mathcal{P}^{T_2-T_1}_{\lambda_i}(j_2) \\
&A_{T_0} e^{(r-\delta-\lambda\nu)(T_2-T_0)-\lambda_i\nu_i T_2+(n_1+n_2)m+(j_1+j_2)m_i+(n_1+n_2)\frac{v}{2}+(j_1+j_2)\frac{v_i}{2}}\mathcal{N}_2\left(d_1^+,-d_2^+;-\rho\right),
\end{aligned}$$

where $\mathcal{N}_2$ denotes the bivariate normal cumulative distribution function,

$$\mathcal{P}^T_{\lambda}(n) = e^{-\lambda T}\frac{(\lambda T)^n}{n!} \tag{IA6}$$

is the probability of n jumps over a time interval of length T for a Poisson jump counter with intensity λ, and we define

$$
\begin{aligned}
d_1^- &= \frac{\log\frac{A_{T_0}}{\Phi} + (r-\delta-\lambda\nu)(T_1-T_0) - \lambda_i\nu_i T_1 + n_1 m + j_1 m_i - \frac{1}{2}v_z}{\sqrt{v_z + n_1 v + j_1 v_i}} \\
d_1^+ &= \frac{\log\frac{A_{T_0}}{\Phi} + (r-\delta-\lambda\nu)(T_1-T_0) - \lambda_i\nu_i T_1 + n_1 m + j_1 m_i + \frac{1}{2}v_z + n_1 v + j_1 v_i}{\sqrt{v_z + n_1 v + j_1 v_i}} \\
d_2^- &= \frac{\log\frac{A_{T_0}}{D_2} + (r-\delta-\lambda\nu)(T_2-T_0) - \lambda_i\nu_i T_2 + (n_1+n_2) m + (j_1+j_2) m_i - \frac{1}{2}(v_z+v_x)}{\sqrt{v_z + v_x + (n_1+n_2) v + (j_1+j_2) v_i}} \\
d_2^+ &= \frac{\log\frac{A_{T_0}}{D_2} + (r-\delta-\lambda\nu)(T_2-T_0) - \lambda\nu_i T_2 + (n_1+n_2) m + (j_1+j_2) m_i + \frac{1}{2}(v_z+v_x) + (n_1+n_2) v + (j_1+j_2) v_i}{\sqrt{v_z + v_x + (n_1+n_2) v + (j_1+j_2) v_i}} \\
\rho &= \sqrt{\frac{v_z + n_1 v + j_1 v_i}{v_z + v_x + (n_1+n_2) v + (j_1+j_2) v_i}}.
\end{aligned}
\tag{IA7}
$$

We only show the derivation of the explicit solution for the second expectation, since all the other expectations can be derived similarly. Substituting from Equation (IA5) above and conditioning on the number of jumps we obtain:

$$
\begin{aligned}
\mathbb{E}[A^i_{T_1}\mathbf{1}_{\left\{A^i_{T_1}<\Phi\right\}} \mid A_{T_0}] \quad &= \sum_{n_1,j_1=0}^{\infty} \mathcal{P}_{\lambda}^{T_1-T_0}(n_1)\mathcal{P}_{\lambda_i}^{T_1}(j_1) A_{T_0} e^{(r-\delta-\lambda\nu)(T_1-T_0)-\lambda_i\nu_i T_1} \times \\
&\qquad \mathbb{E}[e^{z+\gamma n_1+\gamma_i j_1}\mathbf{1}_{\left\{A^i_{T_1}<\Phi\right\}} \mid A_{T_0}, N^i_{T_1}=j_1, N_{T_1}-N_{T_0}=n_1].
\end{aligned}
$$

Now, since $z+\gamma n_1+\gamma_i j_1 \sim \mathcal{N}(m_z+mn_1+m_i j_1, v_z+vn_1+v_i j_1)$ we obtain:[11]

$$
\mathbb{E}[e^{z+\gamma n_1+\gamma_i j_1}\mathbf{1}_{\left\{A^i_{T_1}<\Phi\right\}} \mid A_{T_0}, N^i_{T_1}=j_1, N_{T_1}-N_{T_0}=n_1] = e^{m_z+mn_1+m_i j_1+\frac{1}{2}(v_z+vn_1+v_i j_1)}\tilde{\mathbb{E}}[\mathbf{1}_{\left\{\frac{z+\gamma n_1+\gamma_i j_1-\tilde{M}}{\sqrt{\tilde{V}}}<-d_1^+\right\}}],
$$

where d_1^+ is as defined in Equation (IA7) above and the expectation $\tilde{\mathbb{E}}[\cdot]$ is taken with respect to a probability measure $\tilde{P}$ equivalent to Q under which $z+\gamma n_1+\gamma_i j_1 \sim \mathcal{N}(\tilde{M},\tilde{V})$ with the mean and variance under $\tilde{P}$ given by $\tilde{M} = m_z + v_z + (m+v)n_1 + (m_i+v_i)j_1$ and $\tilde{V} = v_z + vn_1 + v_i j_1$.[12] Using the definition of m_z and the fact that $\tilde{\mathbb{E}}[\mathbf{1}_{\left\{\frac{z+\gamma n_1+\gamma_i j_1-\tilde{M}}{\sqrt{\tilde{V}}}<-d_1^+\right\}}] = \mathcal{N}(-d_1^+)$ completes the derivation. Similar derivations apply to all other expectations.

[11] Recall that γn_1 ($\gamma_i j_1$) is our short-hand notation for a sum of n_1 (j_1) i.i.d. normal random variables each distributed like γ (γ_i).

[12] Recall that if $z \sim \mathcal{N}(m_z, v_z)$ then $\mathbb{E}[e^z H(z)] = e^{m_z+\frac{1}{2}v_z}\tilde{\mathbb{E}}[H(z)]$ where under $\tilde{P} \sim Q$ we have $z \sim \mathcal{N}(m_z + v_z, v_z)$. To see that note that $d\tilde{P} = e^{z-m_z-\frac{1}{2}v_z}dQ$ and that the Laplace transform of z under $\tilde{P}$ is $\tilde{\mathbb{E}}[e^{kz}] =$

IA.6.2 Valuation of CDX and SPX options

Again, we obtain closed-form solutions for all the expectations in the CDX option formula

$$\mathbb{E}_0[\mathbf{1}_{\left\{A_{T_0}<\overline{A}\right\}}] = \sum_{n_0=0}^{\infty} \mathcal{P}_\lambda^{T_0}(n_0)\mathcal{N}(-d_0^-)$$

$$\mathbb{E}_0[\mathbf{1}_{\left\{A_{T_0}<\overline{A},A^i_{T_1}<\Phi\right\}}] = \sum_{n_0,n_1,j_1=0}^{\infty} \mathcal{P}_\lambda^{T_0}(n_0)\mathcal{P}_\lambda^{T_1-T_0}(n_1)\mathcal{P}_{\lambda_i}^{T_1}(j_1)\mathcal{N}_2(-d_0^-;-d_1^-;\rho_{01})$$

$$\mathbb{E}_0[A^i_{T_1}\mathbf{1}_{\left\{A_{T_0}<\overline{A},A^i_{T_1}<\Phi\right\}}] = \sum_{n_0,n_1,j_1=0}^{\infty} \mathcal{P}_\lambda^{T_0}(n_0)\mathcal{P}_\lambda^{T_1-T_0}(n_1)\mathcal{P}_{\lambda_i}^{T_1}(n_2)$$

$$A_0 e^{(r-\delta-\lambda\nu-\lambda_i\nu_i)T_1+(n_0+n_1)m+j_1m_i+\frac{1}{2}(n_0+n_1)v+\frac{1}{2}j_1v_i}\mathcal{N}_2(-d_0^+,-d_1^+;\rho_{01})$$

$$\mathbb{E}_0[\mathbf{1}_{\left\{A_{T_0}<\overline{A},A^i_{T_1}\geq\Phi,A^i_{T_2}<D_2\right\}}] = \sum_{n_0,n_1,n_2,j_1,j_2=0}^{\infty} \mathcal{P}_\lambda^{T_0}(n_0)\mathcal{P}_\lambda^{T_1-T_0}(n_1)\mathcal{P}_\lambda^{T_2-T_1}(n_2)\mathcal{P}_{\lambda_i}^{T_1}(j_1)\mathcal{P}_{\lambda_i}^{T_2-T_1}(j_2)$$

$$\mathcal{N}_3(-d_0^-,d_1^-,-d_2^-;-\rho_{01},\rho_{02},-\rho_{12})$$

$$\mathbb{E}_0[A^i_{T_2}\mathbf{1}_{\left\{A_{T_0}<\overline{A},A^i_{T_1}\geq\Phi,A^i_{T_2}<D_2\right\}}] = \sum_{n_0,n_1,n_2,j_1,j_2=0}^{\infty} \mathcal{P}_\lambda^{T_0}(n_0)\mathcal{P}_\lambda^{T_1-T_0}(n_1)\mathcal{P}_\lambda^{T_2-T_1}(n_2)\mathcal{P}_{\lambda_i}^{T_1}(j_1)\mathcal{P}_{\lambda_i}^{T_2-T_1}(j_2)$$

$$A_0 e^{(r-\delta-\lambda\nu-\lambda_i\nu_i)T_2+(n_0+n_1+n_2)m+(j_1+j_2)m_i+\frac{1}{2}(n_0+n_1+n_2)v+\frac{1}{2}(j_1+j_2)v_i}\mathcal{N}_3(-d_0^+,d_1^+,-d_2^+;-\rho_{01},\rho_{02},-\rho_{12}),$$

and the SPX option formula

$$\mathbb{E}_0[\mathbf{1}_{\left\{A_{T_0}\geq\overline{A}\right\}}] = \sum_{n_0=0}^{\infty} \mathcal{P}_\lambda^{T_0}(n_0)\mathcal{N}(d_0^-)$$

$$\mathbb{E}_0[A_{T_0}\mathbf{1}_{\left\{A_{T_0}\geq\overline{A}\right\}}] = \sum_{n_0=0}^{\infty} \mathcal{P}_\lambda^{T_0}(n_0)A_0 e^{(r-\delta-\lambda\nu)T_0+n_0m+\frac{1}{2}n_0v}\mathcal{N}(d_0^+)$$

$$\mathbb{E}_0[\mathbf{1}_{\left\{A_{T_0}\geq\overline{A},A^i_{T_1}\geq\Phi\right\}}] = \sum_{n_0,n_1,j_1=0}^{\infty} \mathcal{P}_\lambda^{T_0}(n_0)\mathcal{P}_\lambda^{T_1-T_0}(n_1)\mathcal{P}_{\lambda_i}^{T_1}(j_1)\mathcal{N}_2(d_0^-,d_1^-;\rho_{01})$$

$$\mathbb{E}_0[A^i_{T_1}\mathbf{1}_{\left\{A_{T_0}\geq\overline{A},A^i_{T_1}<\Phi\right\}}] = \sum_{n_0,n_1,j_1=0}^{\infty} \mathcal{P}_\lambda^{T_0}(n_0)\mathcal{P}_\lambda^{T_1-T_0}(n_1)\mathcal{P}_{\lambda_i}^{T_1}(n_2)$$

$$A_0 e^{(r-\delta-\lambda\nu-\lambda_i\nu_i)T_1+(n_0+n_1)m+j_1m_i+\frac{1}{2}(n_0+n_1)v+\frac{1}{2}j_1v_i}\mathcal{N}_2(d_0^+,-d_1^+;-\rho_{01})$$

$$\mathbb{E}_0[\mathbf{1}_{\left\{A_{T_0}\geq\overline{A},A^i_{T_1}\geq\Phi,A^i_{T_2}\geq D_2\right\}}] = \sum_{n_0,n_1,n_2,j_1,j_2=0}^{\infty} \mathcal{P}_\lambda^{T_0}(n_0)\mathcal{P}_\lambda^{T_1-T_0}(n_1)\mathcal{P}_\lambda^{T_2-T_1}(n_2)\mathcal{P}_{\lambda_i}^{T_1}(j_1)\mathcal{P}_{\lambda_i}^{T_2-T_1}(j_2)$$

$$\mathcal{N}_3(d_0^-,d_1^-,d_2^-;\rho_{01},\rho_{02},\rho_{12})$$

$$\mathbb{E}_0[A^i_{T_2}\mathbf{1}_{\left\{A_{T_0}\geq\overline{A},A^i_{T_1}\geq\Phi,A^i_{T_2}<D_2\right\}}] = \sum_{n_0,n_1,n_2,j_1,j_2=0}^{\infty} \mathcal{P}_\lambda^{T_0}(n_0)\mathcal{P}_\lambda^{T_1-T_0}(n_1)\mathcal{P}_\lambda^{T_2-T_1}(n_2)\mathcal{P}_{\lambda_i}^{T_1}(j_1)\mathcal{P}_{\lambda_i}^{T_2-T_1}(j_2)$$

$\mathbb{E}[e^{z-m_z-\frac{1}{2}v_z+kz}] = e^{k(m_z+v_z)+\frac{1}{2}k^2v_z}$.

$$A_0 e^{(r-\delta-\lambda\nu-\lambda_i\nu_i)T_2+(n_0+n_1+n_2)m+(j_1+j_2)m_i+\frac{1}{2}(n_0+n_1+n_2)v+\frac{1}{2}(j_1+j_2)v_i}\mathcal{N}_3(d_0^+, d_1^+, -d_2^+; \rho_{01}, -\rho_{02}, -\rho_{12}),$$

where $\mathcal{N}_2$ and $\mathcal{N}_3$ denote the bivariate and trivariate normal cumulative distribution functions, $\mathcal{P}_\lambda^T(n)$ is given in (IA6), and we define

$$d_0^- = \frac{\log(\frac{A_0}{A}) + (r-\delta-\lambda\nu)T_0 + n_0 m - \frac{1}{2}v_y}{\sqrt{v_y + n_0 v}}$$

$$d_0^+ = \frac{\log(\frac{A_0}{A}) + (r-\delta-\lambda\nu)T_0 + n_0 m + \frac{1}{2}v_y + n_0 v}{\sqrt{v_y + n_0 v}}$$

$$d_1^- = \frac{\log\frac{A_0}{\Phi} + (r-\delta-\lambda\nu-\lambda\nu_i)T_1 + (n_0+n_1)m + j_1 m_i - \frac{1}{2}(v_y+v_z)}{\sqrt{v_y + v_z + (n_0+n_1)v + j_1 v_i}}$$

$$d_1^+ = \frac{\log\frac{A_0}{\Phi} + (r-\delta-\lambda\nu-\lambda\nu_i)T_1 + (n_0+n_1)m + j_1 m_i + \frac{1}{2}(v_y+v_z) + (n_0+n_1)v + j_1 v_i}{\sqrt{v_y + v_z + (n_0+n_1)v + j_1 v_i}}$$

$$d_2^- = \frac{\log\frac{A_0}{D_2} + (r-\delta-\lambda\nu-\lambda\nu_i)T_2 + (n_0+n_1+n_2)m + (j_1+j_2)m_i - \frac{1}{2}(v_y+v_z+v_x)}{\sqrt{v_y + v_z + v_x + (n_0+n_1+n_2)v + (j_1+j_2)v_i}}$$

$$d_2^+ = \frac{\log\frac{A_0}{D_2} + (r-\delta-\lambda\nu-\lambda\nu_i)T_2 + (n_0+n_1+n_2)m + (j_1+j_2)m_i + \frac{1}{2}(v_y+v_z+v_x) + (n_0+n_1+n_2)v + (j_1+j_2)v_i}{\sqrt{v_y + v_z + v_x + (n_0+n_1+n_2)v + (j_1+j_2)v_i}}$$

$$\rho_{01} = \sqrt{\frac{v_y + n_0 v}{v_y + v_z + (n_0+n_1)v + j_1 v_i}}$$

$$\rho_{02} = \sqrt{\frac{v_y + n_0 v}{v_y + v_z + v_x + (n_0+n_1+n_2)v + (j_1+j_2)v_i}}$$

$$\rho_{12} = \sqrt{\frac{v_y + v_z + (n_0+n_1)v + j_1 v_i}{v_y + v_z + v_x + (n_0+n_1+n_2)v + (j_1+j_2)v_i}}.$$

IA.7 Details on model estimation and implementation

This section provides details on the estimation procedure (IA.7.1), the implementation of pricing formulas (IA.7.2), and how to fix σ_ω and ρ_ω in accordance with recent time series studies (IA.7.3).

IA.7.1 Estimation procedure

Consider a CDX series that is on-the-run for the following set of dates: $t_1, ..., t_n$. We partition the parameters into two sets,

$$\Theta_{1,t_j} = \{A_{t_j}, \sigma_{i,t_j}, \lambda_{i,t_j}, \ell_{1,t_j}, \ell_{2,t_j}, \delta_{t_j}\} \tag{IA8}$$

and

$$\Theta_2 = \{\omega_{t_1}, ..., \omega_{t_n}, \kappa, \bar{\omega}, \lambda_0, \lambda_\omega, m, v\}, \tag{IA9}$$

where Θ_2 determines the amount of systematic risk in the asset process. The optimization procedure has two "layers". In the outer layer, we search for the Θ_2 that minimizes the sum of squared pricing errors for index options over the entire 6-month period that a CDX series is on-the-run.[13] In the inner layer, for each Θ_2-guess, we solve for the Θ_{1,t_j}, $j = 1, ..., n$ that achieves an exact match to the 1Y and 5Y CDX upfronts, the SPX level, the SPX dividend yield, and the index leverage ratios on each observation date.

In general, the optimization procedure is very stable and convergence is not sensitive to (reasonable) starting values. We did, however, find that leaving $\bar{\omega}$ unconstrained could cause non-convergence. Imposing the constraint $\bar{\omega} \leq 0.04$ solved this issue.

Note that CDX Series 33 is on-the-run from September 25, 2019 to March 18, 2020. However, market turmoil due to COVID-19 starts on March 11, 2020 in the weekly time series.[14] It turns out that the extreme market prices observed on the last two observation dates for this series (March 11 and 18) adversely affects the fit for the entire time that Series

[13] Ideally, we would want to express option pricing errors in terms of implied volatilities. However, this is not practical because computing implied volatilities from prices requires a numerical inversion for each option, which adds an extra layer of complexity to the calibration procedure. Instead, we fit to option prices scaled by their Black-Scholes vegas (when fitting to CDX options, the option vegas are computed from the Black-type formula described in Section IA.1.3). This converts option pricing errors in terms of prices into option pricing errors in terms of implied volatilities via a linear approximation.

[14] Figure IA11 shows daily time series of index levels, ATM implied volatilities, and implied volatility skews for CDX and SPX during the COVID-19 crisis.

33 is on-the-run. To avoid this effect, we push these two observation dates to Series 34. Series 34 therefore starts on March 11, 2020 and becomes a "crisis" series. We make two observations on the fit during this time: First, the tumultuous market conditions cause the fit to the option surfaces to deteriorate markedly relative to normal times. Second, there are two observation dates (March 18 and 25, 2020) on which the model is not able to perfectly fit the CDX term structure and the SPX level; therefore, we allow for (small) pricing errors on these dates.

Table 4 in the paper, reports parameter estimates averaged over the entire sample period. As a supplement to that table, Tables IA.1 and IA.2 report parameter estimates for each time period over which a CDX series is on-the-run. Table IA.1 is when calibrating to SPX options, and Table IA.2 is when calibrating to CDX options.

IA.7.2 Implementation of pricing formulas

The integrals in Theorem 1 are computed using Gauss-Legendre quadrature with 41 integration points in each dimension. The integrals are truncated conservatively. The default and option exercise boundaries are linearized around the expected future ω-value; i.e., $\mathbb{E}_0[\omega_{T_0}]$ for the option exercise boundaries and $\mathbb{E}_0[\omega_{T_1}]$ for the default boundary.

IA.7.3 Time-series consistency

Consider a general risk-premium specification that results in the following $\mathbb{P}$-dynamics of A_t:

$$\frac{dA_t}{A_t} = (\mu_0 + \mu_\omega \omega_t)dt + \sqrt{\omega_t} dW_t^{\mathbb{P}} + (e^{\gamma^{\mathbb{P}}} - 1)dN_t^{\mathbb{P}} \tag{IA10}$$

$$d\omega_t = (\beta_0 + \beta_\omega \omega_t)dt + \sigma_\omega \sqrt{\omega_t}\{\rho_\omega dW_t^{\mathbb{P}} + \sqrt{1 - \rho_\omega{}^2} dZ_t^{\mathbb{P}}\}, \tag{IA11}$$

where $W_t^{\mathbb{P}}$ and $Z_t^{\mathbb{P}}$ are independent Brownian motions, $N_t^{\mathbb{P}}$ is an independent Poisson counting processes with intensity $\lambda_t^{\mathbb{P}} = \lambda_0^{\mathbb{P}} + \lambda_\omega^{\mathbb{P}} \omega_t$, and $\gamma^{\mathbb{P}} \sim \mathcal{N}(m^{\mathbb{P}}, v^{\mathbb{P}})$ is an independent normal

random variable. Only the parameters σ_ω and ρ_ω are invariant under a change of measure. We seek to set those parameters such that the corresponding vol-of-vol and correlation parameters for SPX returns are consistent with recent time series studies. This way we impose time-series consistency as advocated by Broadie, Chernov, and Johannes (2007).

Given (IA10)-(IA11), the resulting $\mathbb{P}$-dynamics of S_t are given by:

$$\begin{aligned}\frac{dS_t}{S_t} &= \cdots dt + \frac{A_t}{S_t}\Bigg(\underbrace{\frac{\partial S_t}{\partial A_t}}_{\approx 1}\frac{dA_t^c}{A_t} + \underbrace{\frac{\partial S_t}{\partial \omega_t}\frac{1}{A_t}}_{\approx 0}d\omega_t + \underbrace{\frac{S(A_{t-}e^{\gamma^{\mathbb{P}}},\omega_t) - S(A_{t-},\omega_t)}{A_{t-}}}_{\approx e^{\gamma^{\mathbb{P}}}-1}dN_t^{\mathbb{P}}\Bigg) \\ &\approx \cdots dt + \frac{A_t}{S_t}\frac{dA_t}{A_t}, \end{aligned} \tag{IA12}$$

that is, the SPX return is approximately equal to the return on the common asset factor times a coefficient that depends on leverage. The intuition is that the equity index is a very in-the-money option on the common asset factor resulting in a delta that is close to one and low sensitivity to variance (because the "vega" is scaled by A_t). To illustrate, using the same parameter values as in Section IA.5, we get $\frac{\partial S_t}{\partial A_t} = 0.9879$ and $\frac{\partial S_t}{\partial \omega_t}\frac{1}{A_t} = 0.0147$. Further, the jump size distributions $\frac{S(A_{t-}e^{\gamma^{\mathbb{P}}},\omega_t)-S(A_{t-},\omega_t)}{A_{t-}}$ and $e^{\gamma^{\mathbb{P}}} - 1$ are very similar; for instance, assuming $m^{\mathbb{P}} = -0.05$ and $\sqrt{v^{\mathbb{P}}} = 0.10$, we get mean, standard deviation, skewness, and excess kurtosis of -0.043, 0.094, 0.314, and 0.171 for the former and -0.044, 0.096, 0.302, and 0.162 for the latter.

The coefficient on the common factor return in (IA12) depends on leverage, which is relatively stable over time. As a further approximation we therefore treat this coefficient as a constant. To estimate its magnitude during our sample period, we use the return on the common asset factor, r_t^A, that we construct in Section IA.12.3. Then, running the regression

$$r_t^S = k_0 + k r_t^A + \epsilon_t$$

on daily returns we get $k_0 = 0.000$, $k = 1.350$, and $R^2 = 0.996$.

The upshot is that our model for A_t implies the following approximate $\mathbb{P}$-dynamics of S_t:

$$\frac{dS_t}{S_t} = \cdots dt + \sqrt{\omega_t^S} dW_t^{\mathbb{P}} + k(e^{\gamma^{\mathbb{P}}} - 1) dN_t^{\mathbb{P}} \tag{IA13}$$

$$d\omega_t^S = (\beta_0^S + \beta_{\omega} \omega_t^S) dt + \sigma_{\omega}^S \sqrt{\omega_t^S} \{\rho_{\omega} dW_t^{\mathbb{P}} + \sqrt{1 - \rho_{\omega}{}^2} dZ_t^{\mathbb{P}}\}, \tag{IA14}$$

where $\omega_t^S = k^2 \omega_t$ and $\sigma_{\omega}^S = k\sigma_{\omega}$.

Many papers have estimated the process (IA13)-(IA14) using SPX returns. A number of prominent studies are listed in Table IA.3 along with their estimates of σ_{ω}^S and ρ_{ω}. These studies differ in terms of estimation methodology and sample period, and whether they assume a constant or stochastic (i.e., variance-dependent) jump intensity. The range of σ_{ω}^S-estimates is from 0.07 to 0.31, which corresponds to a range of σ_{ω} from 0.05 to 0.23. The range of ρ_{ω}-estimates is from -0.33 to -0.73. To ensure a role for stochastic volatility in the analysis, we choose values of σ_{ω} and ρ_{ω} towards the high end of these intervals. Specifically, we set $\sigma_{\omega} = 0.20$ and $\rho_{\omega} = -0.70$.

IA.8 Computation of leverage

This section shows how to compute index leverage. We distinguish between short-term debt maturing within one year and long-term debt maturing later than one year. For each index constituent, we compute "short-term leverage" as book value of short-term debt relative to the sum of market value of equity and book value of total debt and "long-term leverage" as book value of long-term debt relative to the sum of market value of equity and book value of total debt. We use quarterly Compustat data, where the book values of short-term and long-term debt are items *DLCQ* and *DLTTQ*, respectively, and market value of equity equals shares outstanding (item *CSHOQ*) times share price (item *PRCCQ*). Leverage ratios

for CDX and SPX are obtained by averaging the leverage ratios of the index constituents, and the final leverage ratios used in calibration are obtained by averaging the leverage ratios across the two indexes.

Figure 6 in the paper shows the distributions of leverage across index constituents. Figure IA12 goes one step further and shows the distributions of short- and long-term leverage across index constituents. Panels A and B show the distribution of firm-quarter short-term leverage observations for CDX and SPX constituents, respectively. Panels C and D do the same for long-term leverage. On average, short- and long-term leverage is similar across the two indexes. The mean (median) short-term leverage is 0.033 and 0.034 (0.021 and 0.015) for the CDX and SPX, respectively, while the mean (median) long-term leverage is 0.244 and 0.204 (0.220 and 0.175) for the CDX and SPX, respectively.

IA.9 Understanding the pure-diffusion model credit skew

In the paper (Figure 5) we find that the implied credit skew has a negative slope in case of the pure-diffusion version of the model. To understand this result, in this section we prove analytically that the slope of the credit (and equity) skew is negative in the special case where i) the underlying model is the classic Merton (1974) model, ii) the CDS is paid in full-upfront (i.e., with no periodic coupon payments), and iii) the credit implied volatility is expressed in full-upfront (rather than spread) terms.

Recall that in the Merton (1974) model the equity value equals the price of a European call option written on the underlying asset value A_t with strike equal to the outstanding debt notional D and maturity T. Let's denote this price by $C(A_t, t)$. It follows from risk-neutral pricing and Itô's lemma that

$$\frac{dC}{C} = rdt + \sigma_C(A_t, t)dZ_t,$$

where $\sigma_C(A,t) = \frac{C_A A\sigma}{C}$ and σ is the volatility of the underlying asset value. Now, as is well-known, the sign of the option implied volatility skew will be determined by the sign of the correlation between the underlying and its variance. Specifically, the implied volatility skew will be negatively (positively) sloped if the covariance of $\frac{dC}{C}$ and $d\sigma_C^2$ is negative (positive). In the present model, we have

$$\rho_C = \frac{1}{dt} Cov\left(\frac{dC}{C}, d\sigma_C^2\right) = 2\sigma_C^2 \frac{\partial \sigma_C}{\partial A}\sigma A.$$

Thus, we have

$$\text{sign}(\rho_C) = \text{sign}\left(\frac{\partial \sigma_C}{\partial A}\right) = \text{sign}\left(\frac{\partial \frac{C_A A}{C}}{\partial A}\right) = -\text{sign}\left(\frac{\partial \frac{C}{C_A A}}{\partial A}\right).$$

Now, by homogeneity we have $C = AC_A + DC_D$. It follows that

$$\frac{\sigma}{\sigma_C} = \frac{C}{AC_A} = 1 + \frac{DC_D}{AC_A} = 1 - \frac{De^{-rT}N(d_2)}{AN(d_1)}.$$

We can then compute

$$\frac{\partial \frac{C}{AC_A}}{\partial A} = \frac{De^{-rT}}{A^2 N(d_1)^2 \sigma\sqrt{T}} \left(n(d_1)N(d_2) + N(d_1)N(d_2)\sigma\sqrt{T} - N(d_1)n(d_2))\right).$$

The sign of the expression is that of the function

$$f_s(x) = n(x+s)N(x) + N(x+s)N(x)s - N(x+s)n(x), \tag{IA15}$$

for the positive constant $s = \sigma\sqrt{T}$ and for $x = d_2$. Note in particular that $\lim_{x\to-\infty} f_s(x) = 0$, $\lim_{x\to+\infty} f_s(x) = s > 0$. Thus, if we can show that $f_s'(x) > 0$ this suffices to establish that $f_s(x) > 0\ \forall x$. We find that $f_s'(x) = N(x+s)n(x)(x+s) - N(x)n(x+s)x = n(x)n(x+s)(\frac{N(x+s)(x+s)}{n(x+s)} - \frac{N(x)x}{n(x)})$. Since $g(x) = \frac{N(x)x}{n(x)}$ is an increasing function, it follows that $f_s'(x) >$

0.[15]

We have established:

Lemma 3. $\frac{\partial \sigma_C}{\partial A} < 0$ *and thus* $\rho_C < 0$.

It follows that when A drops (because of a negative shock $dZ < 0$), the value of the call (i.e., the equity value) decreases, but its variance increases generating the negative equity implied volatility skew.

Turning to the credit side, we assume for analytical purposes that the CDS is paid in full-upfront (so that the underlying of a CDS option is the full-upfront CDS price) and we study the slope of the implied volatility skew expressed in full-upfront terms.[16] In the Merton setting, the CDS value equals the price of a European put option on A_t with strike D and maturity T. Let's denote this price by $P(A_t, t)$. Its risk-neutral dynamics are

$$\frac{dP}{P} = rdt + \sigma_P(A_t, t)dZ_t,$$

where $\sigma_P(A, t) = \frac{P_A A \sigma}{P}$. Similar to before, the credit-option implied volatility skew will be negatively (positively) sloped if the covariance of $\frac{dP}{P}$ and $d\sigma_P^2$ is negative (positive). In the present model, we have

$$\rho_P = \frac{1}{dt} Cov\left(\frac{dP}{P}, d\sigma_P^2\right) = 2\sigma_P^2 \frac{\partial \sigma_P}{\partial A} \sigma A.$$

Thus,

$$\text{sign}(\rho_P) = \text{sign}\left(\frac{\partial \sigma_P}{\partial A}\right) = \text{sign}\left(\frac{\partial \frac{P_A A}{P}}{\partial A}\right) = -\text{sign}\left(\frac{\partial \frac{P}{P_A A}}{\partial A}\right).$$

[15] It can be shown that $g'(x) = \frac{\int_{-\infty}^{x} (x-y)^2 n(y) dy}{n(x)} > 0$.

[16] Instead, and to be consistent with the market convention, in the paper we present implied credit-spread volatilities, where the upfront-to-spread conversion is done using a standard reduced-form model as described in Section IA.1.

Now, by homogeneity we have $P = AP_A + DP_D$. It follows that

$$\frac{\sigma}{\sigma_P} = \frac{P}{AP_A} = 1 + \frac{DP_D}{AP_A} = 1 - \frac{De^{-rT}N(-d_2)}{AN(-d_1)}.$$

We can then compute

$$\frac{\partial \frac{P}{AP_A}}{\partial A} = \frac{De^{-rT}}{A^2 N(-d_1)^2 \sigma\sqrt{T}} \left(N(-d_1)N(-d_2)\sigma\sqrt{T} + n(-d_2)N(-d_1) - n(-d_1)N(-d_2) \right).$$

We see that the sign of the right-hand side is that of the function $f_s(x)$ defined in equation (IA15) above with $x = -d_1$. It follows then immediately from our previous analysis that:

Lemma 4. $\frac{\partial \sigma_P}{\partial A} < 0$ *and thus* $\rho_P < 0$.

Thus, when A drops (because of a negative shock $dZ < 0$), and since $\sigma_P < 0$, the value the put (i.e., the CDS value) increases, but its variance decreases generating a negative credit implied volatility skew.

Combining both lemmas, we see that the classic Merton diffusion framework generates the same (negative) slope for the equity and credit implied volatility skew, contrary to what is observed in the data.

IA.10 Option pricing with heterogeneity in leverage

In the paper, we assume that firms are ex-ante identical. In this section, we investigate the effect of heterogeneity in leverage on the relative valuation of CDX and SPX options. Figure IA13 shows time series of the mean, standard deviation, and skewness of the distribution of long-term leverage for SPX constituents. Consistent with Panel D in Figure IA12, the leverage distribution is consistently positively skewed. The time-series averages of the mean,

standard deviation, and skewness are 0.204, 0.143, and 0.887, respectively. We focus on the impact of this "average" degree of heterogeneity.

IA.10.1 Homogeneous benchmark

For the homogenous benchmark, we use the same parameterization as in Section IA.5, with the only difference being that we match the index leverage ratios for SPX ($lev_1 = 0.034$ and $lev_2 = 0.204$) instead of the average of the index leverage ratios for SPX and CDX. The resulting parameters are $A_t = 2842.9$, $\sigma_i = 0.300$, $\lambda_i = 0.002$, $\ell_1 = 0.035$, $\ell_2 = 0.208$, and $\delta = 0.015$.[17] Then, we compute implied volatilities for CDX and SPX options with a wide set of strikes. These are displayed in the top panels in Figure IA14 (blue lines).

IA.10.2 Heterogenous model

Next, we consider a model that allows for heterogeneity in leverage. Specifically, along the lines of Bai, Goldstein, and Yang (2019), we assume that there are two types of firms, L and H, that are ex-ante identical except in terms of their long-term leverage, lev_2^L and lev_2^H (type L being the low-leverage firms). A fraction w of index constituents are of type L, while the remaining fraction $1 - w$ are of type H.

Note that equity and CDS values for type L and H firms are obtained with the pricing formulas in the paper, and that the SPX and CDX values are given by

$$S_0(x_0) = wS_0^{i,L}(x_0) + (1-w)S_0^{i,H}(x_0)$$
$$U_0(x_0) = wU_0^{i,L}(x_0) + (1-w)U_0^{i,H}(x_0).$$

The pricing formulas for index options are given below.

As a first step, we search for w, lev_2^L, and lev_2^H so that we match the time-series averages

[17] The equity value and 1Y and 5Y CDS spreads are 2202.6, 15.2 bps, and 72.2 bps, respectively.

of the first three moments of the distribution of long-term leverage for SPX. The solution is $w = 0.703$, $lev_2^L = 0.111$, and $lev_2^H = 0.424$. The two types of firms are assumed to have the same short-term leverage so that $lev_1^L = lev_1^H = 0.034$.

Next, we parameterize the model as for the homogeneous benchmark, only now we have four leverage parameters, ℓ_1^L, ℓ_2^L, ℓ_1^H, and ℓ_2^H, and four leverage targets

$$\begin{aligned} lev_1^L &= \frac{D_1^L}{S_0^{i,L} + D_1^L + D_2^L} \\ lev_2^L &= \frac{D_2^L}{S_0^{i,L} + D_1^L + D_2^L} \\ lev_1^H &= \frac{D_1^H}{S_0^{i,H} + D_1^H + D_2^H} \\ lev_2^H &= \frac{D_2^H}{S_0^{i,H} + D_1^H + D_2^H}. \end{aligned}$$

The resulting parameters are $A_t = 2841.4$, $\sigma_i = 0.238$, $\lambda_i = 0.002$, $\ell_1^L = 0.034$, $\ell_2^L = 0.112$, $\ell_1^H = 0.036$, $\ell_2^H = 0.448$, and $\delta = 0.015$.[18]

Finally, we compute implied volatilities for CDX and SPX options with the same set of strikes as for the homogeneous model. These are also displayed in the top panels in Figure IA14 (red lines). The bottom panels in Figure IA14 display the relative difference between the implied volatilities from the heterogeneous and homogeneous models. The heterogeneous model generates somewhat lower option prices than the benchmark model across the entire moneyness spectrum, but the effect is significantly greater for CDX options than for SPX options (for ATM options, the CDX option price is 12.4% lower while the SPX option price is 1.1% lower). Therefore, taking heterogeneity in leverage into account only exacerbates the valuation puzzle.

[18] The equity value and 1Y and 5Y CDS spreads for the low-leverage (high-leverage) firm are 2446.9 (1625.2), 14.7 (16.4) bps, and 19.3 (207.0) bps, respectively.

IA.10.3 Pricing formulas for index options

The index upfront amount, conditional on the common factors x_{T_0}, is given by

$$
\begin{aligned}
U_{T_0}(x_{T_0}) &= w\mathbb{E}[U_{T_0}^{i,L}|x_{T_0}] + (1-w)\mathbb{E}[U_{T_0}^{i,H}|x_{T_0}] \\
&= we^{-r(T_1-T_0)}\Big((1+C_1)\mathbb{E}[\mathbf{1}_{\left\{A_{T_1}^i<\Phi_{T_1}^L\right\}}\,|\,x_{T_0}] - \frac{\alpha}{D_1^L+D_2^L}\mathbb{E}[A_{T_1}^i\mathbf{1}_{\left\{A_{T_1}^i<\Phi^L\right\}}\,|\,x_{T_0}]\Big) \\
&\quad + we^{-r(T_2-T_0)}\Big(\mathbb{E}[\mathbf{1}_{\left\{A_{T_1}^i\geq\Phi_{T_1}^L,A_{T_2}^i<D_2^L\right\}}\,|\,x_{T_0}] - \frac{\alpha}{D_2^L}\mathbb{E}[A_{T_2}^i\mathbf{1}_{\left\{A_{T_1}^i\geq\Phi_{T_1}^L,A_{T_2}^i<D_2^L\right\}}\,|\,x_{T_0}]\Big) \\
&\quad + (1-w)e^{-r(T_1-T_0)}\Big((1+C_1)\mathbb{E}[\mathbf{1}_{\left\{A_{T_1}^i<\Phi_{T_1}^H\right\}}\,|\,x_{T_0}] - \frac{\alpha}{D_1^H+D_2^H}\mathbb{E}[A_{T_1}^i\mathbf{1}_{\left\{A_{T_1}^i<\Phi_{T_1}^H\right\}}\,|\,x_{T_0}]\Big) \\
&\quad + (1-w)e^{-r(T_2-T_0)}\Big(\mathbb{E}[\mathbf{1}_{\left\{A_{T_1}^i\geq\Phi_{T_1}^H,A_{T_2}^i<D_2^H\right\}}\,|\,x_{T_0}] - \frac{\alpha}{D_2^H}\mathbb{E}[A_{T_2}^i\mathbf{1}_{\left\{A_{T_1}^i\geq\Phi_{T_1}^H,A_{T_2}^i<D_2^H\right\}}\,|\,x_{T_0}]\Big) \\
&\quad - C_0 - C_1e^{-r(T_1-T_0)}.
\end{aligned}
$$

Therefore, the time-0 value of a CDX call option with strike K and expiration at T_0 is

$$
\begin{aligned}
C_0^{CDX} &= e^{-rT_0}\mathbb{E}_0[\max(U_{T_0}(A_{T_0})-K,0)] \\
&= we^{-rT_1}\Big((1+C_1)\mathbb{E}_0[\mathbf{1}_{\left\{A_{T_0}<\underline{A}(\omega_{T_0}),A_{T_1}^i<\Phi_{T_1}^L\right\}}] - \frac{\alpha}{D_1^L+D_2^L}\mathbb{E}_0[A_{T_1}^i\mathbf{1}_{\left\{A_{T_0}<\underline{A}(\omega_{T_0}),A_{T_1}^i<\Phi_{T_1}^L\right\}}]\Big) \\
&\quad + we^{-rT_2}\Big(\mathbb{E}_0[\mathbf{1}_{\left\{A_{T_0}<\underline{A}(\omega_{T_0}),A_{T_1}^i\geq\Phi_{T_1}^L,A_{T_2}^i<D_2^L\right\}}] - \frac{\alpha}{D_2^L}\mathbb{E}_0[A_{T_2}^i\mathbf{1}_{\left\{A_{T_0}<\underline{A}(\omega_{T_0}),A_{T_1}^i\geq\Phi_{T_1}^L,A_{T_2}^i<D_2^L\right\}}]\Big) \\
&\quad + (1-w)e^{-rT_1}\Big((1+C_1)\mathbb{E}_0[\mathbf{1}_{\left\{A_{T_0}<\underline{A}(\omega_{T_0}),A_{T_1}^i<\Phi_{T_1}^H\right\}}] - \frac{\alpha}{D_1^H+D_2^H}\mathbb{E}_0[A_{T_1}^i\mathbf{1}_{\left\{A_{T_0}<\underline{A}(\omega_{T_0}),A_{T_1}^i<\Phi_{T_1}^H\right\}}]\Big) \\
&\quad + (1-w)e^{-rT_2}\Big(\mathbb{E}_0[\mathbf{1}_{\left\{A_{T_0}<\underline{A}(\omega_{T_0}),A_{T_1}^i\geq\Phi_{T_1}^H,A_{T_2}^i<D_2^H\right\}}] - \frac{\alpha}{D_2^H}\mathbb{E}_0[A_{T_2}^i\mathbf{1}_{\left\{A_{T_0}<\underline{A}(\omega_{T_0}),A_{T_1}^i\geq\Phi_{T_1}^H,A_{T_2}^i<D_2^H\right\}}]\Big) \\
&\quad - e^{-rT_0}\tilde{K}\mathbb{E}_0[\mathbf{1}_{\left\{A_{T_0}<\underline{A}(\omega_{T_0})\right\}}],
\end{aligned}
$$

where

$$\tilde{K} = K + C_0 + C_1e^{-r(T_1-T_0)}$$

and $\underline{a}(\omega) = \log \underline{A}(\omega)$ is the exercise boundary such that it is optimal to exercise the CDX call at T_0 when $a_{T_0} \leq \underline{a}(\omega_{T_0})$. It is implicitly defined by the equation $U_{T_0}(\underline{a}(\omega), \omega) = K$ (using the fact that, for a given ω, $U_{T_0}(a, \omega)$ is decreasing in a).

To value CDX options analytically, we approximate the exercise boundary with an affine function:

$$\underline{a}(\omega) = \underline{a}_0 + \underline{a}_1 \omega.$$

Note that, even though formally the exercise barrier solves the same equation as in the benchmark model, the estimated exercise barrier (and the parameters $\underline{a}_0, \underline{a}_1$ of its linear approximation) will be affected by heterogeneity, because the expression for the upfront, $U_{T_0}(a, \omega)$, obtained above for the case with heterogeneity is a different function than that obtained in Section (4.5) for the benchmark model.

Similarly, the value of the SPX, conditional on the common factors x_{T_0}, is given by

$$\begin{aligned}
S_{T_0}(x_{T_0}) &= w\mathbb{E}[S^{i,L}_{T_0}|x_{T_0}] + (1-w)\mathbb{E}[S^{i,H}_{T_0}|x_{T_0}] \\
&= A_{T_0} - we^{-r(T_1-T_0)}\Big(D_1^L\mathbb{E}[\mathbf{1}_{\left\{A^i_{T_1}\geq\Phi^L_{T_1}\right\}} \,|\, x_{T_0}] + \mathbb{E}[A^i_{T_1}\mathbf{1}_{\left\{A^i_{T_1}<\Phi^L\right\}} \,|\, x_{T_0}]\Big) \\
&\quad - we^{-r(T_2-T_0)}\Big(D_2^L\mathbb{E}[\mathbf{1}_{\left\{A^i_{T_1}\geq\Phi^L, A^i_{T_2}\geq D^L_2\right\}} \,|\, x_{T_0}] + \mathbb{E}[A^i_{T_2}\mathbf{1}_{\left\{A^i_{T_1}\geq\Phi^L, A^i_{T_2}<D^L_2\right\}} \} \,|\, x_{T_0}]\Big) \\
&\quad - (1-w)e^{-r(T_1-T_0)}\Big(D_1^H\mathbb{E}[\mathbf{1}_{\left\{A^i_{T_1}\geq\Phi^H\right\}} \,|\, x_{T_0}] + \mathbb{E}[A^i_{T_1}\mathbf{1}_{\left\{A^i_{T_1}<\Phi^H\right\}} \,|\, x_{T_0}]\Big) \\
&\quad - (1-w)e^{-r(T_2-T_0)}\Big(D_2^H\mathbb{E}[\mathbf{1}_{\left\{A^i_{T_1}\geq\Phi^H, A^i_{T_2}\geq D^H_2\right\}} \,|\, x_{T_0}] + \mathbb{E}[A^i_{T_2}\mathbf{1}_{\left\{A^i_{T_1}\geq\Phi^H, A^i_{T_2}<D^H_2\right\}} \} \,|\, x_{T_0}]\Big).
\end{aligned}$$

Therefore, the time-0 value of an SPX call option with strike K and expiration at T_0 is

$$
\begin{aligned}
C_0^{SPX} &= e^{-rT_0}\mathbb{E}_0[\max(S_{T_0}(A_{T_0}) - K, 0)] \\
&= e^{-rT_0}\mathbb{E}_0[A_{T_0}\mathbf{1}_{\left\{A_{T_0}\geq \overline{A}(\omega_{T_0})\right\}}] - we^{-rT_1}\left(D_1^L\mathbb{E}_0[\mathbf{1}_{\left\{A_{T_0}\geq \overline{A}(\omega_{T_0}),A^i_{T_1}\geq \Phi^L\right\}}] + \mathbb{E}_0[A^i_{T_1}\mathbf{1}_{\left\{A_{T_0}\geq \overline{A}(\omega_{T_0}),A^i_{T_1}< \Phi^L\right\}}]\right) \\
&\quad - we^{-rT_2}\left(D_2^L\mathbb{E}_0[\mathbf{1}_{\left\{A_{T_0}\geq \overline{A}(\omega_{T_0}),A^i_{T_1}\geq \Phi^L,A^i_{T_2}\geq D_2^L\right\}}] + \mathbb{E}_0[A^i_{T_2}\mathbf{1}_{\left\{A_{T_0}\geq \overline{A}(\omega_{T_0}),A^i_{T_1}\geq \Phi^L,A^i_{T_2}< D_2^L\right\}}]\right) \\
&\quad - (1-w)e^{-rT_1}\left(D_1^H\mathbb{E}_0[\mathbf{1}_{\left\{A_{T_0}\geq \overline{A}(\omega_{T_0}),A^i_{T_1}\geq \Phi^H\right\}}] + \mathbb{E}_0[A^i_{T_1}\mathbf{1}_{\left\{A_{T_0}\geq \overline{A}(\omega_{T_0}),A^i_{T_1}< \Phi^H\right\}}]\right) \\
&\quad - (1-w)e^{-rT_2}\left(D_2^H\mathbb{E}_0[\mathbf{1}_{\left\{A_{T_0}\geq \overline{A}(\omega_{T_0}),A^i_{T_1}\geq \Phi^H,A^i_{T_2}\geq D_2^H\right\}}] + \mathbb{E}_0[A^i_{T_2}\mathbf{1}_{\left\{A_{T_0}\geq \overline{A}(\omega_{T_0}),A^i_{T_1}\geq \Phi^H,A^i_{T_2}< D_2^H\right\}}]\right) \\
&\quad - e^{-rT_0}K\mathbb{E}_0[\mathbf{1}_{\left\{A_{T_0}\geq \overline{A}(\omega_{T_0})\right\}}],
\end{aligned}
$$

where $\overline{a}(\omega) = \log \overline{A}(\omega)$ is the exercise boundary such that it is optimal to exercise the SPX call at T_0 if $a_{T_0} \geq \overline{a}(\omega_{T_0})$, and which is implicitly defined by the equation $S_{T_0}(\underline{a}(\omega), \omega) = K$ (using the fact that, for a given ω, $S_T(a, \omega)$ is increasing in a). To value SPX options analytically, we approximate the exercise boundary with an affine function:

$$\overline{a}(\omega) = \overline{a}_0 + \overline{a}_1\omega.$$

IA.11 Option pricing with a finite number of index constituents

In the paper, we obtain analytical solutions to index options by letting the number of index constituents go to infinity. In actuality, indexes are composed of a finite number of constituents (125 in case of CDX and 500 in case of SPX). In this section, we conduct a simulation exercise to verify that the number of index constituents is sufficiently high that index option prices are well approximated by our analytical formulas.

We use the same parameterization of the model as in Section IA.5. We consider two-month equity index put options that are ATM (strike equal to the forward SPX value,

$K = 2199.5$) and roughly one standard deviation OTM ($K = 2052.6$). The analytical option prices are 52.74 and 14.56, respectively. We also consider two-month credit index call options that are ATM (strike equal to the upfront value of the 5Y FEP forward-starting CDX, $K = -114.9$ bps) and roughly one standard deviation OTM ($K = -63.2$ bps). The analytical option prices are 17.17 and 5.39 bps, respectively.

Next, we use simulation to price the options for a finite number, N, of index constituents. We use $M = 50,000$ simulations. In each simulation, we first simulate the systematic factors $\{A_{T_0}, \omega_{T_0}\}$ using the "full truncation" scheme of Lord, Koekkoek, and Dijk (2010). Conditional on A_{T_0}, we then simulate the individual firm asset values $A^i_{T_0}$ from (14). The estimated equity index put option price is given by

$$e^{-rT_0} \frac{1}{M} \sum_{j=1}^{M} \max \left(K - \frac{1}{N} \sum_{i=1}^{N} S^i_{T_0}(A^{i,j}_{T_0}, \omega^j_{T_0}), 0 \right),$$

and the credit index call option price is given by

$$e^{-rT_0} \frac{1}{M} \sum_{j=1}^{M} \max \left(\frac{1}{N} \sum_{i=1}^{N} U^i_{T_0}(A^{i,j}_{T_0}, \omega^j_{T_0}) - K, 0 \right).$$

Figure IA15 shows index option prices as a function of N.[19] The left panels show CDX options, and the right panels shows SPX options. The top panels show ATM options, and the bottom panels show OTM options. The grey areas indicate 95% confidence intervals. The blue lines show the analytical option prices for $N \to \infty$.

Consider first the equity index options with $N = 500$. The ATM option has a simulated price of 53.18 with a 95% confidence interval of [52.26,54.10], and the OTM option has a simulated price of 14.77 with a 95% confidence interval of [14.17,15.38]. For both options, the analytical price is within the 95% confidence interval of the finite-N option price.

Consider next the credit index options with $N = 125$. The ATM option has a simulated

[19] $N = 1$ corresponds to an option on a single-name CDS or single stock.

price of 18.36 bps with a 95% confidence interval of [18.00,18.73] bps, and the OTM option has a simulated price of 6.09 bps with a 95% confidence interval of [5.83,6.36] bps. For both options, the analytical price lies outside of the 95% confidence interval of the finite-N option price. The finite-N option prices are 7.0% and 13.0%, respectively, higher than the analytical option prices.

The upshot is that while the analytical SPX option prices are very good approximations to the $N = 500$ index option prices, the analytical CDX option prices are downward-biased compared to the $N = 125$ index option prices.[20] However, the magnitudes of the biases are small relative to the size of the mispricing that we document in the paper.

Figure IA16 compares index distributions for finite N (estimated from the simulated data using a normal kernel function with optimal bandwidth) with the limiting distributions for $N \to \infty$ (obtained using the analytical option price formulas together with the Breeden-Litzenberger Theorem). The left panels show CDX options, and the right panels shows SPX options. The top panels show results for $N = 125$, and the bottom panels show results for $N = 500$. Visually, the distributions are very similar, with the distributions for finite N having only slightly more dispersion than the limiting distribution.

IA.12 Computation of asset return volatility

This section describes how we compute asset returns and total and systematic asset volatility.

IA.12.1 Data

We build our sample for computing asset volatilities of CDX and SPX constituents from several databases. Daily stock price data come from the Center for Research in Secu-

[20] Note that for $N = 500$, the analytical CDX option prices are within the 95% confidence intervals of the finite-N option prices. In this case, the ATM option has a simulated price of 17.50 bps with a 95% confidence interval of [17.14,17.86] bps, and the OTM option has a simulated price of 5.42 bps with a 95% confidence interval of [5.28,5.79] bps.

rity Prices' (CRSP's) US stock database. Quarterly company fundamentals come from the CRSP/Compustat Merged database. One- and five-year CDS spreads and expected recovery rates come from Markit. Finally, corporate actions and reference entity data come from Markit's Reference Entity Database (RED).

We use six-digit Committee on Uniform Security Identification Procedures (CUSIP) codes to identify companies that are present in both the CRSP and Markit data. Specifically, we associate with each RED code the CRSP permanent company identifier whose six-digit CUSIP—that is, the first six characters of CRSP's historic eight-character issue identifier (the *NCUSIP* item)—corresponds to the six-digit CUSIP available in Markit RED data.[21]

Then, we incorporate corporate actions among reference entities, exclusively focusing on events in which a RED code was changed because the reference entity was renamed. We do not incorporate other corporate action types, such as mergers and acquisitions, directly; i.e., via the corresponding events in the RED database. Instead, we incorporate them indirectly whenever there are two RED codes with the same CRSP permanent company identifier that have not yet been linked. This ensures that mergers are consistent across the two data sets in that the surviving company is identical in both CRSP and Markit data.

Finally, we use CRSP's permanent company identifier to obtain company fundamentals from the CRSP/Compustat Merged database. In case of companies with multiple share classes, we drop the share class that is less liquid in terms of trading volume over the 2012–2019 sample period.

[21]The RED code is the primary identifier of a CDS's reference entity.

IA.12.2 Asset returns

We compute asset returns as the leverage-weighted average of equity and synthetic short- and long-term bond returns; that is,

$$r_t^{A^i} = (1 - lev_1^i - lev_2^i) r_t^{S^i} + lev_1^i r_t^{B_1^i} + lev_2^i r_t^{B_2^i},$$

where $r_t^{S^i}$ denotes firm i's daily equity return from CRSP for date t (CRSP's *RET* item), and $r_t^{B_1^i}$ and $r_t^{B_2^i}$ denote synthetic short- and long-term bond returns based on firm i's one- and five-year Markit CDS spreads, respectively, for the same period.[22] The leverage ratios, lev_1^i and lev_2^i, are computed as described in Section IA.8.

The synthetic bond return computation is based on no-arbitrage arguments. As shown in Duffie (1999), selling CDS protection on firm i and buying a risk-free floating rate note produces the same cash flow stream as a floating rate note with matching payment dates issued by the same firm. In the same spirit, the cash flow stream of a fixed-rate bullet bond approximately equals selling CDS protection, buying a risk-free floating rate note, and swapping the risk-free floating rate payments to a fixed rate via an interest rate swap (IRS). In this case, the excess return on the fixed-rate bullet bond can be decomposed into

$$r_t^{B_j^i} = r_t^{CDS_j^i} + r_t^{IRS_j},$$

where $r_t^{CDS_j^i}$ denotes firm i's one- (if $j = 1$) or five-year (if $j = 2$) CDS return and $r_t^{IRS_j}$ denotes the return on a one- (if $j = 1$) or five-year (if $j = 2$) IRS.

Specifically, the CDS return over the period from date s to date t is

$$r_t^{CDS_j^i} = -\big(C_{j,t}^i - C_{j,s}^i\big) PVBP_t\big(C_{j,t}^i, R_t^i\big) + C_{j,s}^i \frac{t-s}{360},$$

[22] CRSP's return computation takes into account all distributions to shareholders, such as dividend payments.

where $C^i_{j,t}$ denotes firm i's one- (if $j = 1$) or five-year (if $j = 2$) par spread on date t and R^i_t denotes firm i's expected recovery rate.[23] The risky present value of a basis point for a given par spread and recovery rate, $PVBP_t(C, R)$, is obtained via the ISDA CDS Standard Model and using locked-in LIBOR rates from Markit.[24] For additional details concerning the CDS return computation, see Junge and Trolle (2015).

Similarly, the IRS return is

$$r_t^{IRS_j} = -(S_{j,t} - S_{j,s})PVBP_t$$

where $S_{j,t}$ denotes the date-t fixed rate on a one- (if $j = 1$) or five-year (if $j = 2$) IRS referencing three-month LIBOR. The present value of a basis point, $PVBP_t$, is computed using zero-rates bootstrapped from deposit and swap rates. Specifically, the short-end of the interest rate curve is composed of rates on LIBOR deposit with less than three months to maturity, and the remainder of the curve comprises swap rates.[25]

We compute asset returns both for companies for which we can establish a CRSP/Markit link and for zero-leverage companies for which we cannot expect to find Markit data. In total, we can compute asset returns for 135 companies that were a CDX constituent at some point between 2012 and 2019 and for 430 companies that were at some point a SPX constituent. Panels A of Figure IA17 shows that for roughly 50% of the CDX constituents for which we

[23] If there is a credit event between dates s and t, then the return is

$$r_t^{B^i_j} = -\left(1 - R^i_{\tau_i}\right) + C^i_{j,s}\frac{\tau_{\tau_i} - s}{360},$$

where R^i_τ is the realized recovery rate and τ_i is the credit event date. There are no credit events among CDX and SPX constituents during our sample period.

[24] The ISDA CDS Standard Model is the market standard for marking to market CDSs based on a term structure of par spreads. The simplified version of the model that we use to compute the risky present values actually assumes that the term structure of risk free rates is piecewise constant, and that both the default intensity and the recovery rate are constant. Given a par spread and recovery rate, the model finds that value of the default intensity that makes a par CDS's present value equal to zero.

[25] The swaps are standard USD-denominated fixed for floating swaps. Floating-leg payments occur quarterly and reference three-month LIBOR, and fixed-leg payments occur semi-annually. The swaps have maturities of at least one year.

can compute asset returns, we are able to do so throughout the sample period. For SPX constituents that share is a little lower at roughly 40%, see Panel B of Figure IA17. The varying number of observations for the remaining companies is due to both missing data and index inclusions/exclusions. In our analysis, we disregard a few companies with very few observations by requiring that we have at least one month of data (i.e., 21 observations) for each quarter for which we produce firm-quarter statistics. This leaves a total of 135 and 425 companies in case of CDX and SPX, respectively.

Panel A of Figures IA18 and IA19 show the distributions of asset returns for CDX and SPX constituents, respectively. Panels B, C, and D of the two figures show the distributions of the asset return's components; namely, the equity return (Panel B), and the synthetic one- (Panel C) and five-year (Panel D) bond returns.

IA.12.3 Systematic asset volatility

We decompose asset returns into systematic and idiosyncratic components by assuming that the return of the common systematic component has the same structure as the returns of the individual companies; that is,

$$r_t^A = (1 - lev_1 - lev_2)r_t^S + lev_1 r_t^{B_1} + lev_2 r_t^{B_2},$$

where r_t^S denotes the return on aggregate equity, $r_t^{B_1^i}$ and $r_t^{B_2^i}$ denote returns on aggregate short- and long-term debt, and lev_1 and lev_2 denote aggregate short- and long-term leverage ratios.

In this case, a one-factor linear model

$$r_t^{A^i} = \alpha_i + \beta_i r_t^A + \epsilon_t^{A^i}$$

becomes

$$r_t^{A^i} = \alpha_i + \beta_i^S r_t^S + \beta_i^{B_1} r_t^{B_1} + \beta_i^{B_2} r_t^{B_2} + \epsilon_t^{A^i}, \tag{IA16}$$

where $\beta_i^S = \beta_i(1 - lev_1 - lev_2)$, $\beta_i^{B_1} = \beta_i lev_1$, and $\beta_i^{B_2} = \beta_i lev_2$. We use Equation (IA16) to estimate the systematic component of asset returns.[26] Specifically, r_t^S is given by the daily SPX return from CRSP (CRSP's *SPRTRN* item), and $r_t^{B_1}$ and $r_t^{B_2}$ are computed from CDX and IRS returns as

$$r_t^{B_j} = r_t^{CDX_j} + r_t^{IRS_j},$$

where the CDX return is given by

$$r_t^{CDX_j} = -(U_{j,t} - U_{j,s}) + C\frac{t-s}{360} - (L_t - L_s),$$

using the notation from Section IA.1.

While total asset volatility is estimated as the annualized standard deviation of $r_t^{A^i}$, systematic asset volatility is estimated as the annualized standard deviation of

$$\hat{r}_t^{A^i} = \hat{\alpha}_i + \hat{\beta}_i^S r_t^S + \hat{\beta}_i^{B_1} r_t^{B_1} + \hat{\beta}_i^{B_2} r_t^{B_2}, \tag{IA17}$$

where $\hat{\alpha}_i$, $\hat{\beta}_i^S$, $\hat{\beta}_i^{B_1}$, and $\hat{\beta}_i^{B_2}$ denote OLS estimates of α_i, β_i^S, $\beta_i^{B_1}$, and $\beta_i^{B_2}$, respectively.

IA.13 Details on volatility trading strategies

This section provides more details on the volatility trading strategies. As described in the paper, in addition to holding the option premium in a margin account, we assume that an initial amount of capital is required when selling options. Let P_t denote the straddle price at time t and X_t the required capital. Assuming that capital in the margin account earns

[26] We estimate Equation (IA16) for each firm and quarter, i.e., we do not impose the cross-equation restrictions implied by the explicit expressions for β_i^S, $\beta_i^{B_1}$, and $\beta_i^{B_1}$.

the risk-free rate, the excess return from selling the straddle is

$$R^e_{t+1} = \frac{-P_{t+1} + P_t(1 + r_t)}{X_t}.$$

In the paper, we assume that X_t is proportional to the option premium, $X_t = cP_t$, and adjust c to achieve a 10% unconditional annualized volatility of realized excess returns within each option maturity.

As a robustness check, here we explore an alternative assumption that X_t is constant over time, and again adjust the required amount to achieve a 10% unconditional annualized excess return volatility. Table IA.4 and Figure IA20 are the counterparts to Table 6 and Figure 9 in the paper. Under the alternative assumption about capital, selling CDX volatility is even more attractive relative to selling SPX volatility. For instance, for the full sample, trading the EW portfolios against each other generates an annualized Sharpe ratio of 1.143 (vs. 0.877 with the original assumption about capital).

Note, however, that the return distributions are much more leptokurtic. This is also evident from Figure IA21, which shows daily excess returns for each of the EW strategies assuming constant capital (in the top row) and proportional capital (in the bottom row). Clearly, constant capital leads to extreme return volatility during the COVID-19 crisis, which is not the case with proportional capital.

IA.14 Option pricing with stochastic bankruptcy costs

In the conclusion of the paper, we highlight a potentially fruitful extension of the model with systematic variation in bankruptcy costs. Such variation will impact bond recovery upon default and thus affect credit derivatives, but not equity derivatives since equity always recovers zero in bankruptcy. In this section we show how to add this feature to the model while keeping analytical solutions to all derivatives.

Bankruptcy costs are modeled as

$$\alpha_t = \sum_{i=1}^{n} \alpha_i \mathbf{1}_{\{s_t=i\}},$$

where $s_t \in \{1, 2, \ldots, n\}$ follows a continuous time Markov chain with constant transition intensities q_{ij} and where α_i are constant bankruptcy cost parameters. We assume the jumps in s_t are independent of all other sources of risk. Further, we define the transition matrix Q with off-diagonal element $Q_{ij} = q_{ij}\ \forall i \neq j$ and with diagonal element $Q_{ii} = -\sum_{j\neq i} q_{ij}$. Note that equity prices and thus SPX and SPX option prices are not affected by bankruptcy costs. Thus they are unchanged. As a result, the endogenous default boundary Φ_{T_1} is also unchanged. Instead, the bankruptcy cost process enters the bond and CDS payoffs, and thus also affects CDX and CDX option values. Further, since α_t is independent of A_t, ω_t, and A_t^i, the bond and CDS prices will depend only on the conditional expectation of α_t, $\overline{\alpha}(s_0, t) = \mathbb{E}[\alpha_t \,|\, s_0]$. Instead, the CDX option will also depend on the volatility of α_t, which has the potential to increase CDX option prices relative to those implied by SPX options.

IA.14.1 CDS value

Consider a CDS contract from t to T_2 with unit notional and with a coupon rate of C. Following the same approach as in the main text, the upfront amount of the CDS contract is

$$\begin{aligned} U_t^i = e^{-r(T_1-t)}\mathbb{E}[(1 - \frac{\alpha_{T_1} A_{T_1}^i}{D_1 + D_2} + C_1)\mathbf{1}_{\left\{A_{T_1}^i < \Phi_{T_1}\right\}} \,|\, x_t^i, s_t] \\ + e^{-r(T_2-t)}\mathbb{E}[(1 - \frac{\alpha_{T_2} A_{T_2}^i}{D_2})\mathbf{1}_{\left\{A_{T_1}^i \geq \Phi_{T_1}, A_{T_2}^i < D_2\right\}} \,|\, x_t^i, s_t] - C_0 - C_1 e^{-r(T_1-t)}, \end{aligned}$$

where C_0, C_1 are as defined in the main text.

Since the Markov Chain process is independent of x_t^i we can rewrite this as:

$$U_t^i = e^{-r(T_1-t)}\mathbb{E}[(1 - \frac{\overline{\alpha}(s_t, T_1-t)A_{T_1}^i}{D_1+D_2} + C_1)\mathbf{1}_{\left\{A_{T_1}^i < \Phi_{T_1}\right\}} \mid x_t^i, s_t]$$
$$+ e^{-r(T_2-t)}\mathbb{E}[(1 - \frac{\overline{\alpha}(s_t, T_2-t)A_{T_2}^i}{D_2})\mathbf{1}_{\left\{A_{T_1}^i \geq \Phi_{T_1}, A_{T_2}^i < D_2\right\}} \mid x_t^i, s_t] - C_0 - C_1 e^{-r(T_1-t)},$$

where we define the expected bankruptcy cost $\tau \geq 0$:

$$\begin{aligned}\overline{\alpha}(s, \tau) &= \mathbb{E}[\alpha_\tau \mid s_0 = s] \\ &= \sum_{i=1}^{n} \alpha_i P[s_\tau = i \mid s_0 = s].\end{aligned}$$

Define the (n, n)-matrix $P(t)$ with element $p_{ij}(t) = P[s_t = j \mid s_0 = i]$. Clearly, it satisfies for $j \neq i$:

$$p_{ij}(t + dt) = \sum_{k \neq j} p_{ik}(t) q_{kj} dt + p_{ij}(t)(1 - \sum_{k \neq j} q_{jk} dt)$$

from which it follows that

$$p_{ij}(t)' = \sum_k p_{ik}(t) Q_{kj}.$$

In matrix form:

$$P(t)' = P(t)Q$$

which admits the matrix solution $P(t) = \exp(tQ)$, where $\exp(M) = \sum_k \frac{1}{k!} M^k$.

We can also compute the conditional variance of the bankruptcy cost as

$$\mathbb{V}[\alpha_\tau \mid s_0 = s] = \mathbb{E}[\alpha_\tau^2 \mid s_0 = s] - \overline{\alpha}(s, \tau)^2,$$

where

$$\mathbb{E}[\alpha_\tau^2 \mid s_0 = s] = \sum_{i=1}^{n} \alpha_i^2 p_{si}(\tau).$$

IA.14.2 CDX value

We value the CDX at time $t \leq T_1$. Like in the main text we use the large homogeneous pool approximation to derive the expression. The new feature is that the common factors are now x_t and s_t. The index upfront amount, conditional on x_t, s_t, is given by:

$$\begin{aligned}
U_t(x_t, s_t) &= \lim_{N\to\infty} \frac{1}{N} \sum_{i=1}^{N} U_t^i(x_t^i, s_t) \\
&= \mathbb{E}[U_t^i(x_t^i, s_t) | x_t, s_t] \\
&= e^{-r(T_1-t)} \Big((1+C_1)\mathbb{E}[\mathbf{1}_{\left\{A^i_{T_1} < \Phi_{T_1}\right\}} \,|\, x_t] - \frac{\overline{\alpha}(s_t, T_1-t)}{D_1+D_2} \mathbb{E}[A^i_{T_1} \mathbf{1}_{\left\{A^i_{T_1} < \Phi_{T_1}\right\}} \,|\, x_t] \Big) \\
&\quad + e^{-r(T_2-t)} \Big(\mathbb{E}[\mathbf{1}_{\left\{A^i_{T_1} \geq \Phi_{T_1}, A^i_{T_2} < D_2\right\}} \,|\, x_t] - \frac{\overline{\alpha}(s_t, T_2-t)}{D_2} \mathbb{E}[A^i_{T_2} \mathbf{1}_{\left\{A^i_{T_1} \geq \Phi_{T_1}, A^i_{T_2} < D_2\right\}} \,|\, x_t] \Big) \\
&\quad - C_0 - C_1 e^{-r(T_1-t)}.
\end{aligned}$$

IA.14.3 CDX options

The time-0 value of a CDX call option with strike K and expiration at T_0 is:

$$\begin{aligned}
C_0^{CDX} &= e^{-rT_0} \mathbb{E}_0[\max(U_{T_0}(x_{T_0}, s_{T_0}) - K, 0)] \\
&= e^{-rT_0} \sum_{j=1}^{n} P[s_{T_0} = j \,|\, s_0] \, \mathbb{E}_0[\max(U_{T_0}(x_{T_0}, j) - K, 0)].
\end{aligned}$$

It remains to evaluate $\mathbb{E}_0[\max(U_{T_0}(x_{T_0}, j) - K, 0)] \;\; \forall j = 1, \ldots, n$. But this is similar to

the expression in the main text. Indeed:

$$
\begin{aligned}
&e^{-rT_0}\mathbb{E}_0[\max(U_{T_0}(x_{T_0},j)-K,0)]\\
&\quad= e^{-rT_0}\mathbb{E}_0\Bigg[\Bigg(e^{-r(T_1-T_0)}\Big((1+C_1)\mathbb{E}[\mathbf{1}_{\left\{A^i_{T_1}<\Phi_{T_1}\right\}}\mid x_{T_0}]-\frac{\overline{\alpha}(j,T_1-T_0)}{D_1+D_2}\mathbb{E}[A^i_{T_1}\mathbf{1}_{\left\{A^i_{T_1}<\Phi_{T_1}\right\}}\mid x_{T_0}]\Big)\\
&\qquad+e^{-r(T_2-T_0)}\Big(\mathbb{E}[\mathbf{1}_{\left\{A^i_{T_1}\geq\Phi_{T_1},A^i_{T_2}<D_2\right\}}\mid x_{T_0}]-\frac{\overline{\alpha}(j,T_2-T_0)}{D_2}\mathbb{E}[A^i_{T_2}\mathbf{1}_{\left\{A^i_{T_1}\geq\Phi_{T_1},A^i_{T_2}<D_2\right\}}\mid x_{T_0}]\Big)\Bigg)\mathbf{1}_{\left\{A_{T_0}<\underline{A}(\omega_{T_0},j)\right\}}\Bigg]\\
&\qquad-e^{-rT_0}\tilde{K}\mathbb{E}_0[\mathbf{1}_{\left\{A_{T_0}<\underline{A}(\omega_{T_0},j)\right\}}]\\
&\quad= e^{-rT_1}\Big((1+C_1)\mathbb{E}_0[\mathbf{1}_{\left\{A_{T_0}<\underline{A}(\omega_{T_0},j),A^i_{T_1}<\Phi(\omega_{T_1})\right\}}]-\frac{\overline{\alpha}(j,T_1-T_0)}{D_1+D_2}\mathbb{E}_0[A^i_{T_1}\mathbf{1}_{\left\{A_{T_0}<\underline{A}(\omega_{T_0},j),A^i_{T_1}<\Phi(\omega_{T_1})\right\}}]\Big)\\
&\qquad+e^{-rT_2}\Big(\mathbb{E}_0[\mathbf{1}_{\left\{A_{T_0}<\underline{A}(\omega_{T_0},j),A^i_{T_1}\geq\Phi(\omega_{T_1}),A^i_{T_2}<D_2\right\}}]-\frac{\overline{\alpha}(j,T_2-T_0)}{D_2}\mathbb{E}_0[A^i_{T_2}\mathbf{1}_{\left\{A_{T_0}<\underline{A}(\omega_{T_0},j),A^i_{T_1}\geq\Phi(\omega_{T_1}),A^i_{T_2}<D_2\right\}}]\Big)\\
&\qquad-e^{-rT_0}\tilde{K}\mathbb{E}_0[\mathbf{1}_{\left\{A_{T_0}<\underline{A}(\omega_{T_0},j)\right\}}],
\end{aligned}
$$

where $\tilde{K}=K+C_0+C_1e^{-r(T_1-T_0)}$ and $\underline{a}(\omega,j)=\log\underline{A}(\omega,j)$ is the exercise boundary such that it is optimal to exercise the CDX call at T_0 when $a_{T_0}\leq\underline{a}(\omega_{T_0},j)$ in bankruptcy-cost state $s_{T_0}=j$. It is implicitly defined by the equation $U_{T_0}([\underline{a}(\omega),\omega],j)=K$ (using the fact that, for a given ω, $U_{T_0}([a,\omega],j)$ is decreasing in a for any bankruptcy-cost state j). To value CDX options analytically, we approximate the exercise boundary with an affine function:

$$\underline{a}(\omega,j)=\underline{a}^j_0+\underline{a}^j_1\omega.$$

Note in particular, that the endogenous exercise threshold will be different across different bankruptcy-cost states.

IA.15 Structural demand for CDX options

In the conclusion of the paper we hypothesize that a structural demand for CDX options—along with various limits to arbitrage—could push their prices above fair values implied by SPX options. Indeed, anecdotal evidence suggests that there is a significant regulatory-driven demand from banks who seek to hedge their CVA exposures in order to reduce their regulatory capital. In this section, we provide more details.

Unfortunately, we cannot directly quantify this demand because we do not have access to trader identities in our transaction data set. However, via regulatory filings we can quantify the amount of risk-weighted assets (RWAs) attributed to CVA risk across large banks to get an idea about the magnitudes of CVA exposures and, hence, the potential demand for CDX call options. Figure IA22 shows the evolution of RWAs for CVA risk across the eight US global systemically important banks. Between Q4 2015 and Q1 2020 it averages 228 bln USD (it jumps markedly to 271 bln USD in Q1 2020). Because traded CDX options have short maturities, a bank that hedges CVA risk exposures via options would need to frequently roll over its positions. Therefore, the regulatory-driven demand can potentially account for a large fraction of the trading volume documented in Section 2.3.

References (Internet Appendix)

Andersen, Torben G., Luca Benzoni, and Jesper Lund, 2002, An empirical investigation of continuous-time equity return models, *Journal of Finance* 57, 1239–1284.

Bai, Jennie, Robert S. Goldstein, and Fan Yang, 2019, The leverage effect and the basket-index put spread, *Journal of Financial Economics* 131, 186–205.

Bates, David S., 2006, Maximum likelihood estimation of latent affine processes, *Review of Financial Studies* 19, 909–965.

———, 2012, U.S. stock market crash risk, 1926–2010, *Journal of Financial Economics* 105, 229–259.

Black, Fischer, 1976, The pricing of commodity contracts, *Journal of Financial Economics* 3, 167–179.

Broadie, Mark, Mikhail Chernov, and Michael Johannes, 2007, Model specification and risk premia: Evidence from futures options, *Journal of Finance* 62, 1453–1490.

Duffie, Darrell, 1999, Credit swap valuation, *Financial Analysts Journal* 55, 73–87.

Eraker, Bjorn, 2004, Do stock prices and volatility jump? Reconciling evidence from spot and option prices, *Journal of Finance*, 59, 1367–1403

Eraker, Bjorn, Michael Johannes, and Nicholas Polson, 2003, The impact of jumps in volatility and returns, *Journal of Finance* 58, 1269–1300.

Junge, Benjamin, and Anders B. Trolle, 2015, Liquidity risk in credit default swap markets, Working paper, Swiss Finance Institute.

Lord, Roger, Remmert Koekkoek, and Dick Van Dijk, 2010, A comparison of biased simulation schemes for stochastic volatility models, *Quantitative Finance* 10, 177–194.

Merton, Robert C., 1974, On the pricing of corporate debt: The risk structure of interest rates, *Journal of Finance* 29, 449–470.

———, 1976, Option pricing when underlying stock returns are discontinuous, *Journal of Financial Economics* 3, 125–144.

Li, Haitao, Martin Wells, and Cindy Yu, 2008. A Bayesian analysis of return dynamics with stochastic volatility and Lévy jumps, *Review of Financial Studies* 21, 2345–2378.

Morini, Massimo, and Damiano Brigo, 2011, No-armageddon measure for arbitrage-free pricing of index options in a credit crisis, *Mathematical Finance* 21, 573–593.

Newey, Whitney K., and Kenneth D. West, 1987, A simple, positive semi-definite, heteroskedasticity and autocorrelation consistent covariance matrix, *Econometrica* 55, 703–708.

Pedersen, Claus M., 2003, Valuation of portfolio credit default swaptions, Lehman Brothers Fixed Income Quantitative Credit Research

White, Richard, 2014, Forward CDS, indices and options, OpenGamma Quantitative Research.

Series	ω_t	κ	$\bar{\omega}$	λ_0	λ_ω	m	$\sqrt{v}$	A_t	σ_i	λ_i	ℓ_1	ℓ_2	δ
S17	0.0075	2.834	0.0400	0.000	6.22	-0.199	0.191	1817.6	0.270	0.003	0.037	0.222	0.016
S18	0.0079	2.244	0.0400	0.000	17.12	-0.121	0.118	1843.1	0.266	0.003	0.038	0.231	0.017
S19	0.0099	0.780	0.0400	0.000	10.74	-0.105	0.122	1935.5	0.289	0.002	0.035	0.225	0.016
S20	0.0092	0.780	0.0400	0.000	9.68	-0.093	0.117	2142.7	0.298	0.001	0.033	0.215	0.015
S21	0.0095	0.439	0.0384	0.000	8.23	-0.136	0.147	2324.4	0.298	0.001	0.031	0.206	0.014
S22	0.0077	0.875	0.0208	0.000	9.56	-0.126	0.125	2497.6	0.323	0.001	0.030	0.202	0.015
S23	0.0089	0.969	0.0400	0.000	11.70	-0.160	0.150	2637.3	0.256	0.001	0.031	0.208	0.014
S24	0.0118	0.700	0.0166	0.000	1.77	-0.301	0.212	2752.1	0.312	0.001	0.033	0.225	0.016
S25	0.0132	0.764	0.0400	0.000	3.88	-0.248	0.180	2677.2	0.253	0.003	0.033	0.238	0.018
S26	0.0090	0.585	0.0400	0.000	4.24	-0.207	0.189	2810.9	0.266	0.002	0.033	0.231	0.017
S27	0.0075	0.567	0.0400	0.000	5.76	-0.167	0.174	2947.8	0.279	0.001	0.032	0.225	0.015
S28	0.0066	2.647	0.0073	0.000	8.21	-0.166	0.169	3173.2	0.339	0.001	0.032	0.225	0.013
S29	0.0085	3.248	0.0058	0.000	6.37	-0.209	0.210	3466.8	0.336	0.001	0.032	0.225	0.010
S30	0.0085	0.729	0.0253	0.000	8.34	-0.194	0.179	3570.8	0.303	0.001	0.033	0.226	0.015
S31	0.0144	0.522	0.0323	0.000	5.55	-0.192	0.179	3594.6	0.286	0.001	0.038	0.248	0.015
S32	0.0093	0.697	0.0400	0.000	6.56	-0.154	0.146	3892.5	0.251	0.001	0.038	0.247	0.014
S33	0.0099	0.646	0.0400	0.001	6.57	-0.152	0.153	4244.0	0.229	0.001	0.037	0.245	0.013
S34	0.0421	0.204	0.0021	0.002	37.42	-0.170	0.153	3614.2	0.141	0.002	0.037	0.244	0.021

Table IA.1: Parameter estimates per series, when calibrating to SPX options

The table reports parameter estimates for each time period over which a CDX series is on-the-run. For the common factors and those parameters that change from each observation date to the next (σ_i, λ_i, ℓ_1, ℓ_2, and δ), the table reports sample means within each time period. A number of model parameters are fixed in advance: $m_i = -5$, $v_i = 0$, $\alpha = 0.8$, $\sigma_{_\omega} = 0.20$ and $\rho_{_\omega} = -0.70$. The total sample period is February 29, 2012 to April 29, 2020 (427 weekly observations).

Series	ω_t	κ	$\bar{\omega}$	λ_0	λ_ω	m	$\sqrt{v}$	A_t	σ_i	λ_i	ℓ_1	ℓ_2	δ
S17	0.0376	1.164	0.0400	0.000	8.22	-0.016	0.330	1817.3	0.212	0.003	0.037	0.222	0.016
S18	0.0279	1.040	0.0393	0.002	41.69	-0.022	0.203	1842.8	0.107	0.003	0.038	0.231	0.017
S19	0.0282	2.536	0.0299	0.000	30.94	-0.004	0.175	1935.7	0.266	0.002	0.035	0.225	0.016
S20	0.0272	2.181	0.0296	0.000	31.07	-0.027	0.167	2142.9	0.275	0.001	0.033	0.215	0.015
S21	0.0132	2.170	0.0183	0.000	83.83	-0.021	0.146	2324.8	0.281	0.001	0.031	0.206	0.014
S22	0.0094	1.237	0.0189	0.000	53.26	-0.001	0.201	2497.4	0.261	0.001	0.030	0.202	0.015
S23	0.0130	1.328	0.0279	0.000	111.45	-0.030	0.152	2636.9	0.121	0.002	0.031	0.208	0.014
S24	0.0085	1.251	0.0192	0.000	167.31	-0.030	0.137	2751.6	0.176	0.001	0.033	0.226	0.016
S25	0.0345	1.814	0.0380	0.000	61.12	-0.070	0.120	2677.3	0.164	0.003	0.033	0.238	0.018
S26	0.0122	1.232	0.0280	0.000	114.26	-0.026	0.149	2811.0	0.115	0.001	0.033	0.231	0.017
S27	0.0089	1.007	0.0359	0.000	56.66	-0.024	0.188	2947.6	0.121	0.001	0.032	0.225	0.015
S28	0.0108	1.778	0.0228	0.000	38.96	-0.051	0.156	3172.9	0.276	0.001	0.032	0.225	0.013
S29	0.0179	4.748	0.0188	0.047	18.17	-0.148	0.159	3466.6	0.288	0.001	0.032	0.225	0.010
S30	0.0081	1.515	0.0133	0.000	102.82	-0.045	0.170	3570.8	0.268	0.001	0.033	0.226	0.015
S31	0.0099	0.705	0.0296	0.000	46.61	-0.095	0.198	3594.1	0.167	0.001	0.038	0.248	0.015
S32	0.0171	2.107	0.0109	0.000	56.96	-0.039	0.155	3893.2	0.290	0.001	0.038	0.247	0.014
S33	0.0173	1.796	0.0199	0.000	31.98	-0.073	0.165	4244.6	0.245	0.001	0.037	0.245	0.013
S34	0.1155	0.603	0.0036	0.951	11.20	-0.125	0.198	3614.4	0.074	0.001	0.037	0.244	0.021

Table IA.2: Parameter estimates per series, when calibrating to CDX options

The table reports parameter estimates for each time period over which a CDX series is on-the-run. For the common factors and those parameters that change from each observation date to the next (σ_i, λ_i, ℓ_1, ℓ_2, and δ), the table reports sample means within each time period. A number of model parameters are fixed in advance: $m_i = -5$, $v_i = 0$, $\alpha = 0.8$, $\sigma_{_\omega} = 0.20$ and $\rho_{_\omega} = -0.70$. The total sample period is February 29, 2012 to April 29, 2020 (427 weekly observations).

Paper	Method	Sample period	Stochastic λ	σ_{ω}^{S}	ρ_{ω}
Andersen et al. (2002)	EMM	1980-1996	$\surd$	0.07	-0.33
Andersen et al. (2002)	EMM	1953-1996	$\surd$	0.18	-0.62
Eraker et al. (2003)	MCMC	1980-1999	—	0.10	-0.47
Eraker (2004)	MCMC	1970-1990	—	0.08	-0.47
Bates (2006)	AML	1953-1996	$\surd$	0.24	-0.61
Li et al. (2008)	MCMC	1980-2000	—	0.11	-0.57
Bates (2012)	AML	1957-2006	$\surd$	0.31	-0.73

Table IA.3: Time-series estimates of σ_{ω}^{S} and ρ_{ω}

The table shows estimates of σ_{ω}^{S} and ρ_{ω} in a number of time series studies that estimate the process (IA13)-(IA14) using SPX returns.

	CDX options				SPX options				CDX vs. SPX options			
	M1	M2	M3	EW	M1	M2	M3	EW	M1	M2	M3	EW
Panel A: Full sample												
Mean	0.104	0.115	0.154	0.124	0.008	0.012	0.007	0.009	0.048	0.051	0.073	0.058
t-stat	2.676	2.782	3.698	3.187	0.223	0.335	0.203	0.258	2.579	2.900	4.175	3.412
Std.dev.	0.100	0.100	0.100	0.093	0.100	0.100	0.100	0.098	0.055	0.054	0.055	0.050
SR	1.042	1.147	1.538	1.337	0.079	0.120	0.073	0.092	0.874	0.959	1.322	1.143
Skewness	-5.265	-7.510	-6.063	-7.458	-4.116	-4.612	-4.286	-4.494	2.223	1.154	-0.280	1.742
Kurt	91.258	145.518	114.268	145.778	47.126	72.070	89.650	63.181	36.730	44.154	57.470	43.983
Panel B: Ex-COVID-19 sample												
Mean	0.186	0.231	0.267	0.228	0.082	0.112	0.119	0.104	0.052	0.060	0.074	0.062
t-stat	4.907	5.827	6.728	6.347	2.584	3.498	3.653	3.314	2.579	2.895	3.569	3.285
Std.dev.	0.100	0.100	0.100	0.087	0.100	0.100	0.100	0.099	0.060	0.060	0.059	0.054
SR	1.860	2.312	2.665	2.605	0.816	1.120	1.186	1.055	0.872	0.998	1.246	1.146
Skewness	-1.138	-2.223	-1.206	-1.901	-2.618	-2.408	-2.256	-2.460	-0.047	-0.183	0.194	0.065
Kurt	18.228	20.375	18.449	16.692	26.397	26.304	24.886	26.227	13.047	12.375	11.958	11.874

Table IA.4: Summary statistics of trading strategies, constant required capital
In each market and for each option maturity category, the strategy sells closest-to-ATM straddles each trading day with a holding period of one day. We assume that the strategy requires an initial amount of capital, which we assume is constant over time and which we adjust to achieve a 10% unconditional annualized volatility of realized excess returns for each option maturity. "EW" denotes an equally weighted portfolio of the three option maturities. "CDX vs. SPX options" denotes a short-long strategy then allocates 50% of funds to selling CDX straddles and 50% to buying SPX straddles. Means, standard deviations, and Sharpe ratios ("SR") are annualized. t-statistics are corrected for heteroscedasticity and serial correlation up to four lags using the approach of Newey and West (1987). The full sample consists of 1881 daily returns between February 28, 2012 and April 30, 2020. The ex-COVID-19 sample consists of 1801 daily returns between February 28, 2012 and December 31, 2019.

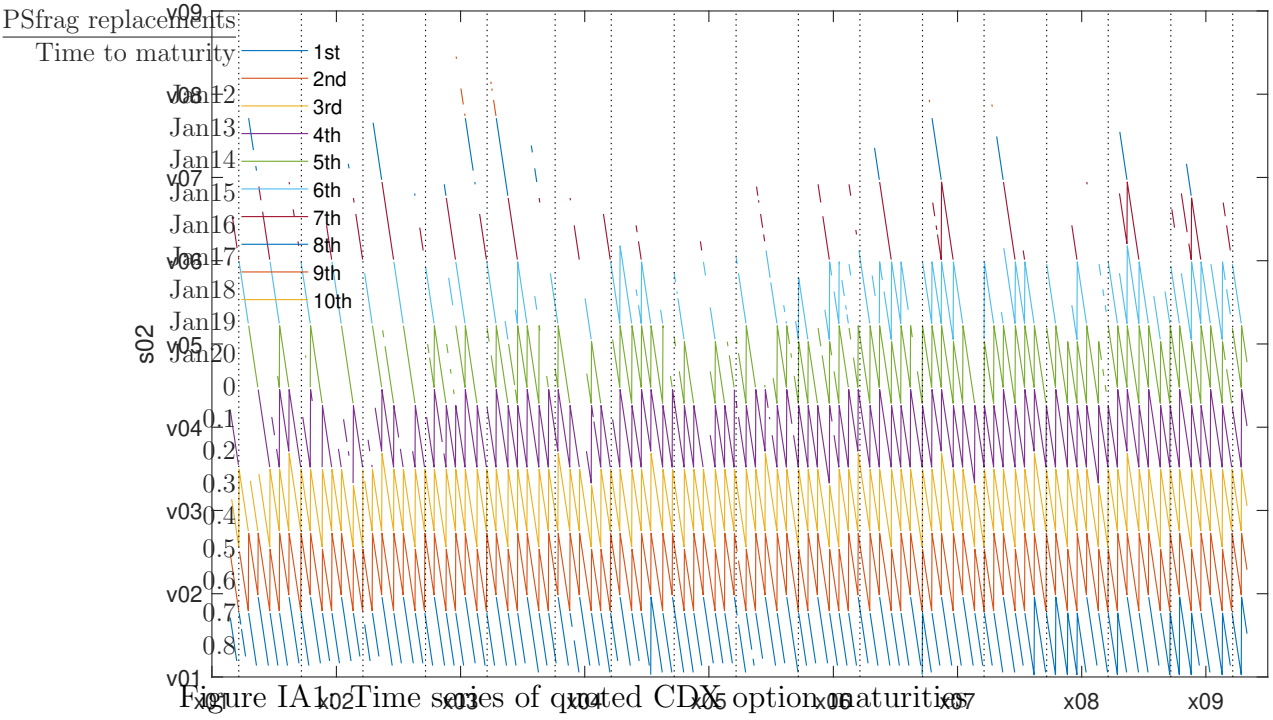

Figure IA.1. Time series of quoted CDX option maturities

Option expiries are 3rd Wednesday of the month. Vertical dotted lines mark roll dates. Daily data from February 24, 2012 until April 30, 2020.

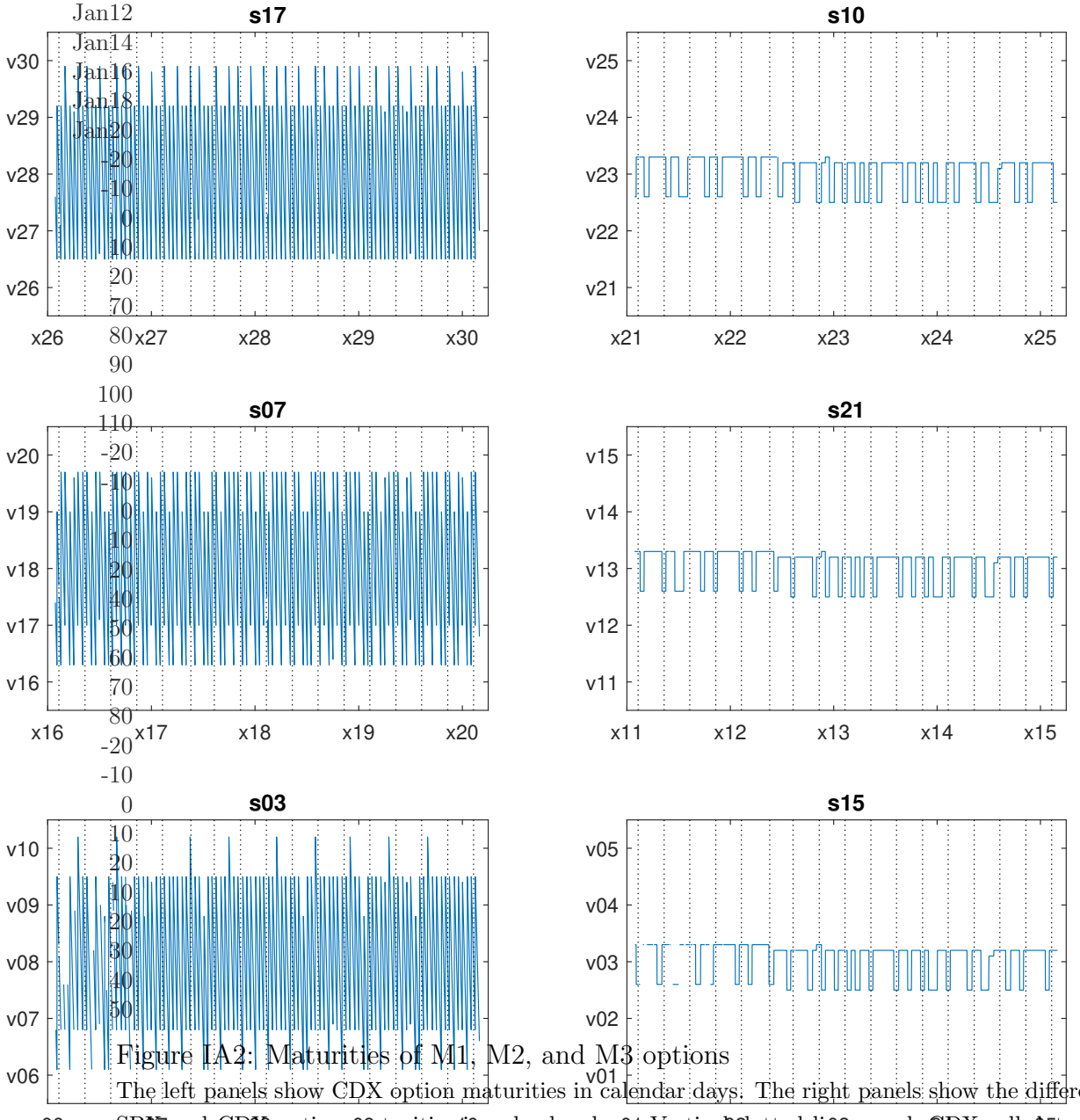

Figure IA2: Maturities of M1, M2, and M3 options

The left panels show CDX option maturities in calendar days. The right panels show the difference between SPX and CDX option maturities in calendar days. Vertical dotted lines mark CDX roll dates. Daily data from February 24, 2012 until April 30, 2020.

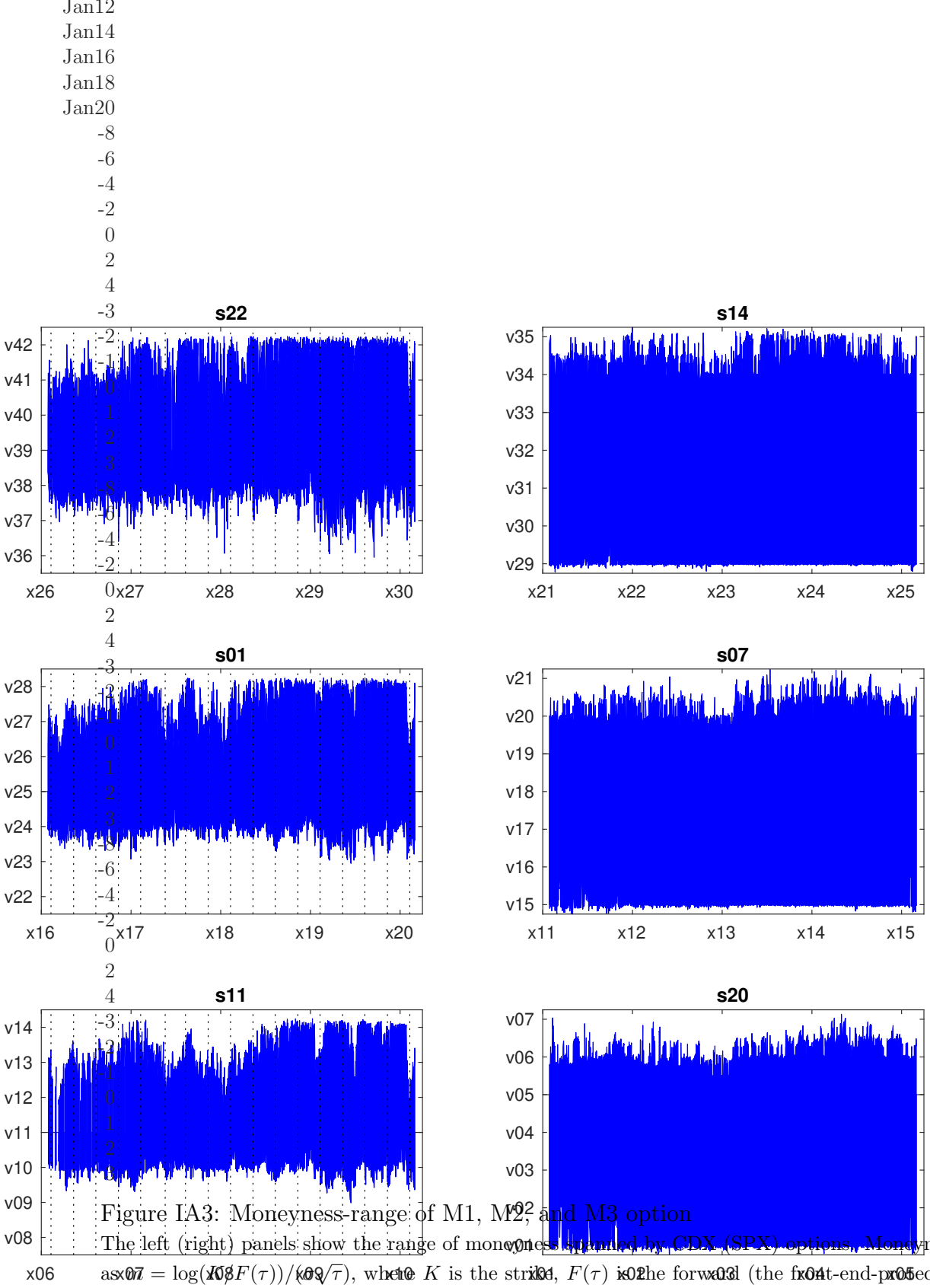

Figure IA3: Moneyness-range of M1, M2, and M3 option

The left (right) panels show the range of moneyness spanned by CDX (SPX) options. Moneyness is defined as $x = \log(K/F(\tau))/(\sigma\sqrt{\tau})$, where K is the strike, $F(\tau)$ is the forward (the front-end-protected spread in case of CDX options and the forward price in case of SPX options), σ is the at-the-money implied volatility, and τ is the maturity. Vertical dotted lines mark CDX roll dates. Daily data from February 24, 2012 until April 30, 2020.

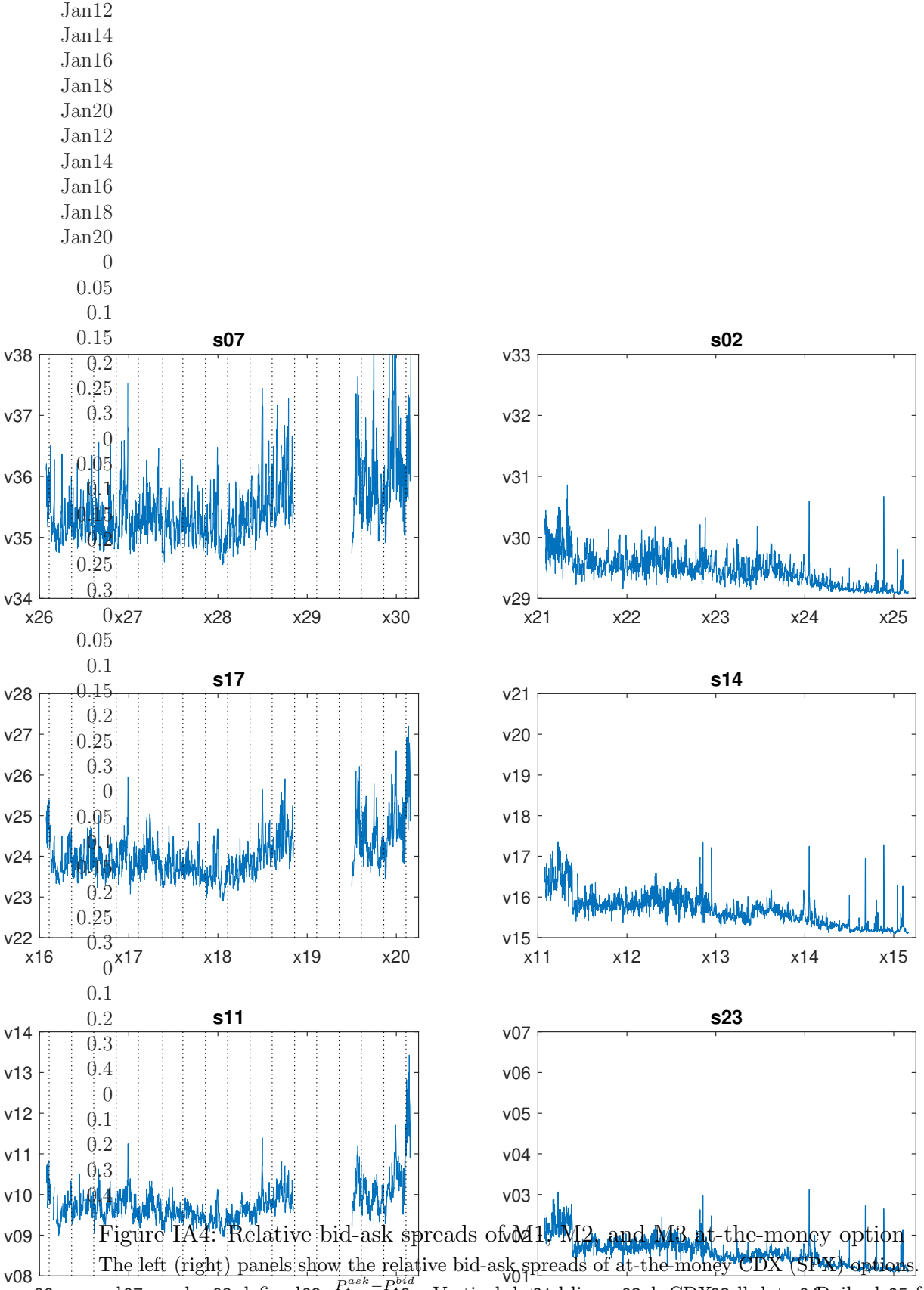

Figure IA4: Relative bid-ask spreads of M1, M2, and M3 at-the-money option

The left (right) panels show the relative bid-ask spreads of at-the-money CDX (SPX) options. Relative bid-ask spreads are defined as $\frac{P_t^{ask}-P_t^{bid}}{P_t^{mid}}$. Vertical dotted lines mark CDX roll dates. Daily data from February 24, 2012 until April 30, 2020.

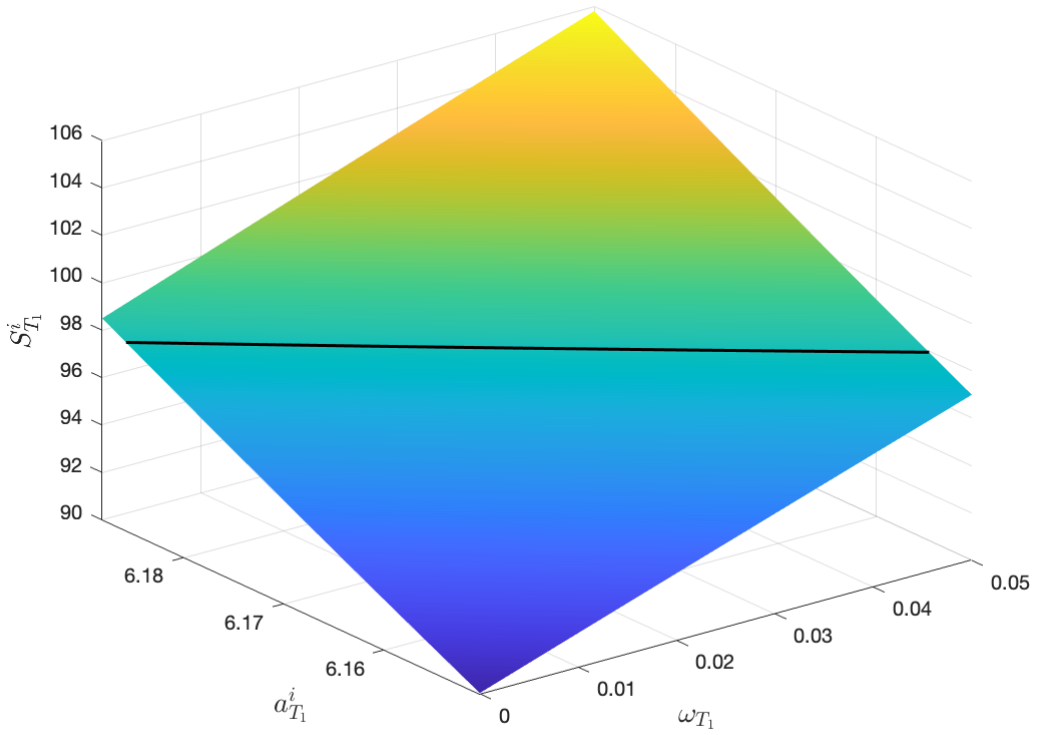

Figure IA5: Equity value and default boundary at T_1

The figure shows the equity value at T_1 as a function of $a^i_{T_1}$ and ω_{T_1}. The black line shows the default boundary.

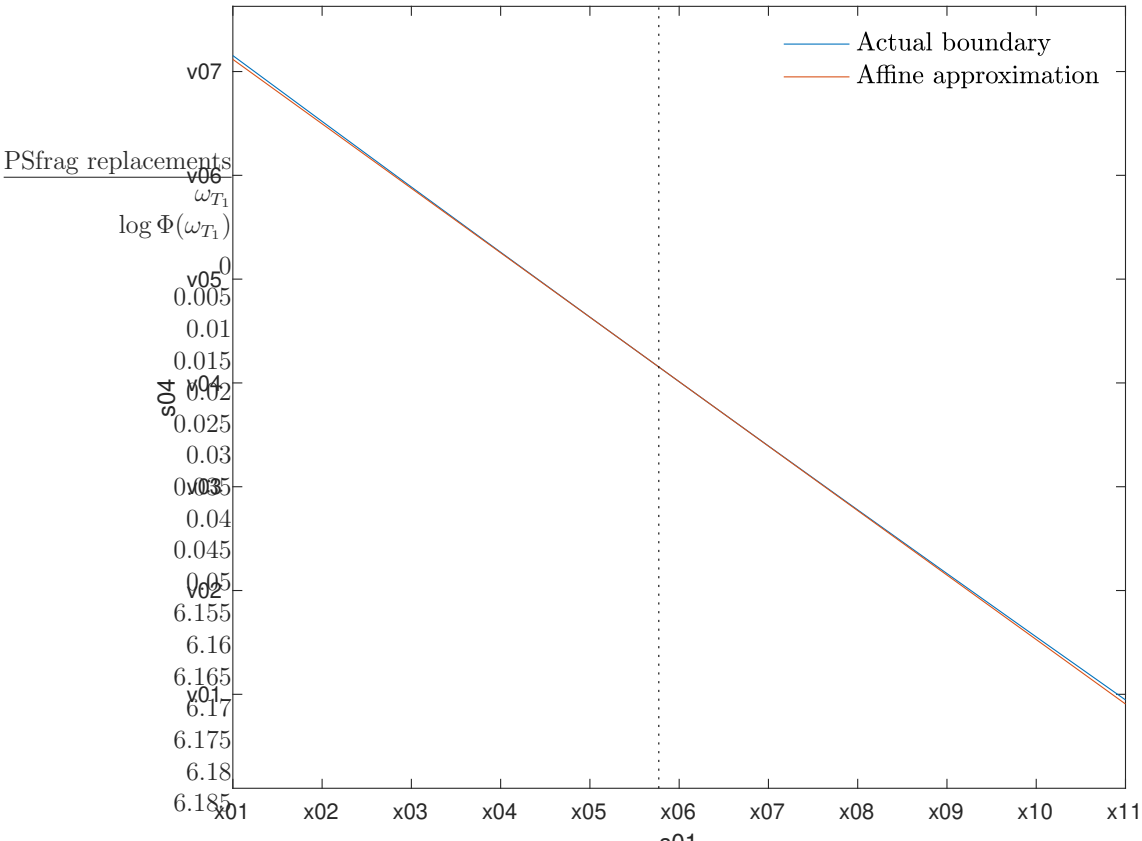

Figure IA6: Default boundary as a function of variance

The approximate boundary is obtained by linearizing the $\log \Phi(\omega)$-function around $\omega = \mathbb{E}_0[\omega_{T_1}] = 0.0239$ (vertical dotted line).

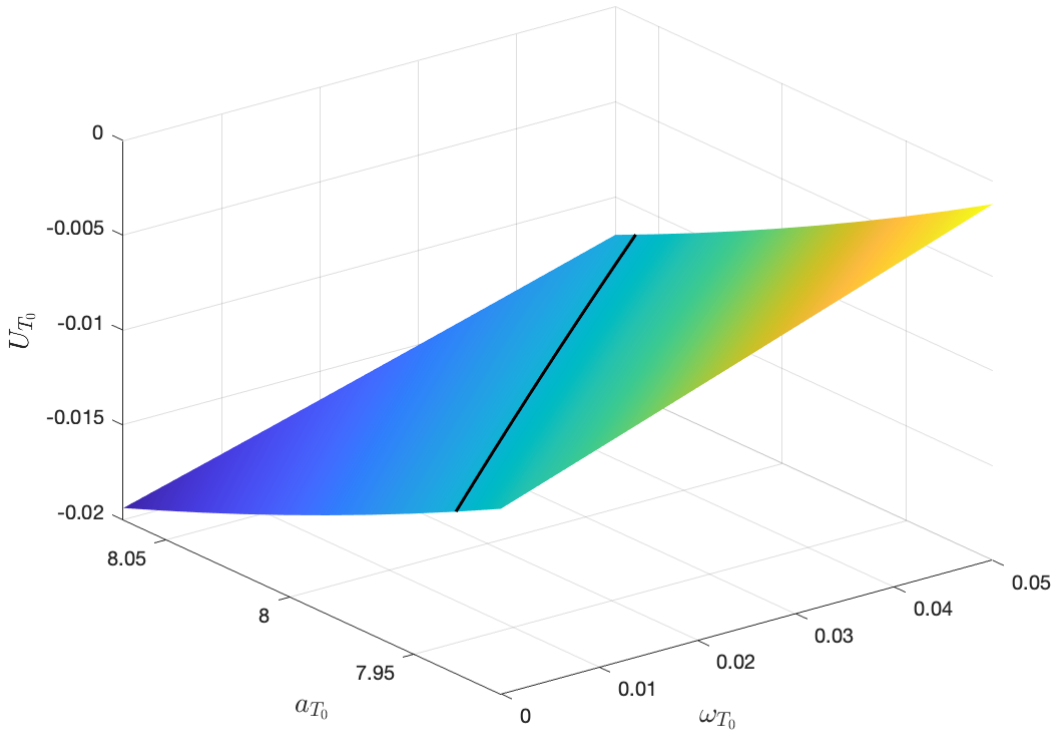

Figure IA7: CDX value and option exercise boundary at T_0

The figure shows the CDX upfront amount at T_0 as a function of a_{T_0} and ω_{T_0}. The black line shows the option exercise boundary.

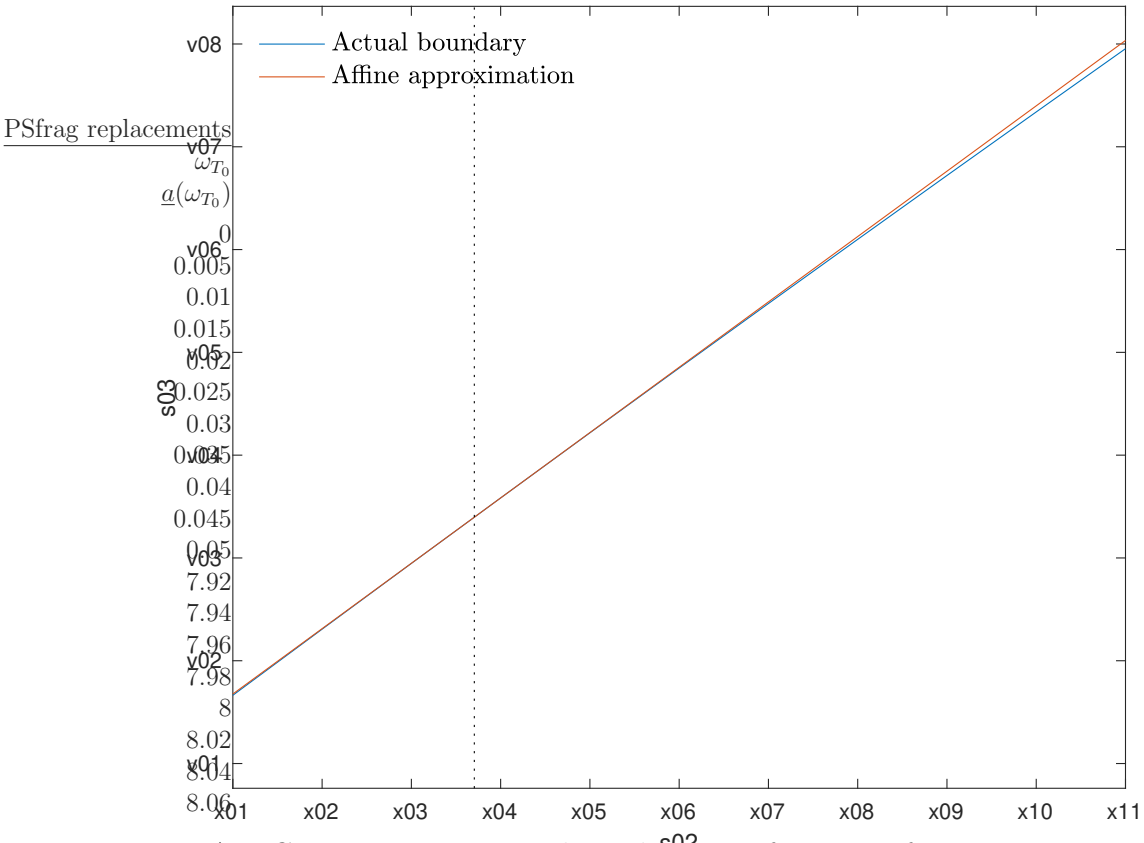

Figure IA8: CDX option exercise boundary as a function of variance

The approximate boundary is obtained by linearizing the $\underline{a}(\omega)$-function around $\omega = \mathbb{E}_0[\omega_{T_0}] = 0.0135$ (vertical dotted line).

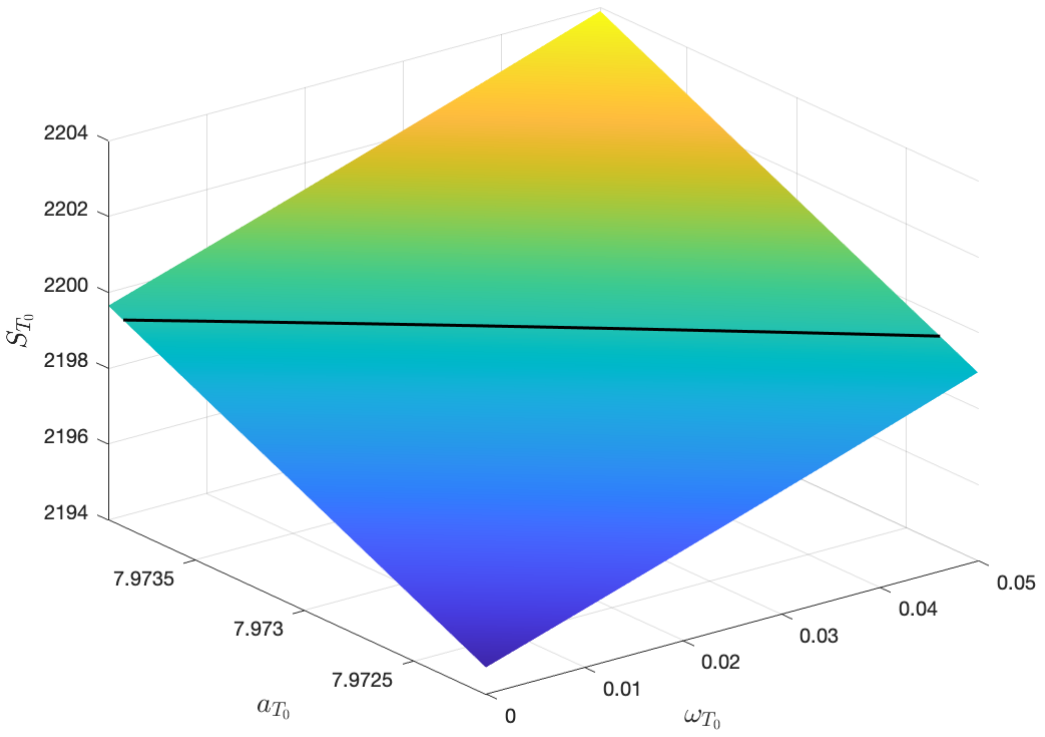

Figure IA9: SPX value and option exercise boundary at T_0

The figure shows the SPX value at T_0 as a function of a_{T_0} and ω_{T_0}. The black line shows the option exercise boundary.

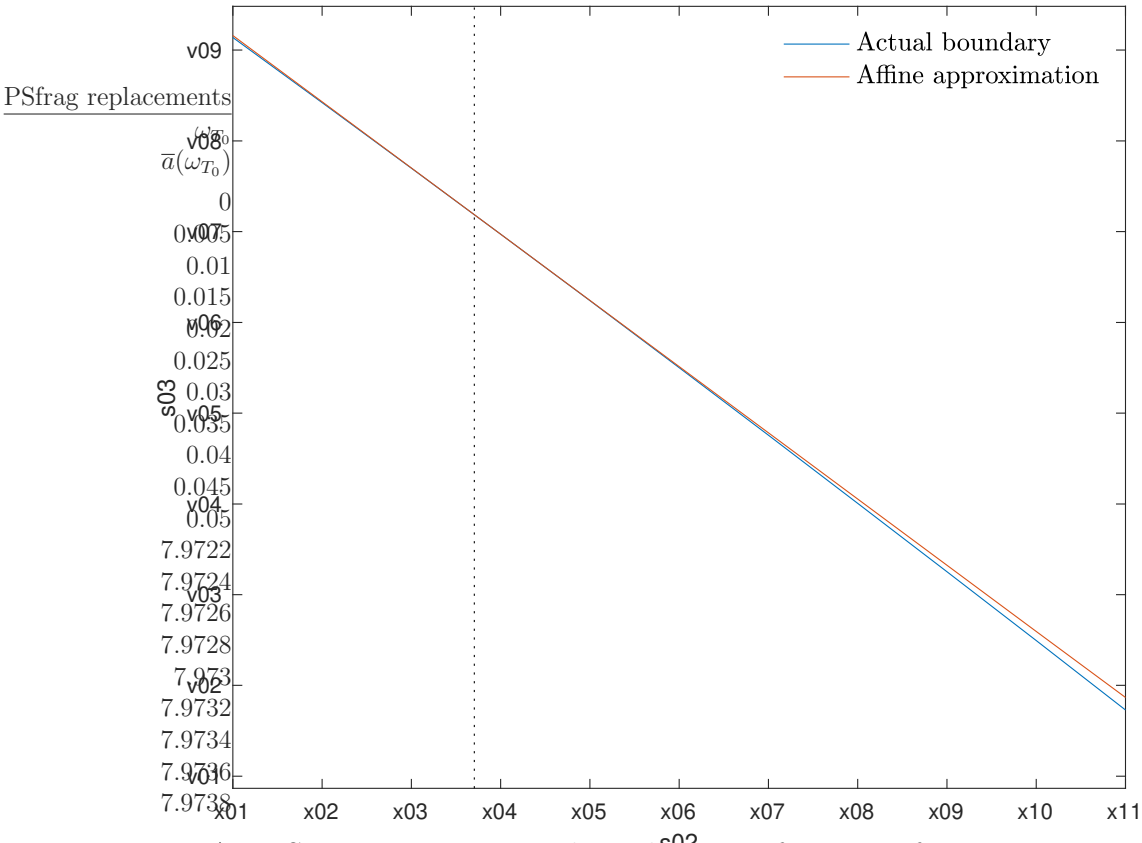

Figure IA10: SPX option exercise boundary as a function of variance

The approximate boundary is obtained by linearizing the $\overline{a}(\omega)$-function around $\omega = \mathbb{E}_0[\omega_{T_0}] = 0.0135$ (vertical dotted line).

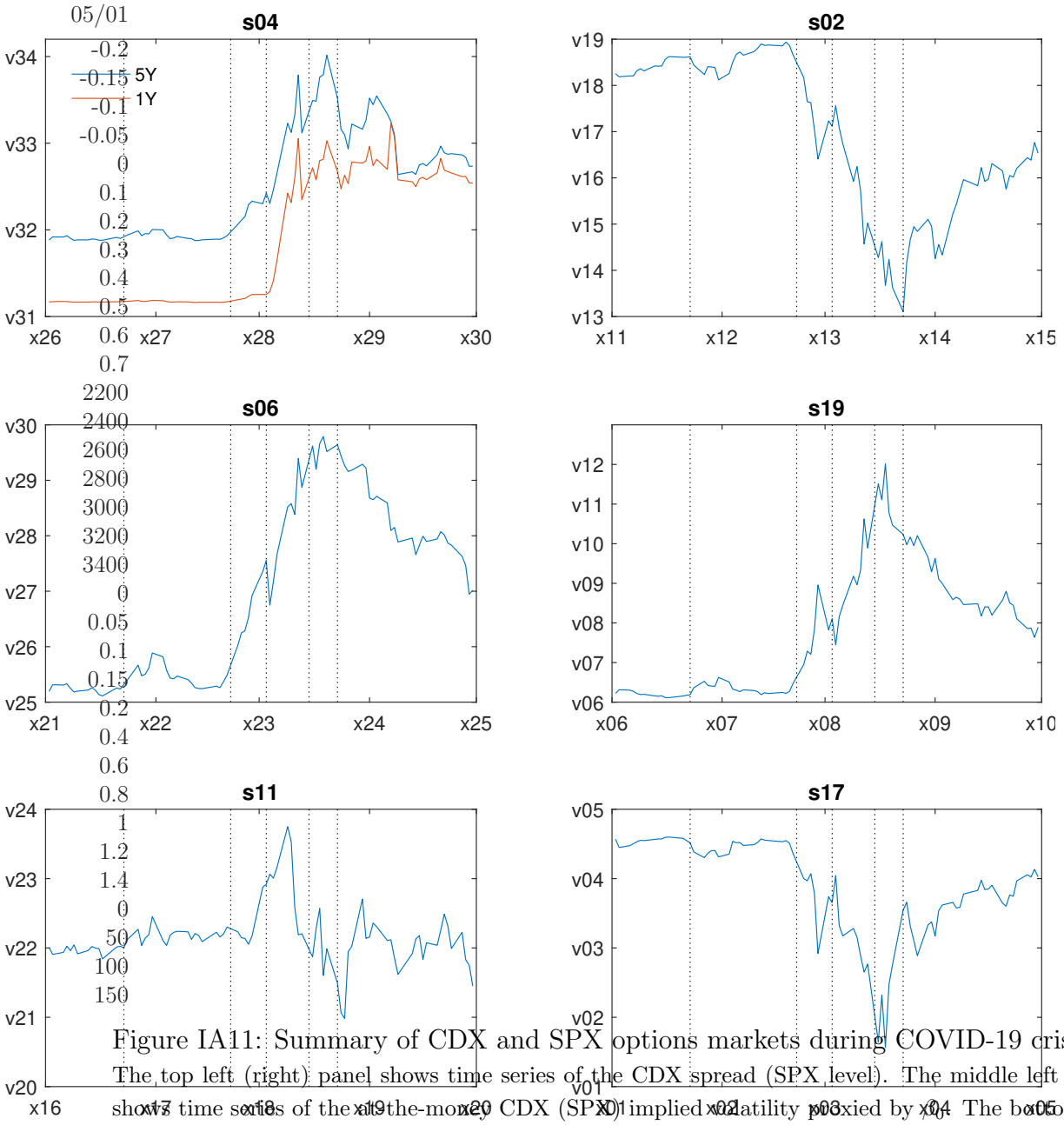

Figure IA11: Summary of CDX and SPX options markets during COVID-19 crisis

The top left (right) panel shows time series of the CDX spread (SPX level). The middle left (right) panel shows time series of the at-the-money CDX (SPX) implied volatility proxied by β_0. The bottom left (right) panel shows time series of the skewness of the CDX (SPX) implied volatility smile proxied by β_1. The vertical dotted lines mark the Wuhan lockdown on January 23, the Italy quarantine on February 22, the 50 bps rate cut by the Federal Reserve on March 3, 2020, the 100 bps rate cut and credit market support by the Federal Reserve on March 15, 2020, and the expansion of credit market support by Federal Reserve on March 23, 2020. Daily data from January 2, 2020 to April 30, 2020.

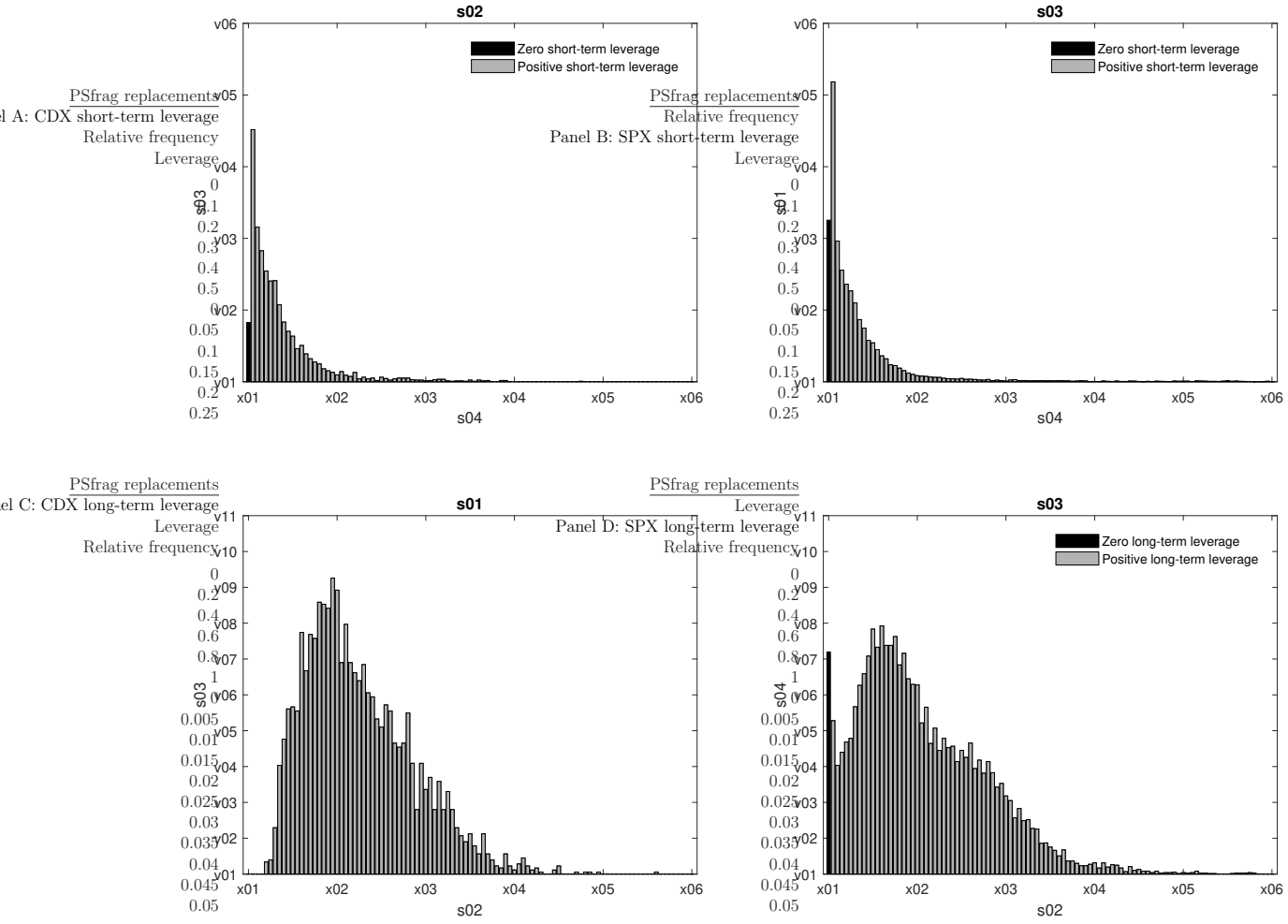

Figure IA12: Distributions of short- and long-term leverage across index constituents

Panels A and B (C and D) show the distribution of firm-quarter short-term (long-term) leverage observations for the constituents of the CDX and SPX, respectively. Short-term (long-term) leverage is defined as book value of short-term (long-term) debt relative to the sum of market value of equity and book value of total debt. The sample is from first quarter of 2012 until first quarter of 2020.

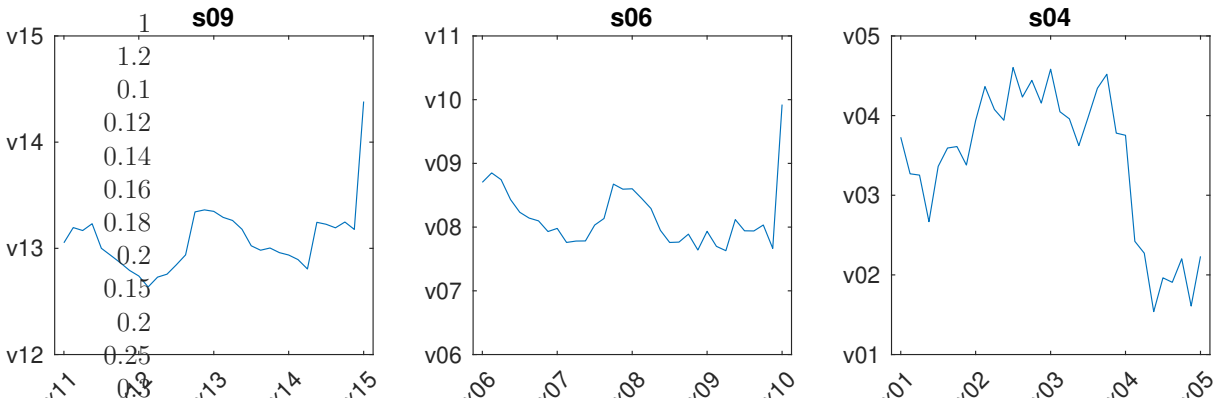

Figure IA13: Time series of moments of leverage distributions

The figure shows the time series of the mean, standard deviation, and skewness of the distribution of long-term leverage for SPX constituents.

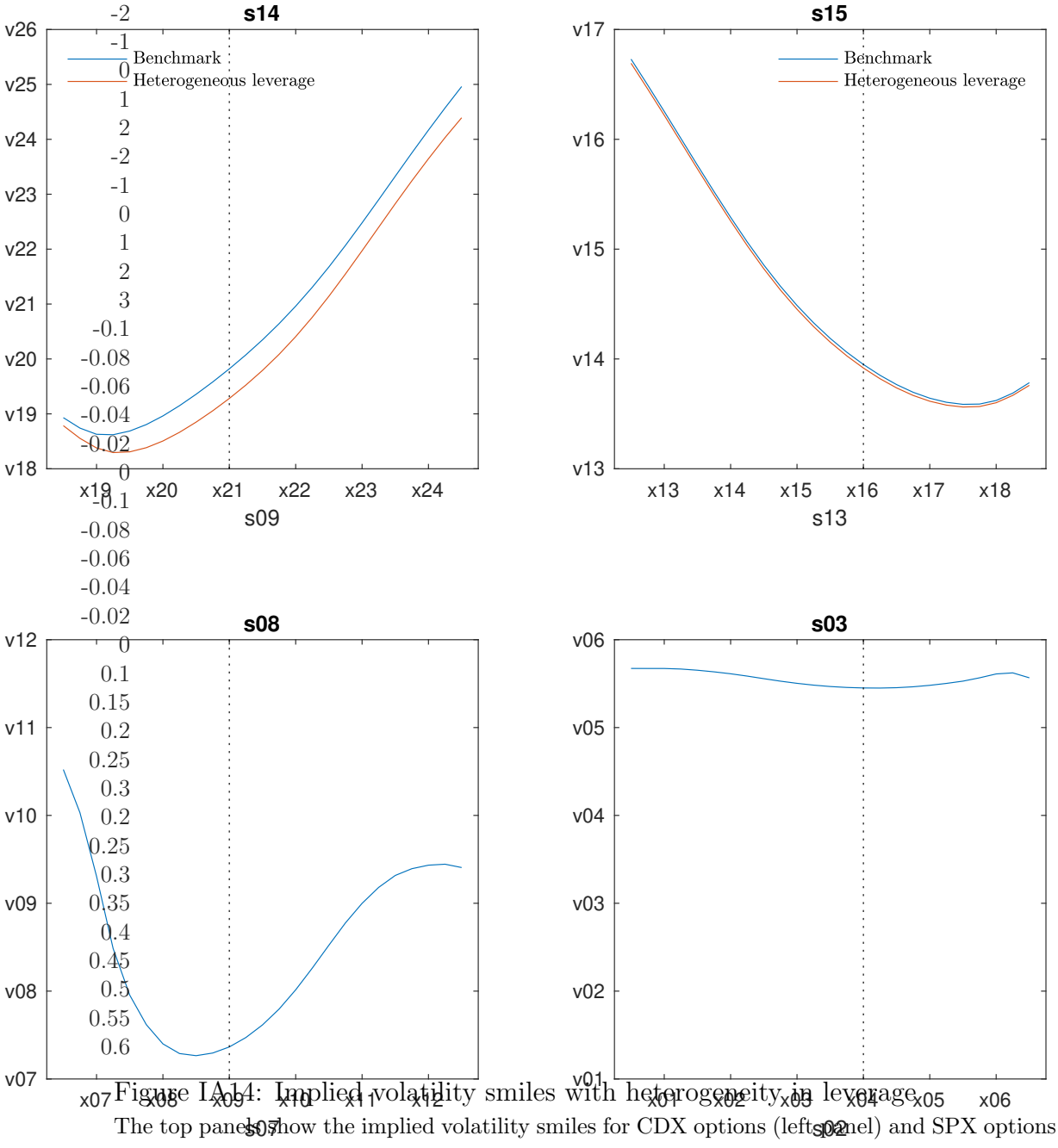

Figure IA.14: Implied volatility smiles with heterogeneity in leverage

The top panels show the implied volatility smiles for CDX options (left panel) and SPX options (right panel) for the benchmark homogeneous model (blue line) and the heterogeneous model (red line) fitted to the same set of SPX options. The bottom panels show the relative difference between the implied volatilities from the heterogeneous and homogeneous models.

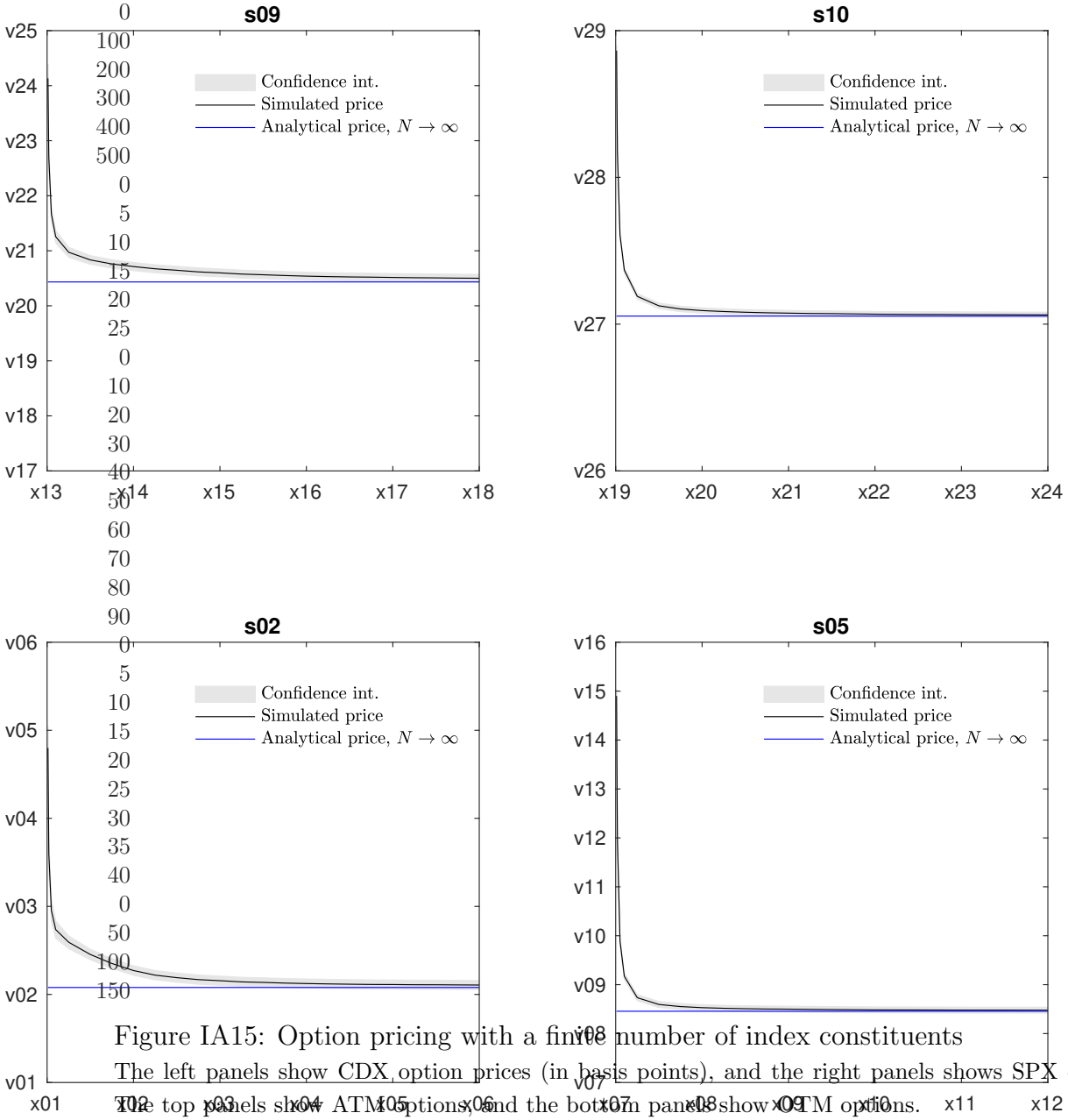

Figure IA15: Option pricing with a finite number of index constituents

The left panels show CDX option prices (in basis points), and the right panels shows SPX option prices. The top panels show ATM options, and the bottom panels show OTM options.

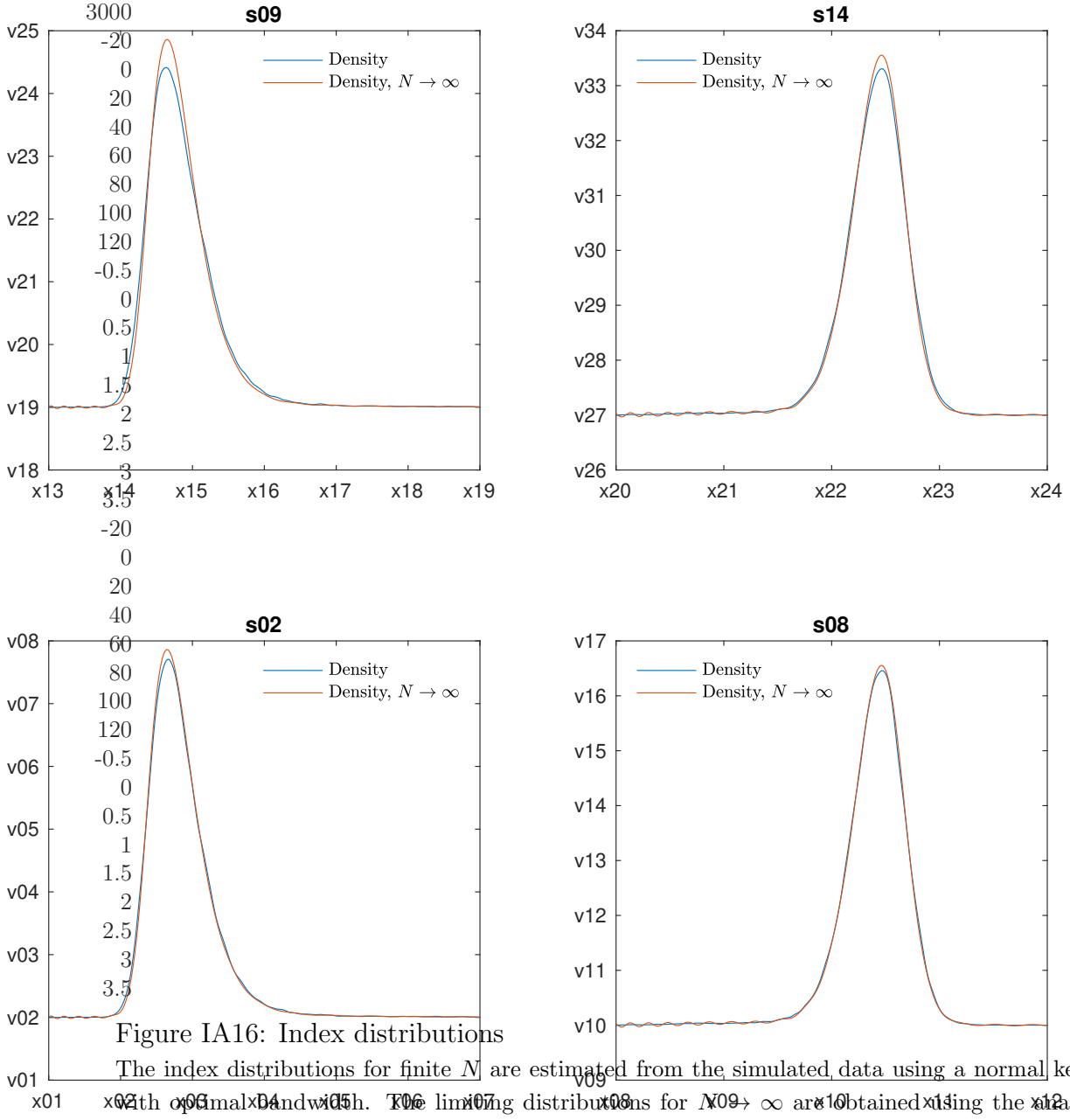

Figure IA16: Index distributions

The index distributions for finite N are estimated from the simulated data using a normal kernel function with optimal bandwidth. The limiting distributions for $N \to \infty$ are obtained using the analytical option price formulas together with the Breeden-Litzenberger Theorem. The left (right) panels show CDX (SPX) distributions (SPX distributions are multiplied by 10^3). The top (bottom) panels show results for $N = 125$ ($N = 500$).

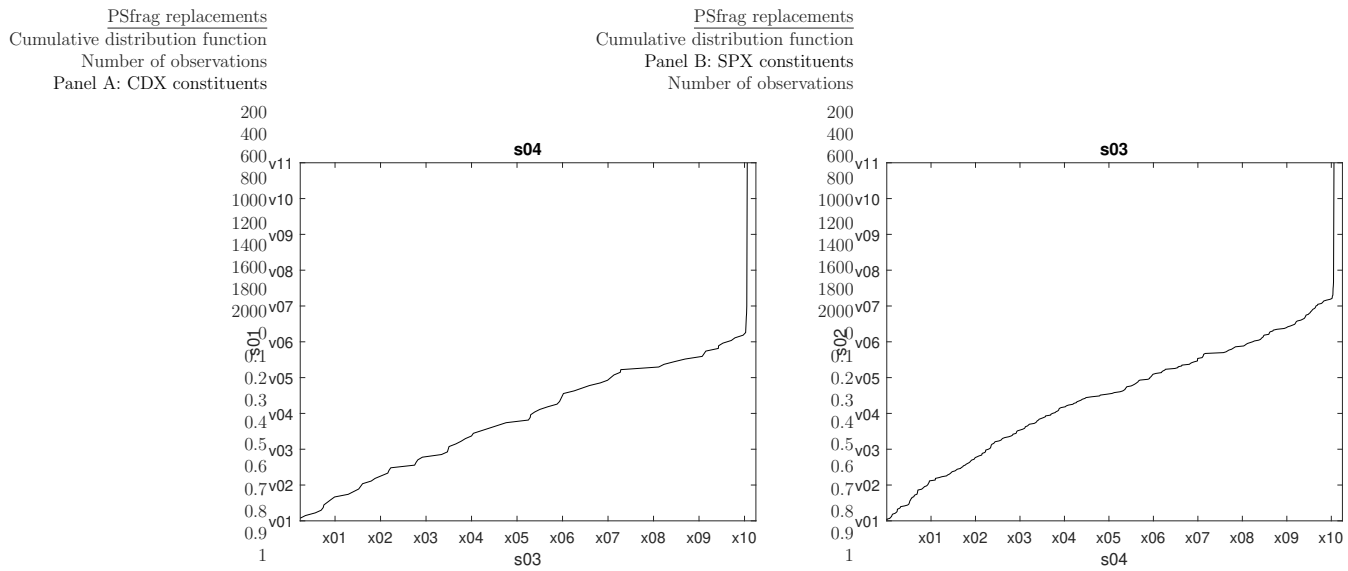

Figure IA17: Cumulative distribution function of asset return observations

Panels A and B show the cumulative distribution function of asset return observations for companies that were a CDX (Panel A) or SPX (Panel B) constituent at some point between 2012 and 2019. Daily data from January 3, 2012 until December 31, 2019.

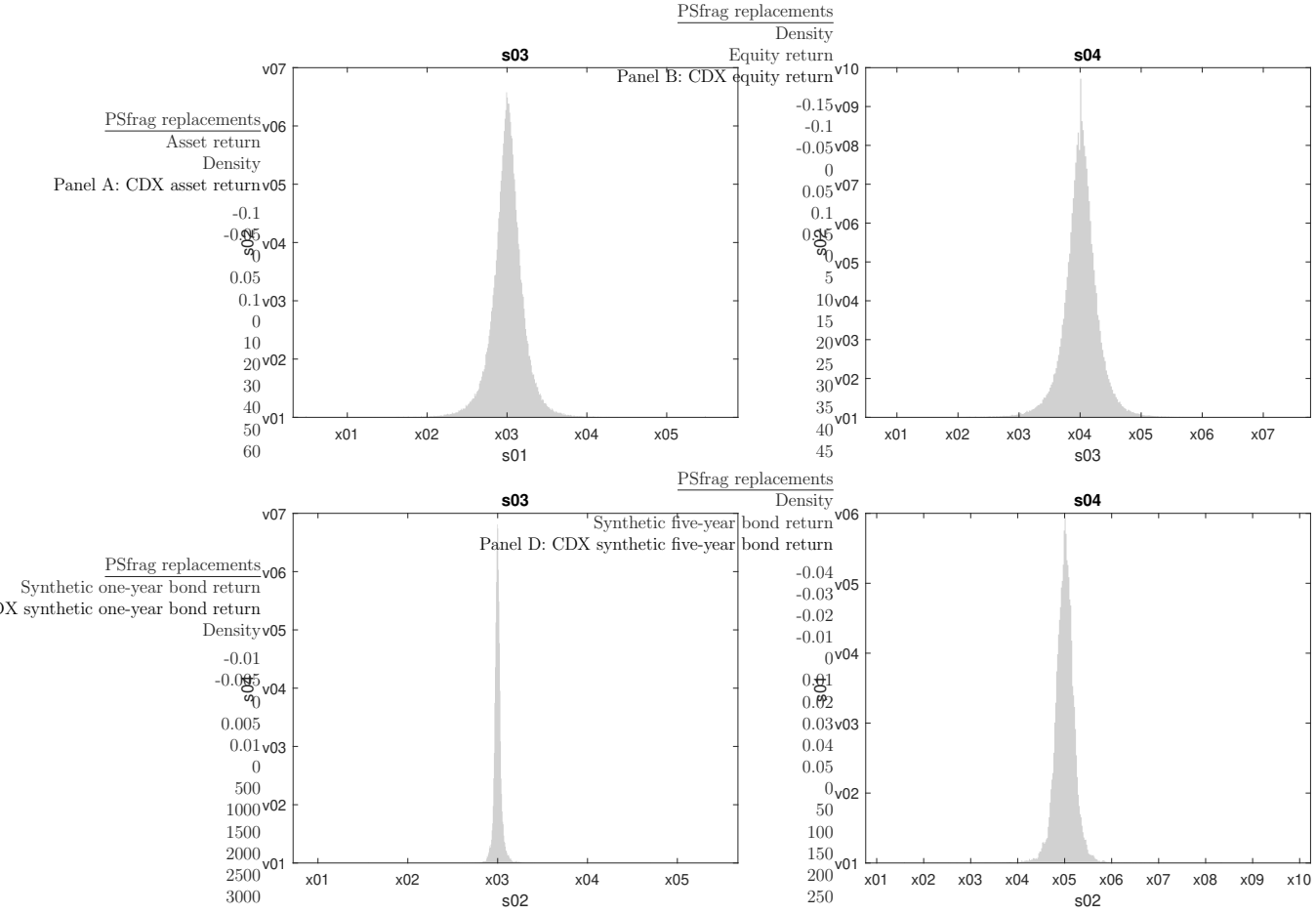

Figure IA18: Return distributions CDX constituents

Panel A shows the density of the asset return distribution for CDX constituents, and Panels B–D show the densities of the distributions of the asset return's components. Panel B shows the density of the equity return distribution, and Panels C and D show the density of the distributions of synthetic one- and five-year bond returns, respectively. Daily data from January 3, 2012 until December 31, 2019.

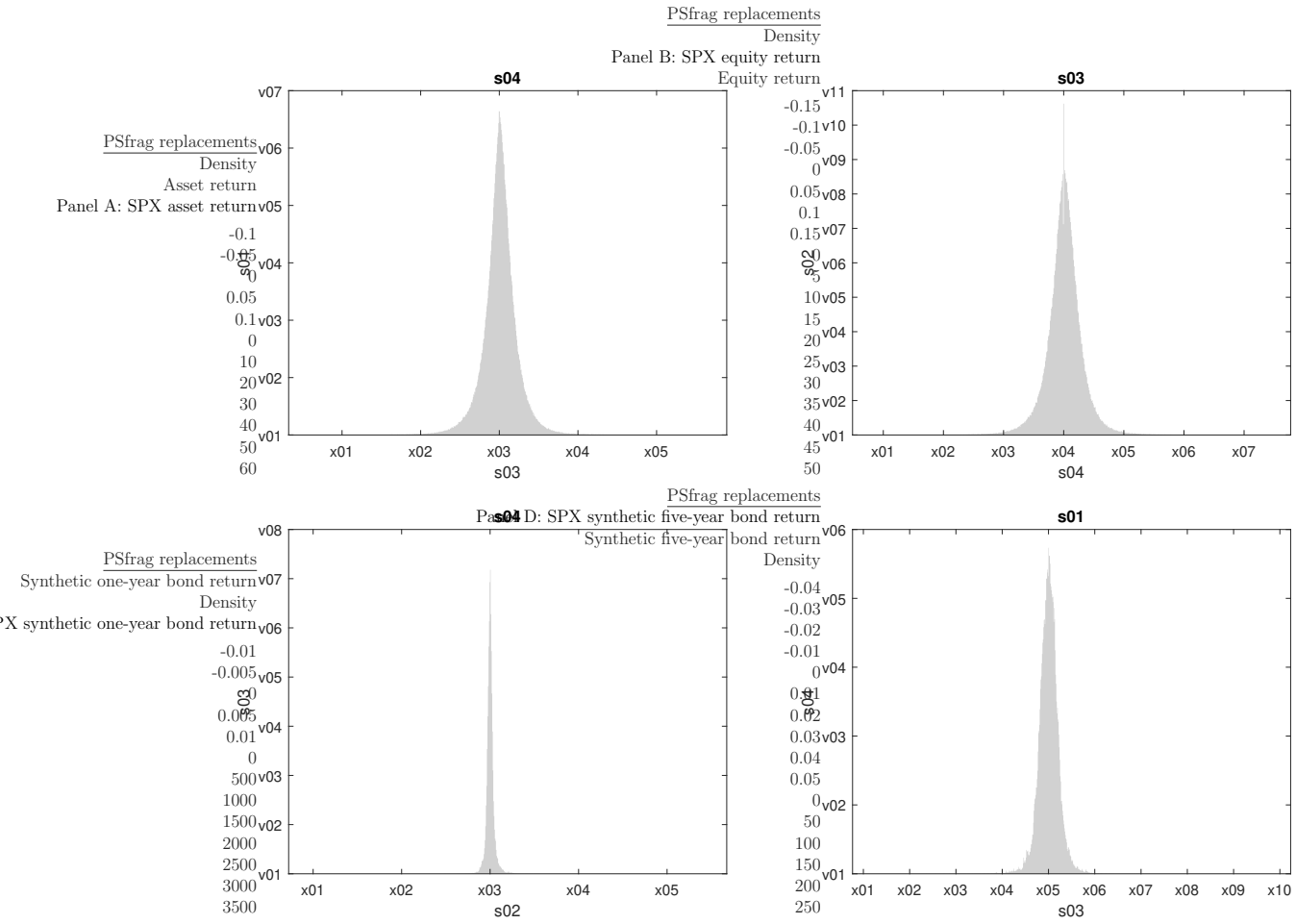

Figure IA19: Return distributions SPX constituents

Panel A shows the density of the asset return distribution for SPX constituents, and Panels B–D show the densities of the distributions of the asset return's components. Panel B shows the density of the equity return distribution, and Panels C and D show the density of the distributions of synthetic one- and five-year bond returns, respectively. Daily data from January 3, 2012 until December 31, 2019.

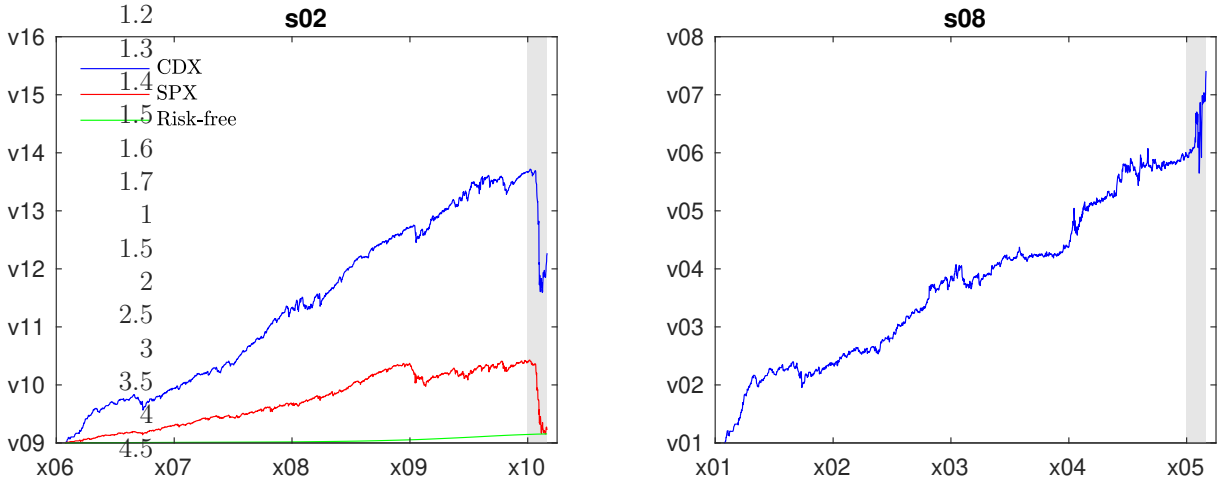

Figure IA20: Cumulative performance of trading strategies, constant required capital

The figure shows shows the evolution of one dollar invested in each of the EW strategies at the beginning of the sample (see Table IA.4 for details on the trading strategies). The left panel shows the performance of selling CDX and SPX straddles outright. The right panel shows the performance of the short-long strategy that allocates 50% of funds to selling CDX straddles and 50% to buying SPX straddles. On those trading days where options returns on unavailable, we invest at the risk-free rate. The sample period is from February 24, 2012 to April 30, 2020 (2042 daily observations). The shaded area marks the COVID-19 period starting on January 1, 2020.

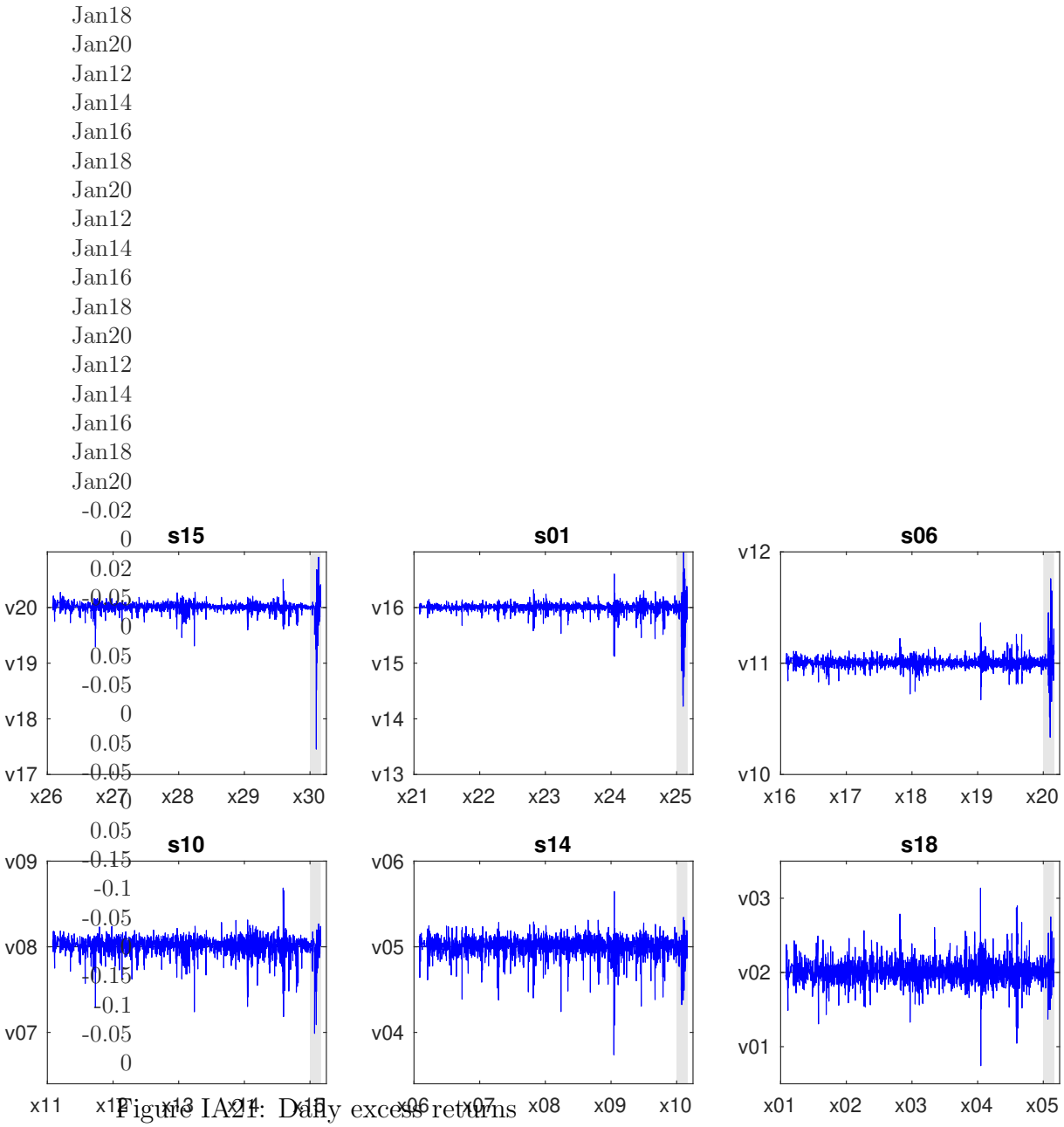

Figure IA21: Daily excess returns

The figure shows daily excess returns for each of the EW strategies. "CDX-SPX" denotes the short-long strategy that allocates 50% of funds to selling CDX straddles and 50% to buying SPX straddles. The top row shows excess returns when the required amount of capital is constant over time. The bottom row shows excess returns when the required amount of capital is proportional to the option premium. Each sample consists of 1881 daily returns between February 28, 2012 and April 30, 2020. The shaded area marks the COVID-19 period starting on January 1, 2020.

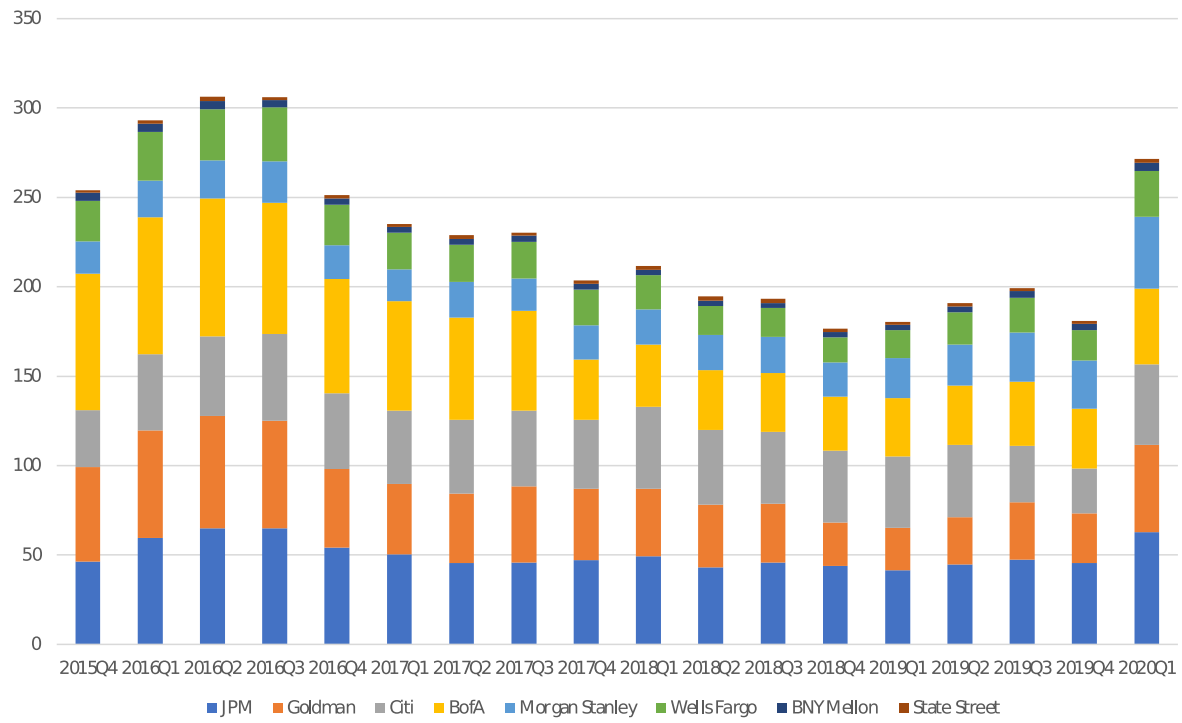

Figure IA22: Risk-weighted assets for CVA risk across the 8 US G-SIBs

The figure shows the risk-weighted assets (RWAs) for counterparty valuation adjustment (CVA) risk across the eight US global systemically important banks (G-SIBs). The data comes from the quarterly "Pillar 3 Regulatory Capital Disclosures". The sample period is Q4 2015 and Q1 2020 (prior to Q4 2015 not all banks reported RWAs specifically for CVA risk).

Swiss Finance Institute

Swiss Finance Institute (SFI) is the national center for fundamental research, doctoral training, knowledge exchange, and continuing education in the fields of banking and finance. SFI's mission is to grow knowledge capital for the Swiss financial marketplace. Created in 2006 as a public–private partnership, SFI is a common initiative of the Swiss finance industry, leading Swiss universities, and the Swiss Confederation.

swiss:finance:institute

c/o University of Geneva, Bd. Du Pont d'Arve 42, CH-1211 Geneva 4
T +41 22 379 84 71, rps@sfi.ch, www.sfi.ch